SENSITIVITY OF H_∞ CONTROLLER DESIGNS TO STRUCTURED UNCERTAINTY

by

IAN KEITH CRAIG

B.Eng. Electronic Engineering, University of Pretoria, South Africa
(1985)

Submitted in partial fulfillment of the
requirements for the degree of

MASTER OF SCIENCE

at the

MASSACHUSETTS INSTITUTE OF TECHNOLOGY

May 1989

Signature of Author _____
Department of Aeronautics and Astronautics
May 12, 1989

Certified by _____
Professor Lena Valavani
Thesis Supervisor

Accepted by _____
Professor Harold Y. Wachman
Chairman, Departmental Graduate Committee

SENSITIVITY OF H_∞ CONTROLLER DESIGNS TO STRUCTURED UNCERTAINTY

by

IAN KEITH CRAIG

Submitted to the Department of Aeronautics and Astronautics on May 12, 1989, in partial fulfillment of the requirements for the degree of Master of Science.

ABSTRACT

The H_∞ design methodology is described in detail, and the sensitivity of H_∞ designs to structured uncertainty is determined using H_∞ controllers designed for two "practical" plants, an advanced fighter aircraft and a milling circuit. The effects of near unstable pole zero cancellations on H_∞ designs are also studied. Methods are developed to determine, before an actual design is done, whether the resulting closed loop system will be sensitive to structured uncertainty. A technique called inner loop compensation is introduced to desensitize H_∞ controller designs to this type of uncertainty. An inner loop compensated H_∞ controller for the advanced fighter aircraft is compared to a traditional classical controller.

Thesis Supervisor: Dr. Lena Valavani

Title: Associate Professor of Aeronautics and Astronautics

ACKNOWLEDGEMENTS

I am grateful to my thesis supervisor Professor Lena Valavani for her guidance, support and insights she shared with me during the course of this research. Her contagious enthusiasm contributed to the successful conclusion of this work.

I would also like to thank my fellow students and colleagues whose friendship and technical advice made my life at M.I.T. a pleasant and rewarding experience. They include Jose Cro Granito, Philippe Le Fur, Mathieu Mercadal, Dragan Obradovic, Dr. Jeff Shamma, Dave Vos, Petros Voulgaris, and Norman Wereley.

In addition, I would like to thank some of the faculty at M.I.T. whose teaching and advice are much appreciated. They are Professors Michael Athans, Munther Dahleh, Gunter Stein, Gilbert Strang, Alar Toomre, Lena Valavani, and Wallace Vander Velde.

Dr. Dave Hulbert of MINTEK who gave me my first taste of "real world" control problems, and who provided the milling circuit model used in this thesis, deserves a special word of thanks.

Next my wife Andrie and I would like to thank our families whose long distance support and encouragement kept us going through the ups and downs of academic life at M.I.T.

Finally, and most importantly, I would like to thank Andrie, who through the years, has become my trusted partner and confidant. Without her love, interest, support, and good humor this research would not have been possible. I therefore dedicate this thesis to her.

TABLE OF CONTENTS

LIST OF FIGURES

LIST OF TABLES

NOTATION AND DEFINITIONS

A^T	transpose of matrix A
A^{-1}	inverse of matrix A
$\lambda_i(A)$	the i^{th} eigenvalue of a matrix A
$\overline{\lambda}(A)$	the maximum eigenvalue of a matrix A
$\sigma_i(A)$	the i^{th} singular value of a matrix A
$\overline{\sigma}(A)$	the maximum singular value of a matrix A
$\underline{\sigma}(A)$	the minimum singular value of a matrix A
$\kappa(A)$	$:= \frac{\overline{\sigma}(A)}{\underline{\sigma}(A)}$ condition number of matrix A
$G(s)$	$:= \left[\begin{array}{c\|c} A & B \\ \hline C & D \end{array}\right] := C(sI - A)^{-1}B + D$ transfer function matrix represented in terms of state space data
sup	least upper bound
$\| G \|_\infty$	$:= \sup_\omega \overline{\sigma}[G(j\omega)]$ the H_∞–norm of a stable transfer function matrix G(s)

CHAPTER 1

INTRODUCTION

1.1 Motivation

The H_∞ design methodology is one of the most recent of the so called robust multivariable feedback control systems synthesis methods [1,2]. This methodology , however, does not take structured uncertainty into account in any direct way but provision can be made for unstructured uncertainty given an upper bound on the magnitude of this uncertainty.

In practical situations, it is often not possible to determine plant parameters very accurately when constructing a nominal plant model. If parametric or structured uncertainty is present, a compensator which was designed based on a nominal model, could behave in an undesirable fashion when implemented on the real plant. The H_∞ compensator inverts the stable part of the plant dynamics and substitutes some desirable dynamics in its place. As this inversion process can be impeded by structured uncertainty, it is important to know for which "size" of such uncertainty the controller will still perform adequately.

Control engineers in industry are often reluctant to apply new multivariable controller design methodologies (e.g. the H_∞ method) to practical problems because of a lack of experience with these methods, and the few "realistic" examples that

exists in the literature [3]. It is often the case that extensions of SISO (single–input–single–output) design methods are applied to inherently multivariable problems. Dealing with the cross–coupling in these multivariable systems then becomes an art based primarily on experience and not on a sound theoretical basis. This thesis should help develop some confidence in the application of the H_∞ methodology to practical design problems.

1.2 Contribution of the Thesis

The are six ways in which this thesis contributes to the understanding of H_∞ designs and control systems in general. They are the following:

- A detailed description is given of the H_∞ design procedure. In particular, the thesis shows how to incorporate frequency domain specifications into weighting functions which form part of an augmented plant to which the H_∞ design methodology is applied.
- The thesis provides two "realistic" design examples of H_∞ compensators, i.e. designs for an advanced fighter aircraft and a milling circuit. The milling circuit example is most likely the first application of the H_∞ methodology to such a plant. An H_∞ design is also done for a fictitious plant with a near unstable pole zero cancellation.
- Equations are derived for the derivatives of singular values and eigenvalues of a square matrix. These equations are tools which help determine whether a closed loop H_∞ controller will be sensitive to structured uncertainty.

- The thesis shows that, by looking at the singular values of the open loop plant, one can determine if the closed loop H_∞ controller will be sensitive to structured uncertainty.
- A practical way is given to desensitize H_∞ controllers to structured uncertainty, called inner loop compensation.
- A comparison is made between a classical and a desensitized H_∞ controller for the advanced fighter aircraft.

1.3 Organization of the Thesis

The thesis is organized into six chapters. The current chapter has described the motivation for and the contributions of this thesis. Chapter 2 gives a detailed description of the H_∞ design methodology. In Chapter 3 H_∞ compensators are designed for an advanced fighter aircraft and a milling circuit.

In Chapter 4, tools are developed to study the effects of structured uncertainty on H_∞ designs. Sensitivity studies are performed on H_∞ designs for the advanced fighter aircraft, the milling circuit, and two fictitious plants. An "artificial" way of making the controller for the aircraft less sensitive to structured uncertainty, is introduced. Chapter 5 focuses on practical ways of desensitizing H_∞ designs to structured uncertainty. A traditional classical compensator for the aircraft is compared to an inner loop compensated H_∞ compensator with regard to stability robustness and performance. The final chapter discusses the results and proposes directions for future research.

CHAPTER 2

THE H_∞ DESIGN METHODOLOGY

2.1 Introduction

This chapter deals with the formal control system synthesis problem, in which the H_∞–norm performance measure is used [1]. Compensators are designed for the class of dynamical systems that are assumed to be finite–dimensional and linear–time–invariant (FDLTI). Although FDLTI systems represent idealizations of actual physical systems, controller designs based on these systems give good results, as long as the approximations made, are justified.

The H_∞ methodology is one of the most recent so called robust (uncertainty–tolerant) multivariable feedback control systems synthesis methods [2]. The design of a fixed parameter compensator is based on a nominal model, and the aim is to maintain stability and reasonable performance in the presence of significant uncertainty (e.g. noise/disturbance signals and modeling errors). However, neither this nor the H_2 (LQG/LTR) [4] design methodology take structured uncertainty into account in any direct way. Provision can, however, be made for unstructured uncertainty given an upper magnitude bound on this uncertainty [5].

The H_∞ design procedure can best be described by the following points, each of which will be elaborated on in this chapter:

- start with a plant model that has to be controlled to desired specifications
- express design specifications in terms of weighting functions
- augment the plant model with these weighting functions
- find the desired compensator by solving the H_∞ synthesis problem
- verify if the design specifications are met and if control rate and magnitude constraints are adhered to
- repeat the design process if necessary

2.2 The Plant Model and Specifications

2.2.1 The Plant Model

The plant model must be FDLTI but can be minimum or nonminimum phase, square or nonsquare, stable or unstable. An upper bound on the unstructured uncertainty of the plant must be known, so that realistic robustness specifications can be set.

2.2.2 Specifications

An obvious specification that is taken care of by the H_∞ synthesis, is that of nominal stability. Other specifications are normally given in terms of singular value loop shapes (frequency domain), e.g.

Robustness specification: 20 db/decade roll–of and at least –40 db at 100 rad/sec

Performance specification: minimize the sensitivity function as much as possible (can also be interpreted as a robustness specification)

The robustness specifications can also be given in more "classical" terms, like multivariable gain and phase margins [6,7]. In each loop of a multivariable feedback system, simultaneously and independently, there are guaranteed gain and phase margins (denoted GM and PM respectively), given by the following equations:

$$\text{downward gain margin} \qquad GM\downarrow \leq \frac{k}{k+1}$$

$$\text{upward gain margin} \qquad GM\uparrow \geq \frac{k}{k-1} \qquad (2.2.2.1)$$

$$\text{phase margin} \qquad |PM| \geq 2\sin^{-1}(1/2k)$$

where

$$k = \|S(s)\|_{\infty}$$

with $S(s) = [I + G(s)K(s)]^{-1}$ the sensitivity transfer function matrix of the standard feedback configuration shown in Figure 2.2.2.1. This means that the gains or phases of all the feedback loops may be changed at the same time within the prescribed limits, without destabilizing the closed loop system. From the equations

above it is evident that minimizing the sensitivity will result in good multivariable gain and phase margins.

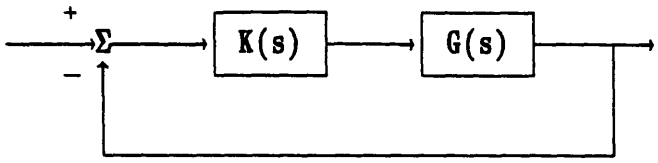

Figure 2.2.2.1: The standard feedback configuration

The following constraint should always be kept in mind when posing specifications:

$$S(s) + C(s) = I \qquad (2.2.2.2)$$

with $C(s) = [I + G(s)K(s)]^{-1}G(s)K(s)$ the closed loop transfer function or complementary sensitivity matrix (see Figure 2.2.2.1). It does not make sense, for example, to ask for output disturbance and measurement noise rejection in the same frequency range, as this violates the constraint given above.

Another performance specification that can be accommodated is zero steady state errors to constant commands or disturbances in all directions. This can be achieved by adding low frequency poles (approximation of integrators) to the weight on the sensitivity transfer function matrix; more on weighting functions in section 2.3. Time domain specifications like rise–time and percentage overshoot, are not treated directly. The time domain response of the system can be observed by doing time simulations after the controller has been designed.

2.3 Singular Value Loop Shaping and the Selection of Weights

Weighting functions are the free parameters in the H_∞ design framework, and can be used to "tune" designs to meet realistic specifications. This section describes how weights are accommodated in the H_∞ synthesis problem.

The standard feedback configuration as shown in Figure 2.2.2.1, will be used to illustrate the selection of weighting functions. Figure 2.3.1 shows how the weights are connected to the feedback system. G(s) is the plant transfer function matrix and K(s) represents the compensator. The transfer function matrices of the weights are given by $W_i(s) = w_i(s)\, I_{nxn}$ (i = 1, 2, 3), and the reference input by u_1. Although the weights used in this thesis are all diagonal, this does not have to be. Diagonal weights have the advantage of forcing decoupled closed loop responses. Matched singular values can be achieved by making the diagonal elements equal.

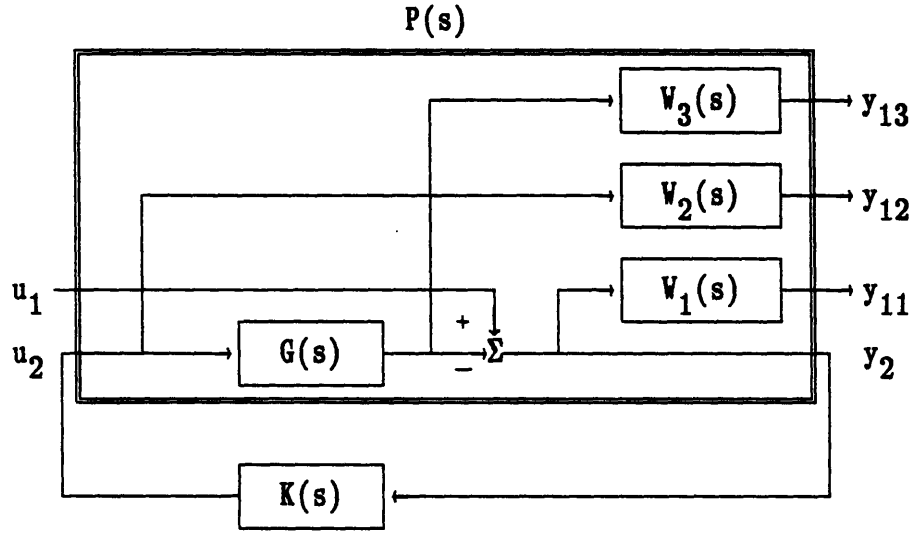

Figure 2.3.1: The standard feedback configuration with weights

The configuration of weights shown in Figure 2.3.1 is by no means the only one that can be accommodated in the H_∞ synthesis problem, but it serves to illustrate the selection of weights in the familiar framework of the standard feedback problem.

Referring to Figure 2.3.1, a disturbance attenuation performance specification up to the crossover frequency ω_c can be expressed as,

$$\lim_{\gamma \to \gamma_{min}} \bar{\sigma}\,[S(j\omega)] \approx \bar{\sigma}\,[W_1^{-1}(j\omega)] \qquad \omega < \omega_c \tag{2.3.1}$$

$$\lim_{\gamma \to \gamma_{min}} \underline{\sigma}\,[S(j\omega)] \approx \underline{\sigma}\,[W_1^{-1}(j\omega)] \qquad \omega < \omega_c$$

where γ_{min} is the optimal gamma in the gamma–iteration discussed in section 2.5.1. Equation 2.3.1 indicates that the attenuation factor is a function of frequency ω, which implies that one frequency range can be emphasized over another, to accommodate, for example, both output disturbance and measurement noise attenuation, subject to the constraint given in equation 2.2.2.2. A good choice for $W_1(s)$ is to set it equal to the inverse of the desired $\bar{\sigma}\,[S(j\omega)]$ at frequencies below crossover (ω_c). A typical weighting function $W_1(j\omega)$, is shown below, with n the number of plant outputs,

$$W_1(s) = \frac{k}{s + \alpha} I_{nxn} \; ; \quad k = \omega_c,\ \alpha = .0001$$

With k equal to the crossover frequency, $W_1(s)$ will help insure that all the singular

values of the loop transfer function crossover at k rad/sec. α is chosen such that $W_1(s)$ approximates a matrix with integrators on the diagonal which will result in the controller having zero steady state errors to constant commands and disturbances.

The weights $W_2(s)$ and $W_3(s)$ both serve the purpose of specifying stability margins. Doyle et al [8] proposed a method for solving the H_∞ feedback problem, named gamma (γ)–iteration which will be discussed in section 2.5.1. Using this method, the weight on the controls $W_2(s)$ has to be present. Safonov [9] relaxed this restriction, and the designer can now choose either between using $W_2(s)$ or using $W_3(s)$. (See section 2.5.1 and Appendix A for more information). Generally, they are not used at the same time, as they serve the same purpose. Stability margins can be expressed using the following equations:

$$\bar{\sigma}\,[R(j\omega)] \leq \bar{\sigma}\,[W_2^{-1}(j\omega)] \qquad \omega > \omega_c \tag{2.3.2}$$

$$\underline{\sigma}\,[R(j\omega)] \leq \underline{\sigma}\,[W_2^{-1}(j\omega)] \qquad \omega > \omega_c$$

$$\bar{\sigma}\,[C(j\omega)] \leq \bar{\sigma}\,[W_3^{-1}(j\omega)] \qquad \omega > \omega_c \tag{2.3.3}$$

$$\underline{\sigma}\,[C(j\omega)] \leq \underline{\sigma}\,[W_3^{-1}(j\omega)] \qquad \omega > \omega_c$$

with $R(s) = K(s)[I + G(s)K(s)]^{-1}$ (see Figure 2.2.2.1). $W_2(s)$ is used when the plant uncertainty is described as additive perturbations, and $W_3(s)$ is used in the face of multiplicative perturbations. These perturbations are illustrated in Figure

2.3.2.

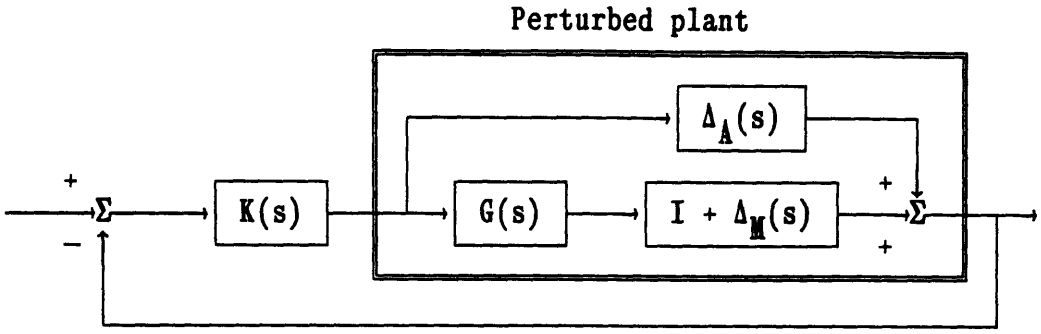

Figure 2.3.2: Additive and Multiplicative uncertainty

The multiplicative plant perturbations are indicated by $\Delta_M(s)$, and the additive perturbations by $\Delta_A(s)$. The multiplicative stability margin is the "size" of the smallest stable $\Delta_M(s)$ which destabilizes the system in Figure 2.3.2 with $\Delta_A(s) = 0$. The "size" of $\Delta_M(s)$, can be expressed in terms of $\bar{\sigma}\ [\Delta_M(j\omega)]$, and gives an indication on how to choose $W_3(s)$ (equation 2.3.3). A good choice for $W_3(s)$ is to set it equal to the inverse of the desired $\bar{\sigma}\ [C(j\omega)]$, at frequencies above ω_c. Similarly, the "size" of the smallest stable $\Delta_A(s)$, which destabilizes the system in Figure 2.3.2 with $\Delta_M(s) = 0$, gives an indication on how to choose $W_2(s)$.

It is intuitively more appealing to lump the effects of all plant uncertainty into multiplicative perturbations. Design specifications can then be expressed in terms of equations 2.3.1 and 2.3.3.

A typical weight on the complementary sensitivity C(s), is given by,

$$W_3(s) = \frac{s}{k} I_{nxn} \; ; \; k = \omega_c \qquad (2.3.4)$$

Thus, with the inclusion of dynamic filters for weights, the order of the compensator that results from the H_∞ design methodology, is equal to the order of the plant plus the order of the weights. There is thus a trade–off between the complexity of the weights and the order of the compensator.

More information on the selection of weighting functions can be found in Chapter 3 where they are actually chosen to meet certain specifications. The milling circuit example is particularly interesting, as the weights are chosen to provide a region of loop (G(s)K(s)) crossover frequencies. Appendix A shows how an improper $W_3(s)$ can be absorbed into a strictly proper plant such that $W_3(s)$ does not contribute to the order of the compensator.

2.4 Plant Augmentation

In order to solve the H_∞ synthesis problem, it is necessary to augment the plant model with specific weighting functions. In this section, the plant and weights shown in Figure 2.3.1, will be used to demonstrate how the plant augmentation is done.

The augmented plant model P(s) can be partitioned as a block (2x2) transfer function matrix.

$$P(s) := \begin{bmatrix} P_{11}(s) & P_{12}(s) \\ P_{21}(s) & P_{22}(s) \end{bmatrix} \tag{2.4.1}$$

with the relationships between the signals in Figure 2.3.1

$$\begin{aligned} y_1 &= P_{11}\, u_1 + P_{12}\, u_2 \\ y_2 &= P_{21}\, u_1 + P_{22}\, u_2 \end{aligned} \tag{2.4.2}$$

or

$$y_1 = \begin{bmatrix} y_{11} \\ y_{12} \\ y_{13} \end{bmatrix} = \begin{bmatrix} W_1 \\ 0 \\ 0 \end{bmatrix} u_1 + \begin{bmatrix} -W_1 G \\ W_2 \\ W_3 G \end{bmatrix} u_2$$

$$y_2 = I\, u_1 - G\, u_2$$

with a detectable and stabilizable state space description

$$P(s) := \left[\begin{array}{c|cc} A & B_1 & B_2 \\ \hline C_1 & D_{11} & D_{12} \\ C_2 & D_{21} & D_{22} \end{array}\right] \tag{2.4.3}$$

To proceed with synthesis next, let the state space descriptions of the plant and the weights be

$$G(s) = \left[\begin{array}{c|c} A_p & B_p \\ \hline C_p & D_p \end{array}\right] \tag{2.4.4}$$

$$W_i(s) = \left[\begin{array}{c|c} A_{wi} & B_{wi} \\ \hline C_{wi} & D_{wi} \end{array}\right]$$

with i = 1, 2, 3.

Let the augmented plant P(s) have a state vector x_{ap} given by

$$x_{ap} = [x_p \;\; x_{w1} \;\; x_{w2} \;\; x_{w3}]^T$$

where x_p and x_{wi} are the state vectors for the plant G(s) and the weights $W_i(s)$, respectively. The augmented plant matrices can now be expressed in terms of block matrices of the plant and the weights, as shown below:

$$A = \begin{bmatrix} A_p & 0 & 0 & 0 \\ -B_{w1}C_p & A_{w1} & 0 & 0 \\ 0 & 0 & A_{w2} & 0 \\ B_{w3}C_p & 0 & 0 & A_{w3} \end{bmatrix}$$

$$[B_1 \mid B_2] = \left[\begin{array}{c|c} 0 & B_p \\ B_{w1} & -B_{w1}D_p \\ 0 & B_{w2} \\ 0 & B_{w3}D_p \end{array}\right]$$

$$\left[\begin{array}{c} C_1 \\ \hline C_2 \end{array}\right] = \left[\begin{array}{cccc} -D_{w1}C_p & C_{w1} & 0 & 0 \\ 0 & 0 & C_{w2} & 0 \\ D_{w3}C_p & 0 & 0 & C_{w3} \\ \hline -C_p & 0 & 0 & 0 \end{array}\right]$$

$$\left[\begin{array}{c|c} D_{11} & D_{12} \\ \hline D_{21} & D_{22} \end{array}\right] = \left[\begin{array}{c|c} D_{w1} & -D_{w1}D_p \\ 0 & D_{w2} \\ 0 & D_{w3}D_p \\ \hline I & -D_p \end{array}\right] \qquad (2.4.5)$$

In this section the standard control problem (Figure 2.3.1) was used to illustrate plant augmentation. Other configurations of plants and weights can be treated in a similar fashion, as equations 2.4.1 and 2.4.3 are generic to all problems that can be accommodated by the H_∞ design methodology.

2.5 H_∞ Synthesis

The H_∞ feedback problem is posed with reference to Figure 2.5.1.

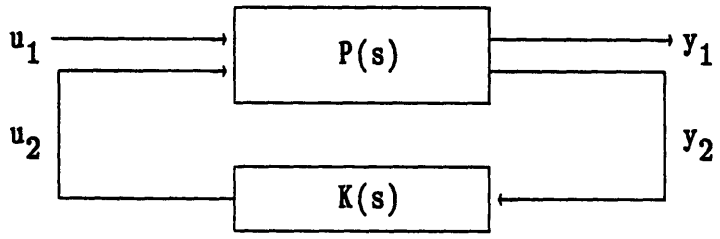

Figure 2.5.1: Synthesis block diagram

Given:	P(s)	FDLTI augmented plant
	$u_1(t)$	exogenous input vector (commands, disturbances etc.)
	$y_1(t)$	output vector (weighted errors, controls etc.)
	$y_2(t)$	measurement vector
	$u_2(t)$	control input vector

Find: K(s) A nonunique FDLTI dynamic compensator such that:

- the closed loop system is nominally stable
- the H_∞–norm of the closed loop transfer function from $u_1(t)$ to $y_1(t)$, $H_{y_1u_1}(s)$, is minimized.

When using weights $W_1(s)$ and $W_3(s)$, the following equation can be given to illustrate the relationship between $H_{y_1u_1}(s)$ and the weights,

$$\| H_{y_1u_1}(j\omega) \|_\infty = \max_\omega \bar{\sigma} \begin{bmatrix} W_1(j\omega)S(j\omega) \\ W_3(j\omega)C(j\omega) \end{bmatrix}$$

The optimal solution to the problem posed above cannot be computed directly. An iterative scheme called γ–iteration, has been formulated to find solutions arbitrary close to the optimal. The γ–iteration procedure is described in the next section.

2.5.1 γ–Iteration

Doyle et al [10,11] devised a procedure to solve the H_∞ output feedback

problem, called γ–iteration. This procedure involves solving two modified Riccati equations, and consists of finding stabilizing compensators K(s), that guarantee

$$\|H_{y_1 u_1}\|_\infty \leq \gamma \qquad (2.5.1.1)$$

with

$$\min_{K(s)} \|H_{y_1 u_1}\|_\infty = \gamma_{optimal}$$

$$\gamma_{optimal} < \gamma$$

The relationship between the signals in Figure 2.5.1 is the same as indicated in equation 2.4.2., with the state space description of P(s) given by equation 2.4.3.

The γ–iteration procedure requires that the augmented plant P(s) have the following properties:

- The state space description of P(s) (equation 2.4.3) must be detectable and stabilizable
- The transfer functions $P_{11}(s)$ and $P_{22}(s)$ must be strictly proper
- The transfer functions $P_{12}(s)$ and $P_{21}(s)$ should be proper but not strictly proper

For $P_{11}(s)$ and $P_{22}(s)$ to be strictly proper, D_{11} and D_{22} must be zero. This can always be achieved by adding high frequency poles to the appropriate weighting functions. From equation 2.4.5 it is evident that the weight $W_1(s)$ needs to be strictly proper in order for D_{11} to be zero. Also, D_{22} will be zero if the plant G(s)

is strictly proper. If this is not the case, u_2 can be weighted to make D_{22} zero.

$P_{21}(s)$ will always be proper in the standard feedback configuration (Figure 2.3.1) where u_1 is fed through to y_2. For $P_{12}(s)$ to be proper, $W_2(s)$ and/or $W_3(s)$ and G(s) has to be proper, as can be seen from equation 2.4.5. $W_2(s)$ and $W_3(s)$ will generally not be used at the same time, which implies that, if the plant is strictly proper ($D_p = 0$), $W_2(s)$ will have to be present. Another alternative is to use the method described in Appendix A, where an improper weight $W_3(s)$ is absorbed into a strictly proper plant. Further requirements on D_{12} and D_{21} in step 3 of the γ–iteration procedure are for D_{12} to have full column rank and D_{21} to have full row rank.

The following steps describe the γ–iteration procedure [12]:

Step 1: Guess the level of achievable performance γ

Step 2: Scale u_1 and/or y_1 so that the upper bound in 2.5.1.1 is unity, i.e. $\|\tilde{H}_{y_1u_1}\|_\infty \leq 1$ where $\tilde{H}_{y_1u_1}$ is appropriately scaled. The scaling in step 2, can be done as shown in Figure 2.5.1.1.

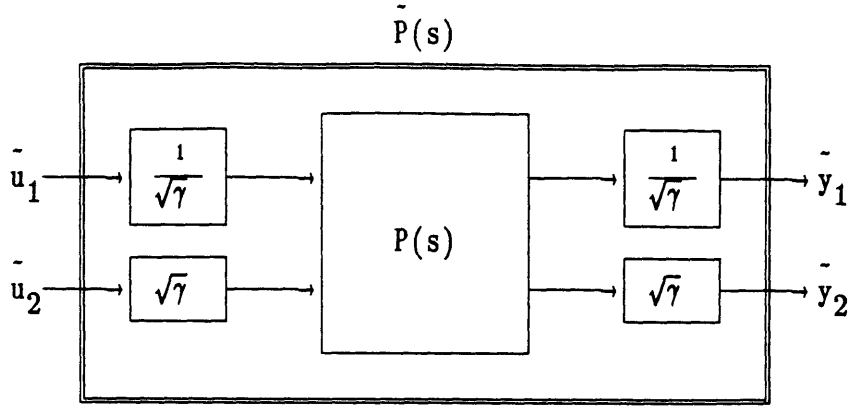

Figure 2.5.1.1: Scaling the augmented plant

The scaled augmented plant $\tilde{P}(s)$, can now be represented as follows:

$$\begin{bmatrix} \tilde{y}_1 \\ \tilde{y}_2 \end{bmatrix} = \begin{bmatrix} \frac{1}{\sqrt{\gamma}} P_{11}(s) & P_{12}(s) \\ P_{21(s)} & \gamma P_{22}(s) \end{bmatrix} \begin{bmatrix} \tilde{u}_1 \\ \tilde{u}_2 \end{bmatrix}$$

$$= \tilde{P}(s) \begin{bmatrix} \tilde{u}_1 \\ \tilde{u}_2 \end{bmatrix}$$

The state space description of $\tilde{P}(s)$ now becomes

$$\tilde{P}(s) = \left[\begin{array}{c|cc} A & \frac{1}{\sqrt{\gamma}} B_1 & \sqrt{\gamma}\, B_2 \\ \hline \frac{1}{\sqrt{\gamma}} C_1 & \frac{1}{\gamma} D_{11} & D_{12} \\ \sqrt{\gamma}\, C_2 & D_{21} & \gamma\, D_{22} \end{array}\right]$$

Step 3: Scale u_2 and y_2 such that

$$D_{12}^T D_{12} = I$$

$$D_{21} D_{21}^T = I$$

Two square, nonsingular matrices S_u and S_y are used for scaling the controls u_2 and the measurements y_2, respectively. These scaling matrices can be computed using the Cholesky decomposition [13] to solve the following equations:

$$S_u^T S_u = D_{12}^T D_{12}$$

$$S_y^{-1} (S_y^{-1})^T = D_{21} D_{21}^T$$

The scaling can be done as shown in Figure 2.5.1.2.

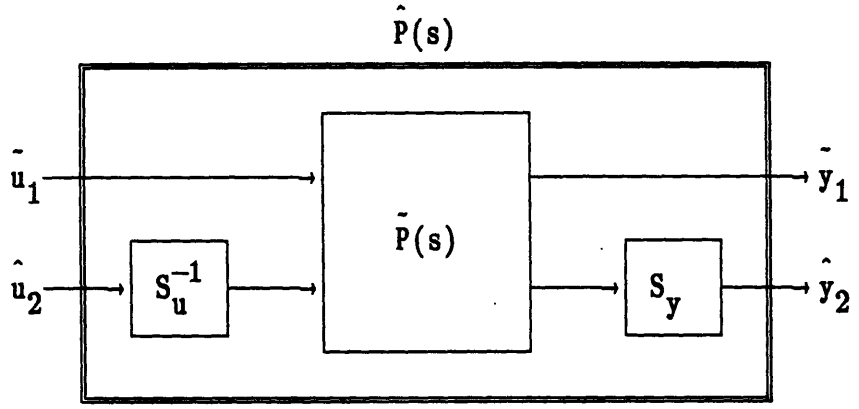

Figure 2.5.1.2: Scaling the controls and measurements

The plant matrices are scaled as follows,

$$\hat{B}_2 = \tilde{B}_2 S_u^{-1}$$
$$\hat{C}_2 = S_y \tilde{C}_2$$
$$\hat{D}_{12} = \tilde{D}_{12} S_u^{-1}$$
$$\hat{D}_{21} = S_y \tilde{D}_{21}$$
$$\hat{D}_{22} = S_y \tilde{D}_{22} S_u^{-1}$$

Step 4: The H_∞ compensator structure is shown in Figure 2.5.1.3

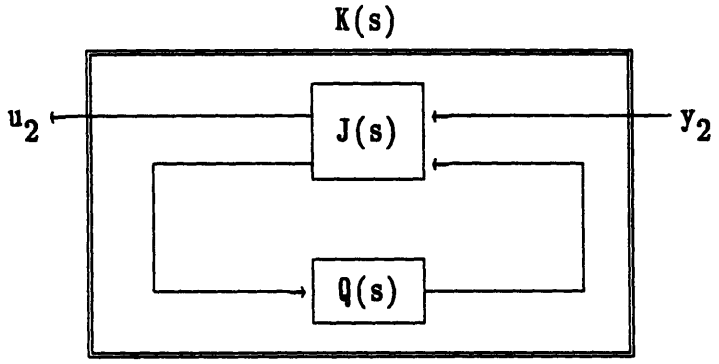

Figure 2.5.1.3: The H_∞ compensator structure

Q(s) is any stable system with $\|Q\|_\infty \leq 1$. Guidelines as to how to choose the free parameter Q are the subject of continuing research [14]. Q(s) = 0 is a legitimate choice for Q, and it will be used throughout this thesis.

The augmented plant matrices (A, B_j, C_i, D_{ij}; i,j = 1,2) used in step 4 are

assumed scaled as indicated in steps 2 and 3. The state space description of J(s) is given by,

$$J(s) := \left[\begin{array}{c|c} A_J & B_J \\ \hline C_J & D_J \end{array}\right]$$

with

$$A_J = A - K_F C_2 - B_2 K_C + Y_\infty C_1^T (C_1 - D_{12} K_C)$$

$$B_J = [K_F \;\; K_{F1}]$$

$$C_J = \begin{bmatrix} -K_C \\ K_{C1} \end{bmatrix}$$

$$D_J = \begin{bmatrix} 0 & -I \\ I & 0 \end{bmatrix}$$

$$K_C = (B_2^T X_\infty + D_{12}^T C_1)(I - Y_\infty X_\infty)^{-1}$$

$$K_{C1} = (D_{12} B_1^T - C_2)(I - Y_\infty X_\infty)^{-1}$$

X_∞ is the unique, real, symmetric solution of the Algebraic Riccati equation

$$(A - B_2 D_{12}^T C_1)^T X_\infty + X_\infty (A - B_2 D_{12}^T C_1) - X_\infty (B_2 B_2^T - B_1 B_1^T) X_\infty + \tilde{C}_1^T \tilde{C}_1 = 0$$

with

$$\tilde{C}_1 = (I - D_{12} D_{12}^T) C_1$$

$$K_F = (Y_\infty C_2^T + B_1 D_{21}^T)$$

$$K_{F1} = (Y_\infty C_1^T D_{12} + B_2)$$

Y_∞ is the unique, real, symmetric solution of the Algebraic Riccati equation

$$(A - B_1 D_{21}^T C_2) Y_\infty + Y_\infty (A - B_1 D_{21}^T C_2)^T - Y_\infty (C_2 C_2^T - C_1 C_1^T) Y_\infty + \tilde{B}_1^T \tilde{B}_1 = 0$$

with

$$\tilde{B}_1 = B_1 (I - D_{21}^T D_{21})$$

The γ chosen in step 1 can be achieved if the following three conditions are met

$$X_\infty \geq 0$$
$$Y_\infty \geq 0$$
$$\overline{\lambda}(Y_\infty X_\infty) \leq 1$$

If these conditions are not satisfied, increase γ and go to step 2. The minimum γ in equation 2.5.1.1 should be found that satisfies these conditions.

Step 5: Incorporate the scaling on u_2 and y_2 into the compensator $\hat{K}(s)$ as shown in Figure 2.5.1.4. The compensator matrices are scaled as follows,

$$B_K = \sqrt{\gamma}\,\hat{B}_K S_y$$
$$C_K = \sqrt{\gamma}\,S_u^{-1}\hat{C}_K$$
$$D_K = \gamma\,S_u^{-1}\hat{D}_K S_y$$

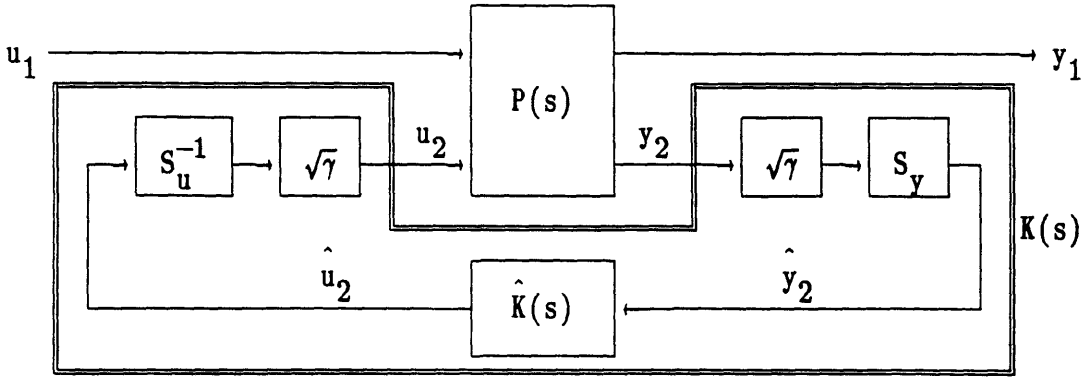

Figure 2.5.1.4: Scaling the designed compensator $\hat{K}(s)$

The state space description of the compensator $\hat{K}(s)$ with $Q(s) = 0$, is given by

$$\hat{K}(s) = \left[\begin{array}{c|c} A - K_F C_2 - B_2 K_C + Y_\infty C_1^T (C_1 - D_{12} K_C) & K_F \\ \hline K_C & 0 \end{array}\right]$$

This concludes the discussion on the γ–iteration procedure.

2.5.2 What does the H_∞ Synthesis Do ?

The basic idea behind the H_∞ compensator is that it "inverts" the stable plant dynamics, and substitutes in its place desirable dynamics prescribed by the weighting functions. In particular, the eigenvalues of the closed loop A matrix include:

- stable plant poles
- poles at the mirror image about the $j\omega-$axis of unstable plant poles
- poles at plant zeros (except nonminimum phase ones)

The zeros of the closed loop system are the zeros of the plant and the compensator.

2.6 Design Verification

This section briefly describes what should be done to check if the controller that was designed meets the required specifications. Two basic analysis tools are used for this purpose, i.e. singular value plots and time simulations.

The first and most obvious specification to check would be that of nominal stability, which is guaranteed by the H_∞ methodology. If this is not achieved, the γ–iteration procedure has been applied incorrectly.

Frequency domain specifications can be verified with singular value plots of the relevant transfer functions, e.g. the sensitivity S(s), and the complementary sensitivity C(s) transfer function matrices.

The H_∞ design methodology does not treat time domain specifications directly. Time simulations of the closed loop controller need to be carried out to check these specifications. This is also the time for the designer to make sure that control rate and magnitude constraints are adhered to. It might be the case that the desired frequency domain specifications cannot be achieved within the constraints on the controls, which would imply that the controller design would have to be repeated with less demanding frequency specifications.

Of course, the ultimate design verification would be to try the controller out on the real plant. This step is usually preceded by extensive time simulations, in which the compensator is "hooked–up" to a realistic model of the plant which includes for example, nonlinearities, unmodeled dynamics, time delays etc.

2.7 Concluding Remarks

A compensator that results from the γ–iteration procedure is computed via the solution of two Riccati equations. Thus, a compensator that meets an H_∞ optimality criterion is no more difficult to obtain than it is to compute an LQG solution [15]. The H_∞ methodology has the advantage that the error is defined directly in terms of frequency domain specifications, and the maximum error is minimized rather than averaged across frequency.

H_∞ solutions can be computed by any software package that can solve an algebraic Riccati equation. There is a commercially available package by Chaing and Safonov [16], for use with PC–MATLAB and PRO–MATLAB, that accommodates plant augmentation, singular value plots, and H_2 and H_∞ synthesis.

CHAPTER 3

H_∞ COMPENSATOR DESIGNS

3.1 Introduction

In this chapter, compensators are designed for two plants, an advanced fighter aircraft, and a milling circuit. These plants were chosen to illustrate the strengths and the weaknesses of the H_∞ design methodology. The nominal designs will be used in Chapter 4 for sensitivity studies.

3.2 Advanced Fighter Aircraft

In this section a lateral–directional flight control system (FCS) for an advanced fighter aircraft is used as an example. The main purpose of the FCS will be to provide bank angle control as an automatic pilot control mode. The model used in this section exhibits special characteristics, some of which were studied in [17].

3.2.1 The Plant

The flight condition and the state space description of the aircraft are given in Appendix B. The plant is controllable and observable, minimum phase and unstable, with poles and transmission zeros as shown below:

$\lambda_i (A_p) =$	$-5.9686e{-}02 \pm 2.8437e{+}00i$	(dutch roll mode)
	$-4.2730e{-}01$	(roll subsidence mode)
	$+4.8718e{-}03$	(unstable spiral mode)
zero =	$-1.6129e{+}02$	

From the poles of the plant the dutch roll mode damping ratio ζ_d can be calculated to be,

$$\zeta_d = 0.021$$

Figure 3.2.1.1 shows a plot of the minimum and maximum singular values of the open loop plant and its condition number versus frequency. The condition number of the aircraft is very high at low frequencies, which implies that different input directions can cause a wide range of plant amplification, at the same frequency.

3.2.2 Design Specifications and the Selection of Weights

The requirements for the control system design include:

(a) bank angle control with crossover at 2 rad/sec

(b) increased dutch roll damping

(c) zero steady state errors to constant commands or disturbances.

(d) unmodeled dynamics and high frequency sensor noise requires the $\bar{\sigma}[C(j\omega)] < -40$ db at $\omega = 100$ rad/sec

(e) and, of course, nominal stability

Requirements (a), (c) and (d) give an indication as to which weighting functions should be used. The H_∞ design methodology automatically takes care of requirement (e), but "circumvents" requirement (b) by canceling the stable portion of the plant (see section 2.5.2), such that the dutch roll mode will not be visible in the plant output. This can cause performance degradation or even instability in the face of structured uncertainty as will be seen in Chapter 4.

Weighting functions which will enable the closed loop control system to meet requirements (a), (c) and (d), are (see Figure 2.3.1)

$$W_1(s) = \frac{2}{s + .0001} I_{2x2}$$

$$W_2(s) = \epsilon I_{2x2}, \quad \epsilon = 0.1$$

$$W_3(s) = \frac{s}{2} I_{2x2}$$

The weights $W_1(s)$ and $W_3(s)$ have crossover frequencies at 2 rad/sec, which will insure that the loop transfer function –plant and compensator– crossover at 2 rad/sec. Singular value plots for the weights $W_1(s)$ and $W_3(s)$ are shown in Figures

3.2.4.3 and 3.2.4.2 respectively. The low frequency poles in $W_1(s)$ takes care of requirement (c). $W_2(s)$ is included to give D_{12} (see section 2.5.1) full column rank without increasing the order of the compensator. ϵ was chosen such that the controller does not command excessive control action. A state space description for $W_3(s)$ cannot be written, as it is improper and, thus, the technique described in Appendix A must be used to calculate the augmented plant.

3.2.3 H_∞ Compensator Design

The γ – iteration procedure described in section 2.5.1, was used to design a compensator for the aircraft augmented with the weights given in section 3.2.2. The minimum γ found via the iteration procedure was $\gamma_{min} = 1.30$. The state space descriptions for the augmented plant and compensator are given in Appendix B.

The poles and transmission zeros for the 6^{th} order compensator are,

$\lambda_i(A_k) =$ – 3.5623e+01
– 9.0694e+00 ± 4.2700e+00i
– 6.6815e+00
2 @ – 1.000e–04

zeros =	– 5.9686e–02 ± 2.8437i	(dutch roll mode)
	– 4.2730e–01	(roll mode)
	– 4.8436e–03	(mirror image of spiral mode)

By looking at the location of the compensator zeros, it would seem that the compensator "inverts" the stable part of the plant. To prove this, a controllability/observability study was performed (Appendix B section B.5) on the closed loop system, and it was found that the stable plant modes are indeed uncontrollable, which implies pole zero cancellations.

The 10^{th} order closed loop system poles and transmission zeros are,

$\lambda_i(A_{cl}) =$	the 3 stable plant poles (see section 3.2.1)
	mirror image of unstable plant pole
	$-3.5995e+01$
	$-8.7283e+00$
	$-6.3733e+00$
	$-3.1521e+00 \pm 1.0167e+00i$
	$-3.0328e+00$
zeros =	1 plant zero
	4 compensator zeros

3.2.4 Design Evaluation

In this section, singular value plots and time simulation will be used to determine if the design in section 3.2.3 meets the specifications that were set in section 3.2.2.

The bandwidth requirement in (a) is met, as can be verified by looking at the minimum and maximum singular value plots of the loop transfer function (T(s) = G(s)K(s)) in Figure 3.2.4.1. The minimum and maximum singular value plots of the closed loop transfer function C(s) in Figure 3.2.4.2 and the bank angle step response in Figure 3.2.4.4 illustrate that bank angle command following is achieved without excessive control action. Requirements (c) and (d) are met, as can be verified from Figure 3.2.4.2.

Figure 3.2.4.3 shows the minimum and maximum singular value plot of the sensitivity function S(s), and from it k as defined in equation 2.2.2.1 can be found to be 1.239. This gives the controller the following gain and phase margins in each loop independently and simultaneously,

$$GM\uparrow \geq 5.2$$

$$GM\downarrow \leq .55$$

$$PM \geq 47.59 \text{ deg}$$

It is evident from Figures 3.2.4.1 to 3.2.4.4 that the dutch roll mode has been canceled, because it does not show up in any of the figures. It is not clear if requirement (b) has been addressed adequately and thus this issue will be explored further in Chapter 4.

The weights $W_1(s)$ and $W_3(s)$ have been included in Figures 3.2.4.3 and 3.2.4.2 respectively, to show how the maximum singular values of S(s) and C(s) approach the inverse Bode plots of these weights as γ goes to its optimal value.

Figure 3.2.4.5 shows the minimum and maximum singular values of $H_{y_1u_1}(s)$ (the transfer function of which the H_∞–norm needs to be minimized) for $\gamma = 2$ and $\gamma = 1.3$.

In conclusion, it can be stated that an H_∞ controller has been designed that meets the posed specifications –except maybe (b)–. Good command following, disturbance rejection, and insensitivity to high frequency sensor noise are evident from the figures presented in this section.

3.3 The Milling Circuit

In this section an H_∞ compensator is designed for a milling circuit that processes gold bearing ore. The main purpose of the controller is to provide particle size control while regulating the mill load and the sump level. An INA (inverse Nyquist array) compensator has previously been designed for this plant, and the successful controller implementation is described in [18].

3.3.1 The Plant

A transfer function model (G(s)) for the plant was derived from "step–tests" done on the actual milling circuit. The G(s), state space description, nomenclature used, and a figure and description of the plant are given in Appendix C. Scaling and model reduction were performed on the plant as described in Appendix C, and this scaled and reduced order version of the plant –referred to as the design plant model–, will be used for the design of the compensator.

The designed plant model is 6^{th} order, controllable and observable, nonminimum phase and stable, with poles and transmission zeros,

$$\lambda_i(A_p) = \begin{matrix} -1.7481e{-}02 \pm 3.7481e{-}03i \\ -1.3158e{-}03 \\ -6.0912e{-}04 \\ -5.0000e{-}06 \\ -5.0006e{-}06 \end{matrix}$$

$$\text{zeros} = \begin{matrix} 5.5624e{-}02 \\ -5.7499e{-}04 \pm 2.8092e{-}04i \end{matrix}$$

← nonminimum phase zero

Figure 3.3.1.1 shows a plot of the minimum and maximum singular values of the design plant model and its condition number versus frequency.

3.3.2 Design Specifications and the Selection of Weights

The specifications for the control system include:

(a) independent PSM, LOAD, and LEVEL control

(b) settling time of 600 sec for the PSM and LOAD

(c) settling time of 1800 sec for the sump level

(d) zero steady state errors to constant commands and disturbances

(e) unmodeled dynamics and "high" frequency sensor noise requires that the $\bar{\sigma}\,[C(j\omega)] < -60$ db at $\omega = 1.0$ rad/sec

(f) and, of course, nominal stability

Requirements (b) through (e) determine which weighting functions should be used. Independent control of the three outputs –requirement (a)– is possible, as there are three independent controls. The H_∞ compensator naturally takes care of requirement (f).

Weighting functions as depicted in Figure 2.3.1, which will enable the closed loop control system to meet the posed specifications, are listed below:

$$W_1(s) = \frac{1}{s + 1.0e{-}06} \begin{bmatrix} 6.00e{-}03 & 0 & 0 \\ 0 & 6.00e{-}03 & 0 \\ 0 & 0 & 1.50e{-}03 \end{bmatrix}$$

$$W_2(s) = \epsilon\, I_{3x3} \quad ; \epsilon = 0$$

$$W_3(s) = s \begin{bmatrix} 8.00e{-}03 & 0 & 0 \\ 0 & 8.00e{-}03 & 0 \\ 0 & 0 & 2.00e{-}03 \end{bmatrix}^{-1}$$

The weighting functions given above are the result of a number of intelligent trial and error iterations. It was found that changes in the parameters in the numerators of $W_1(s)$ had the biggest impact on the speed of the output response. These parameters were chosen such that requirements (b) and (c) were met. The

parameters in the denominators of $W_3(s)$ were then "tuned" to give acceptable multivariable gain and phase margins and meet requirement (e), without the controller demanding excessive control action. Requirement (d) is taken care of by the parameters in the denominator of $W_1(s)$.

A state space description for $W_3(s)$ cannot be written since it is improper, and thus $W_3(s)$ is absorbed into the strictly proper plant, as shown in Appendix A.

3.3.3 H_∞ Compensator Design

The γ – iteration procedure described in section 2.5.1, was used to design a compensator for the scaled milling circuit augmented with the weights given in section 3.3.2. The minimum γ found via the iteration procedure that met the specifications, was $\gamma_{min} = 1.05$. The state space descriptions for the augmented plant is given in Appendix C.

The poles and transmission zeros of the 9^{th} order compensator –same order as the augmented design plant–, are,

$\lambda_i(A_k) =$ $-4.8949e{-}02 \pm 2.4744e{-}02i$

$-5.7528e{-}04 \pm 2.8146e{-}04i$ ← approximate reduced order plant zeros

$-2.6844e{-}02$

$-6.7628e{-}03$

3 @ – 1.0000e–06

zeros = 6 design plant poles (see section 3.3.1)

The location of the compensator zeros are the same as that of the design plant poles (section 3.3.1). The compensator has poles at the same location as the design plant zeros, except for the one nonminimum phase zero.

The closed loop system is 21^{th} order made up of the 9^{th} order compensator and the 12^{th} order full order plant model. The closed loop poles and transmission zeros are as follows,

$\lambda_i(A_{cl}) =$

– 6.8919e–02
– 2.7549e–02 ± 2.0416e–02i
– 2.4912e–02
– 2.0959e–02
– 1.5277e–02
– 7.4999e–03 ± 5.9805e–03i
– 1.1002e–02 ± 3.2040e–04i
– 1.0231e–02
– 4.1474e–03
– 2.3795e–03
– 1.0849e–03 ± 7.4794e–04i
– 2.8364e–04
– 7.1382e–04 ± 2.0308e–05i

$-5.6385e{-}04$

$-5.0006e{-}06$

$-5.0000e{-}06$

zeros = 9 full order plant zeros (given in Appendix C)

6 compensator zeros

3.3.4 Design Evaluation

In this section, singular value plots and time simulation will be used to determine if the design in section 3.3.3 meets the specifications that were set in section 3.3.2. The full 12^{th} order plant model and the compensator based on the reduced order model are used to evaluate the design.

Figure 3.3.4.1 shows the reaction of the outputs and controls to steps in the command inputs. The PSM command step is 2%, the LOAD command step 1%, and that of the LEVEL 3%. From this Figure it can be seen that specifications (a), (b), and (c) are met.

Specifications (d) and (e) can be verified from Figure 3.3.3.2 which shows the maximum and minimum singular values of C(s) versus frequency. The singular values of the weight $1/W_3(s)$ are included in this Figure to illustrate the role of weighting functions in shaping singular value loop shapes.

Figure 3.3.4.3 shows the minimum and maximum singular values of S(s) and

$1/W_1(s)$ versus frequency, and from it the multivariable gain and phase margins discussed in section 2.2.2, can be calculated with k = 1.228 to be,

$$GM\uparrow \geq 5.39$$

$$GM\downarrow \leq 0.55$$

$$|PM| \geq 48.05 \text{ deg}$$

Figure 3.3.4.4 shows the minimum and maximum singular values of the loop transfer function T(s) = G(s)K(s). The crossover frequency range is from 1.5e–3 to 6.0e–3 as dictated by the weighting function $W_1(s)$, which is about a decade below the nonminimum phase zero. This zero does not seem to have a significant influence on the performance of the control system, as would be expected.

The H_∞ controller meets the posed specifications with an 9^{th} order compensator, which is six states less than a 15^{th} order compensator that would have resulted from an H_∞ design if the full order plant was used.

Figure 3.2.1.1 :Singular values and condition no. of the plant

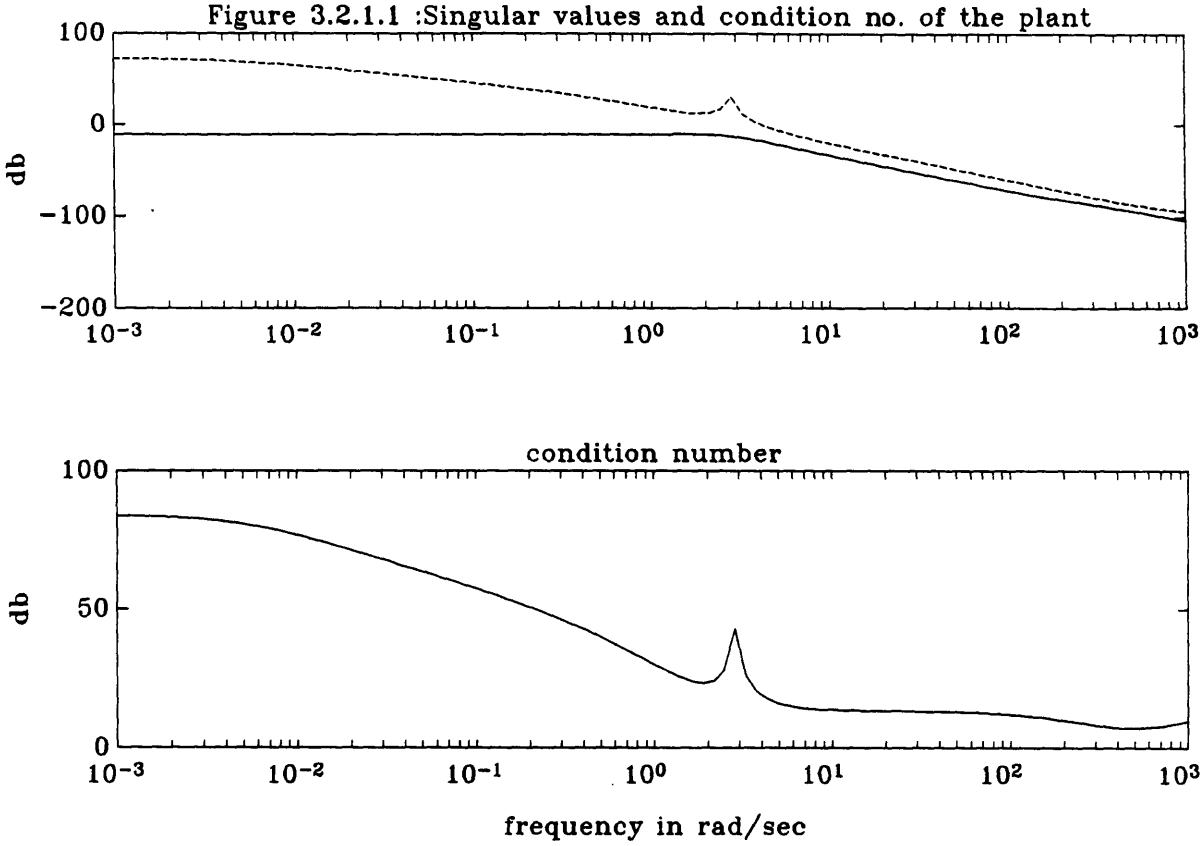

Figure 3.2.4.1 :Singular values of T(s) = G(s)K(s)

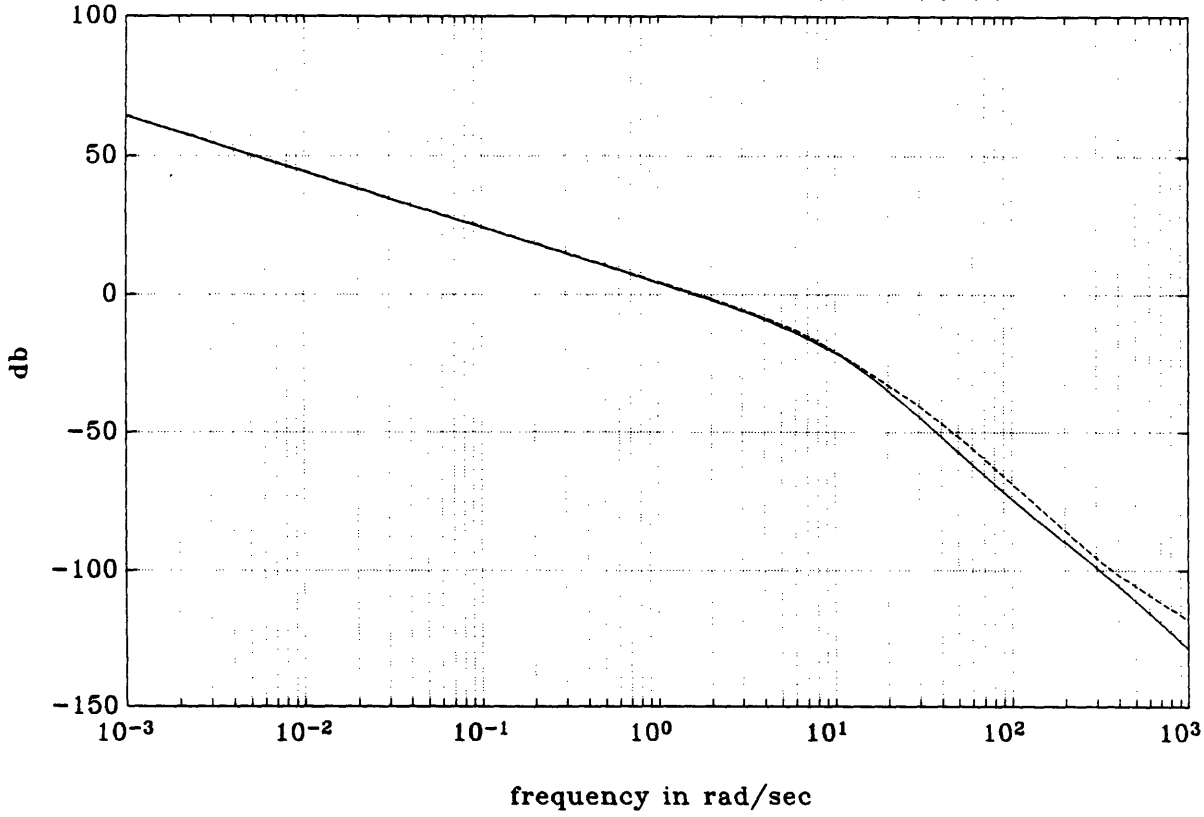

Figure 3.2.4.2 :Singular values of C(s) and 1/W3

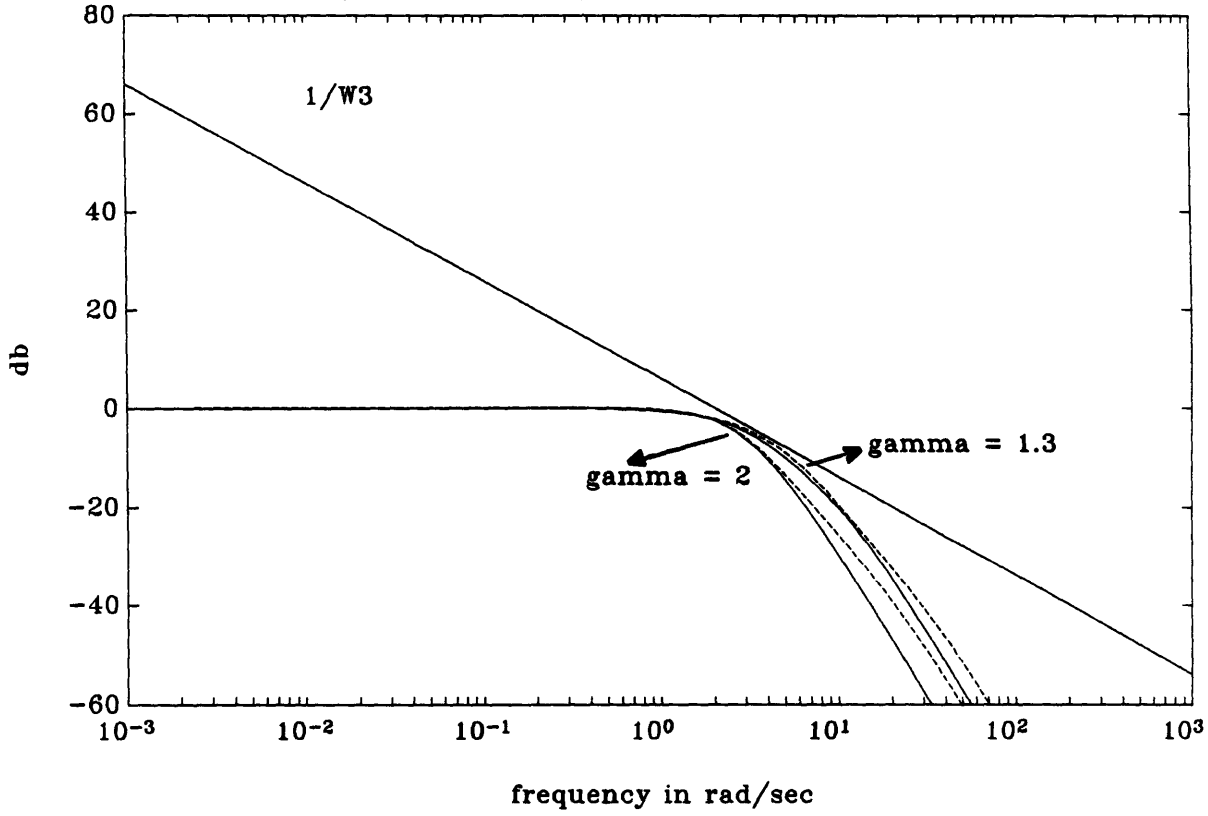

Figure 3.2.4.3 :Singular values of S(s) and 1/W1

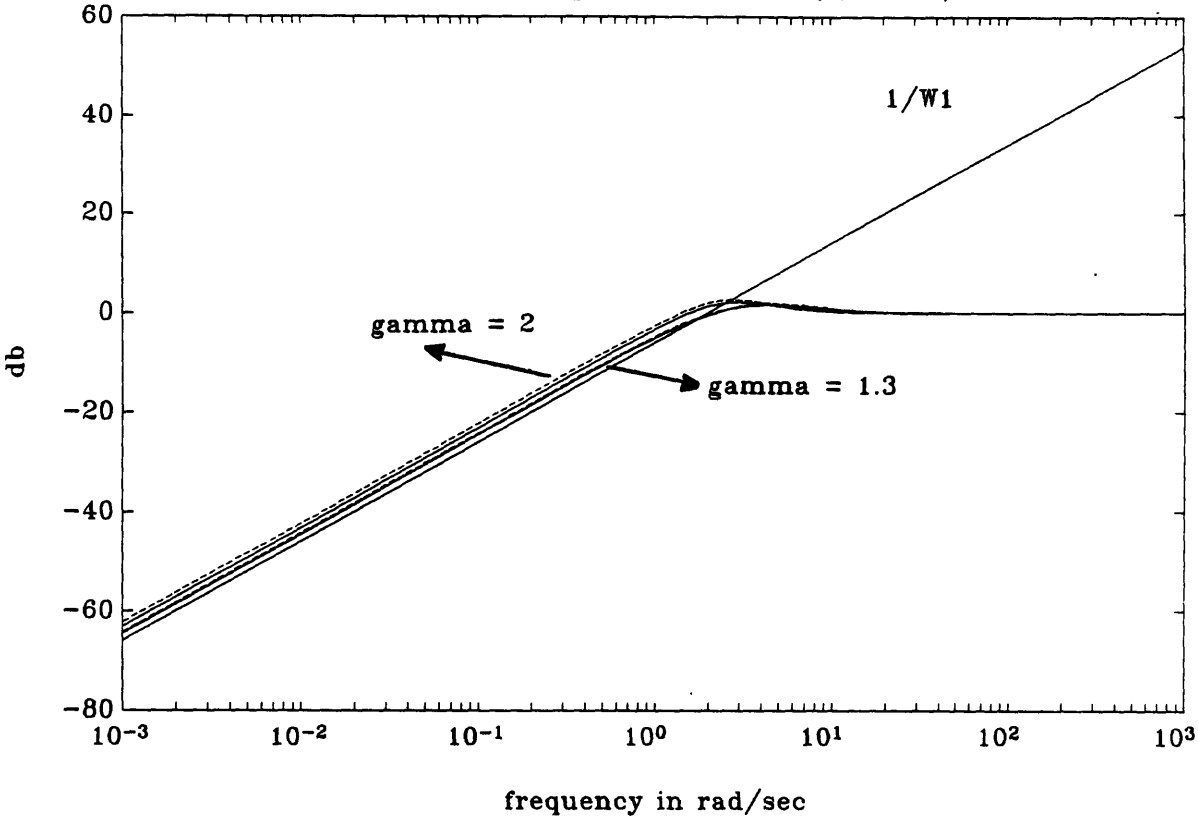

Figure 3.2.4.4 :Response to unit step in bank angle command

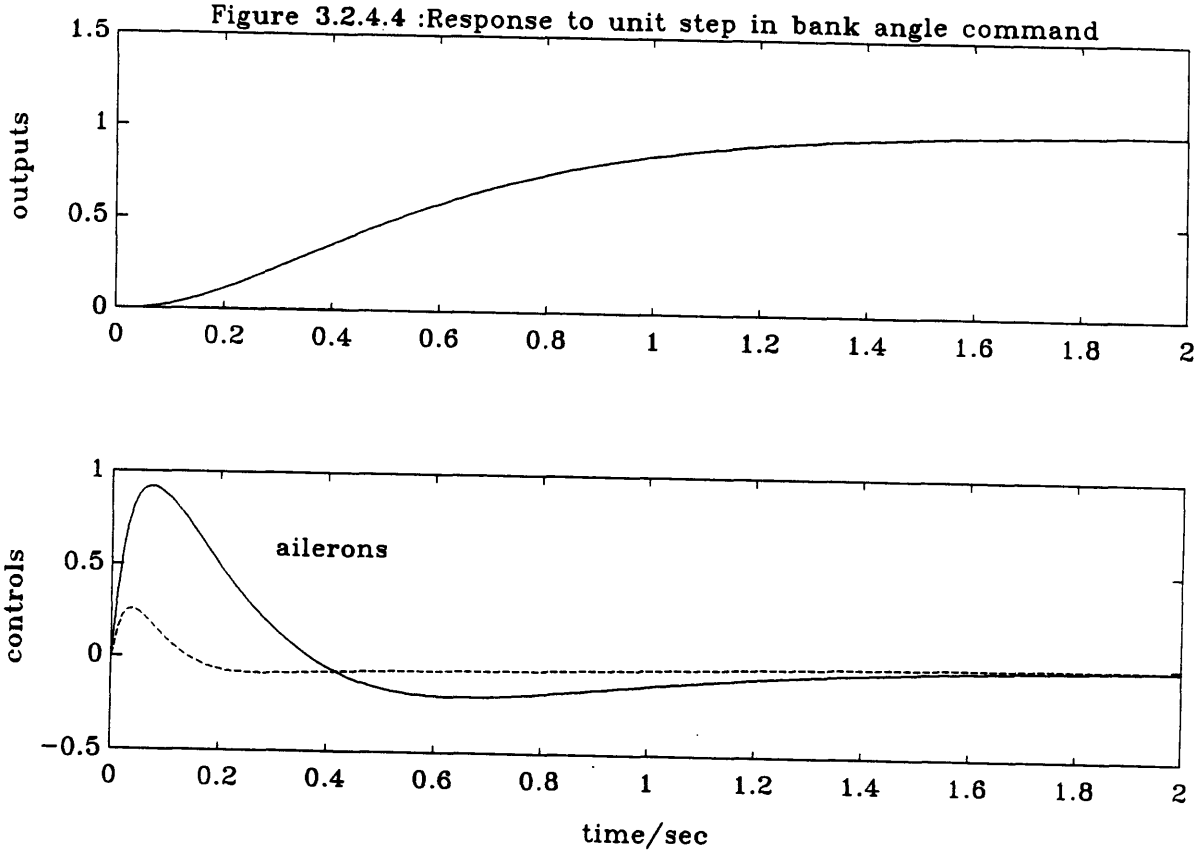

Figure 3.2.4.5 :Singular values of Hy1u1(s)

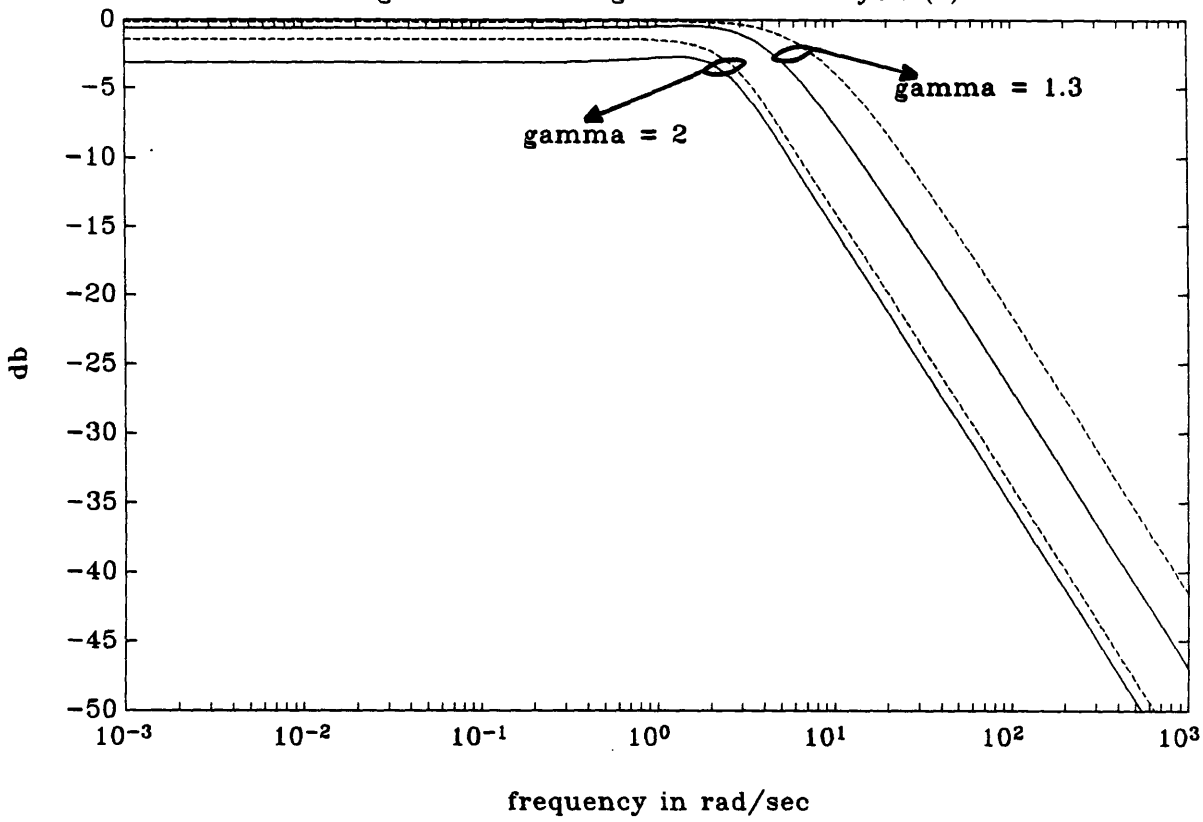

Figure 3.3.1.1 :Singular values and condition no. of the design plant

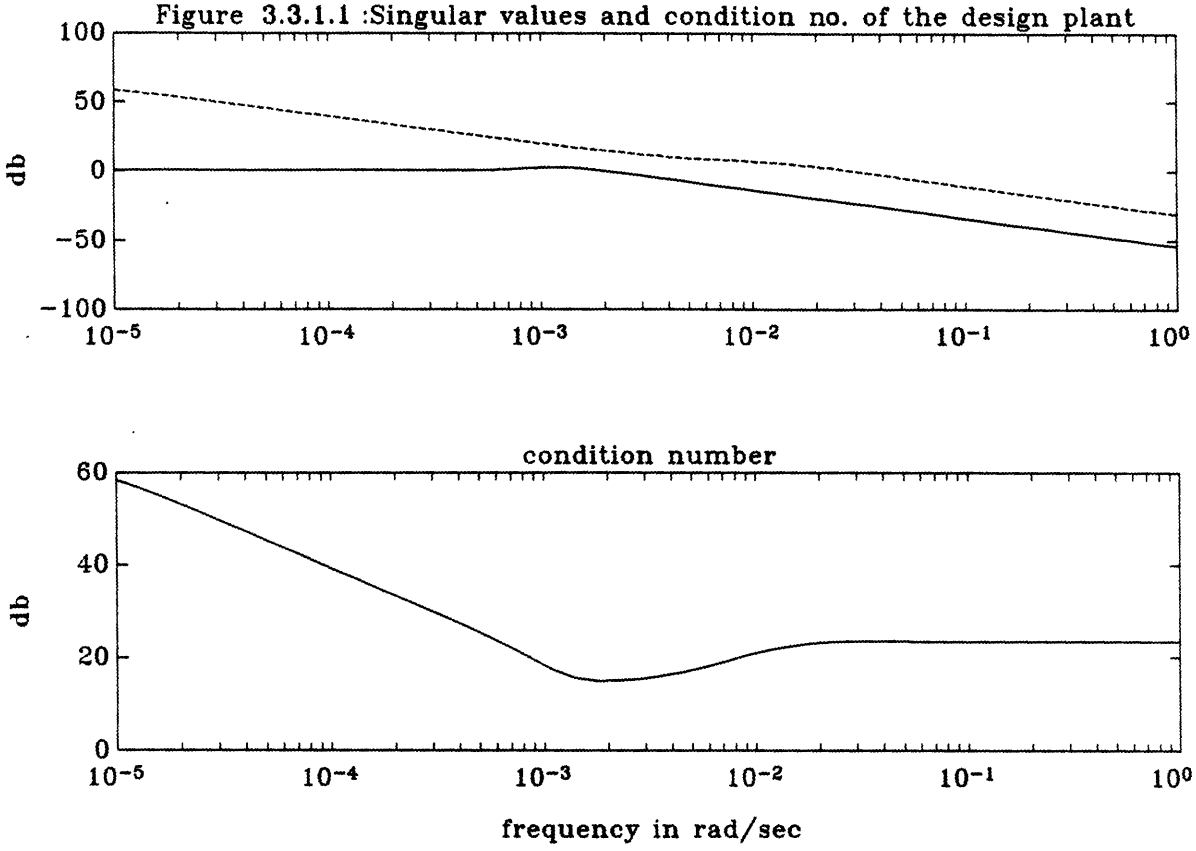

Figure 3.3.4.1 :Response to steps in command inputs

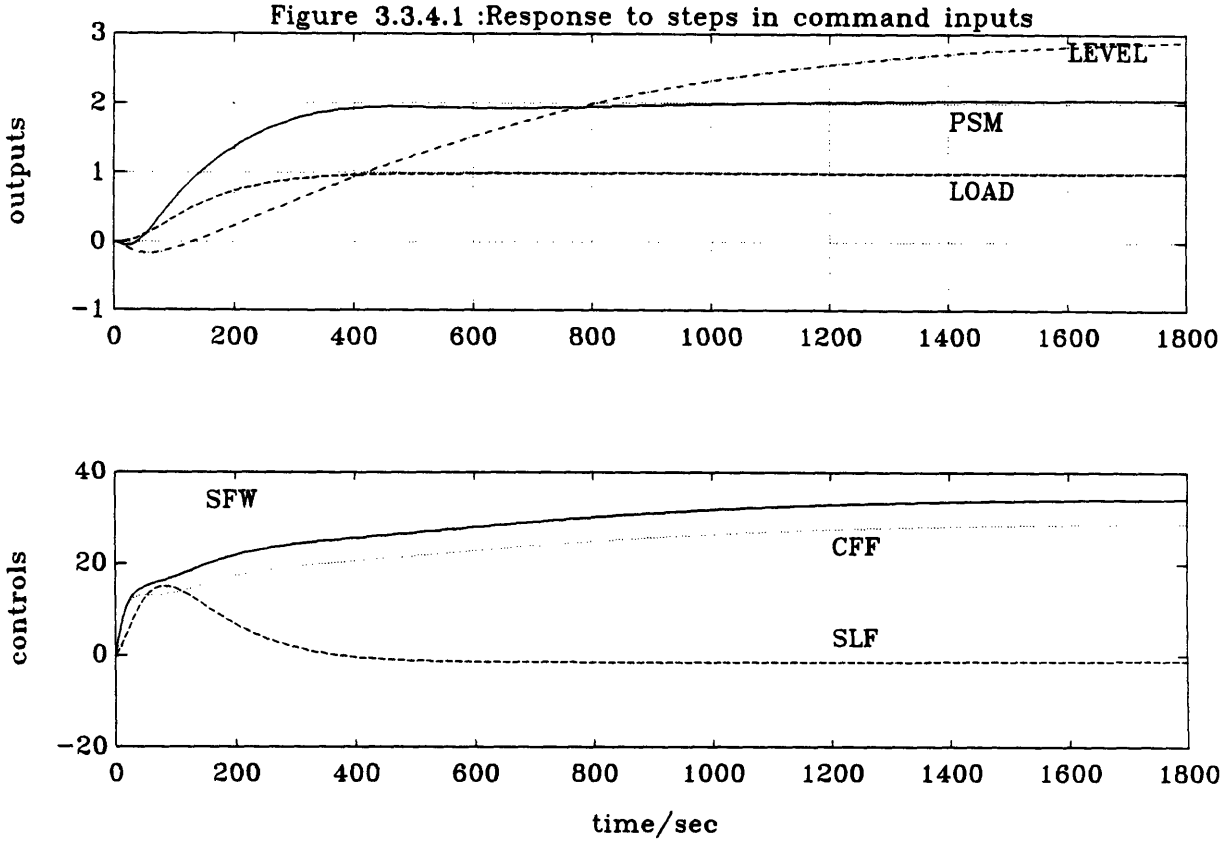

Figure 3.3.4.2 :Singular values of C(s) and 1/W3

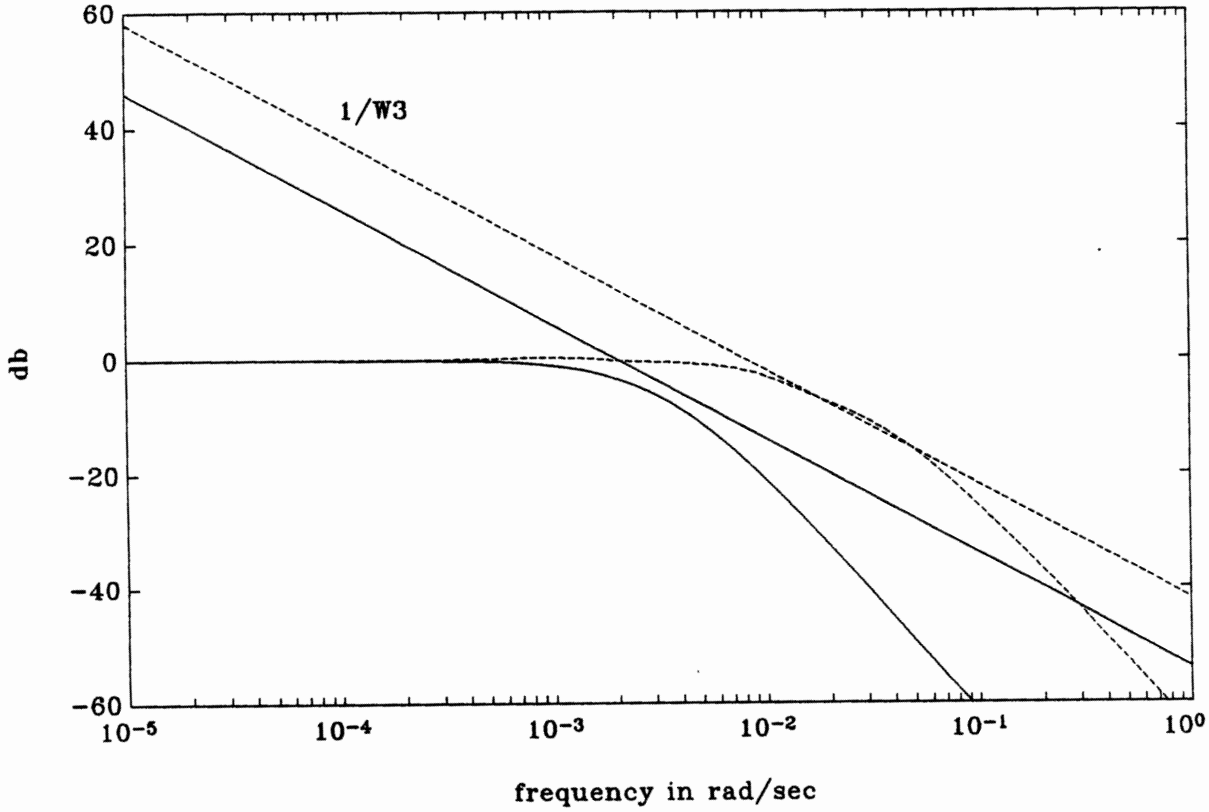

Figure 3.3.4.3 :Singular values of S(s) and 1/W1

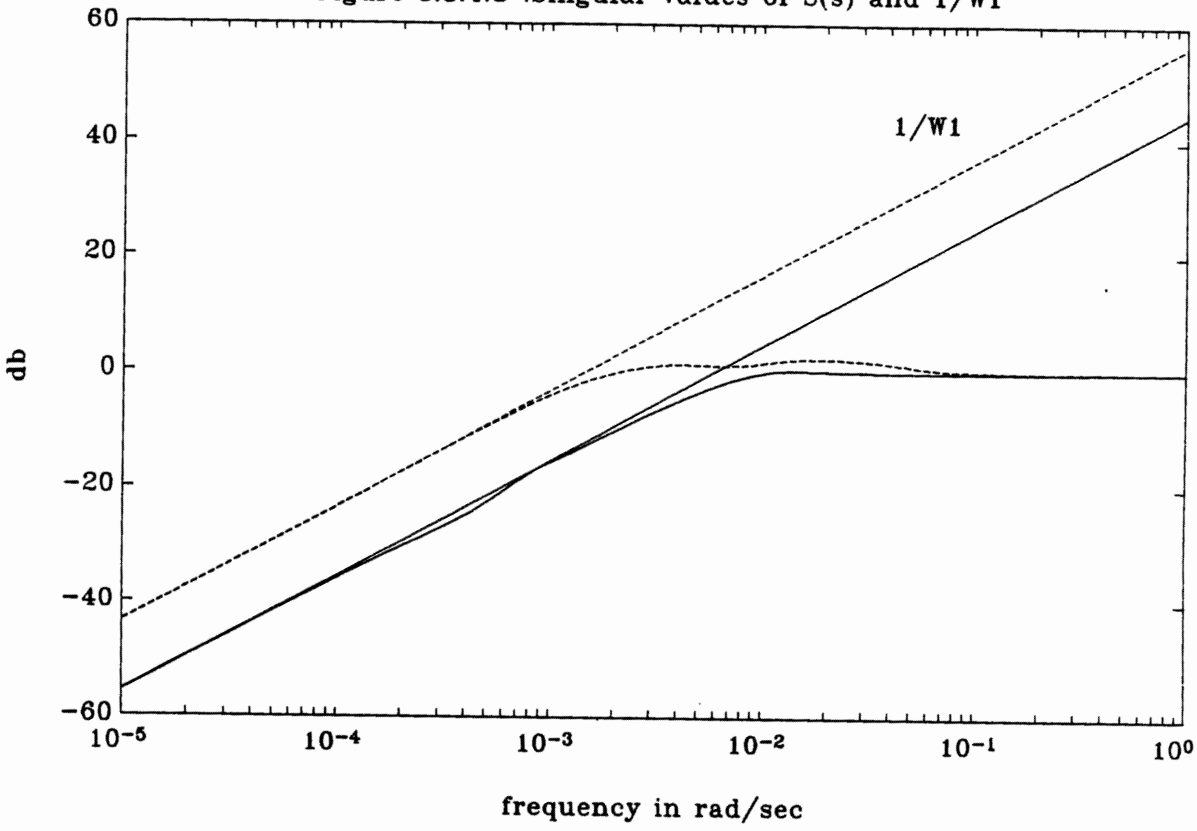

Figure 3.3.4.4 :Singular values of T(s)

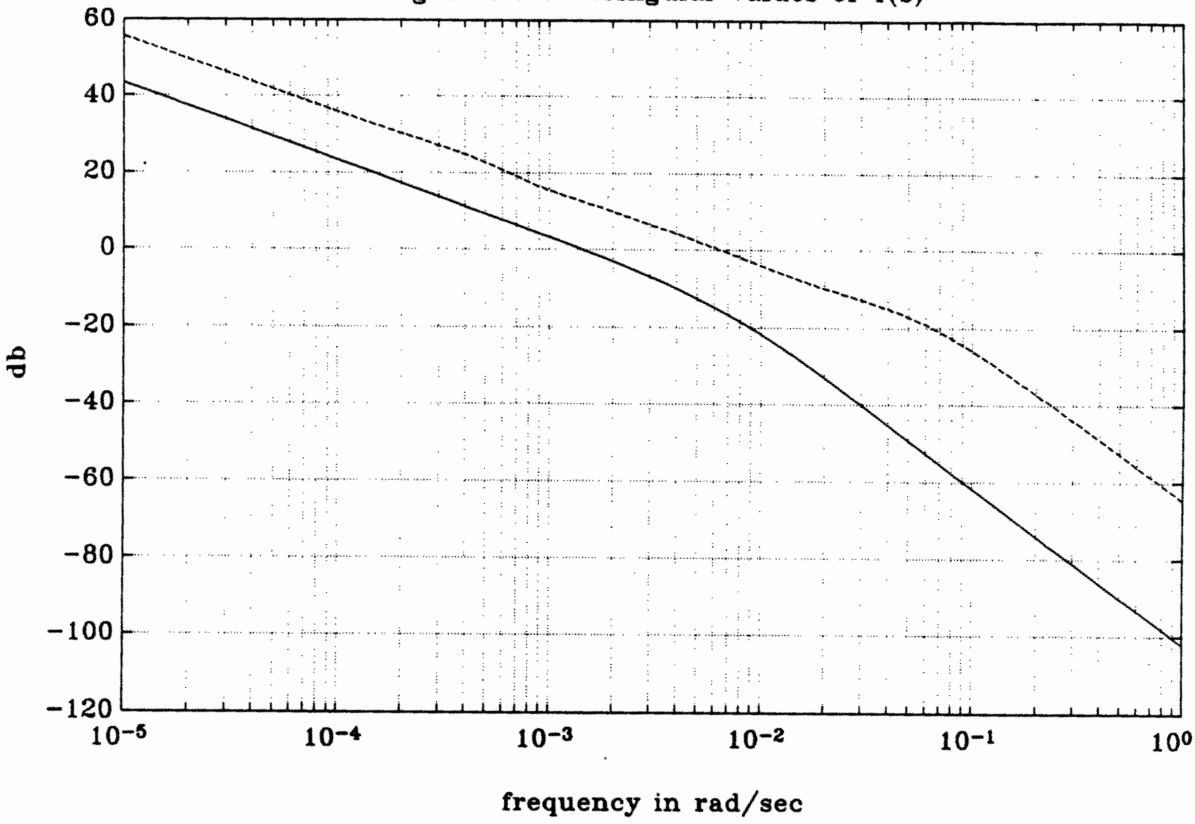

CHAPTER 4

SENSITIVITY STUDIES

4.1 Introduction

In practical situations it is often not possible to determine plant parameters very accurately when constructing a nominal plant model. If parametric (structured) uncertainty is present, a compensator, which was designed based on a nominal model, could behave in an undesirable fashion when implemented on the real plant. In section 2.5.2 it was mentioned that the H_∞ compensator basically "inverts" the plant and substitutes some desirable dynamics in its place. As this inversion process can be impeded by structured uncertainty, it is important to know for which "size" of such uncertainty the controller will still perform adequately.

In this chapter a study is made of the sensitivity of eigenvalues and singular values of a closed loop system to perturbations in the plant matrices, using tools developed in Appendix D. These perturbations are intended to simulate structured uncertainty in the plant.

4.2 Choice of Perturbation Matrices

A perturbation scheme described in this section, will be used to simulate structured uncertainty. The choice of perturbation matrices should represent

realistic possible changes in the physical plant, given the constraints of the nominal linear plant model. Although different plants will behave differently to the same perturbation, it is convenient to study the effect of plant perturbations in a common framework. One such framework is described below.

Let G(s) be the nominal plant, with a state space description of,

$$G(s) = \left[\begin{array}{c|c} A_p & B_p \\ \hline C_p & D_p \end{array}\right]$$

A compensator K(s) is designed based on this plant, and it is represented by,

$$K(s) = \left[\begin{array}{c|c} A_k & B_k \\ \hline C_k & 0 \end{array}\right]$$

The resulting closed loop system, with a configuration as shown in Figure 2.2.2.1, has a state space description given by,

$$C(s) = \left[\begin{array}{c|c} A_{cl} & B_{cl} \\ \hline C_{cl} & 0 \end{array}\right]$$

with

$$A_{cl} = \left[\begin{array}{c|c} A_p & B_pC_k \\ \hline -B_kC_p & A_k - B_kD_pC_k \end{array}\right]$$

$$B_{cl} = \left[\begin{array}{c} 0 \\ \hline B_k \end{array}\right]$$

and

$$C_{cl} = [\, C_p \mid D_p C_k \,]$$

Now, suppose that the A matrix of the real plant is given by,

$$A_r = A_p + dA_p$$

The real closed loop system is then given by,

$$C_r(s) = \left[\begin{array}{c|c} A_{cl} + dA_{cl} & B_{cl} \\ \hline C_{cl} & D_{cl} \end{array}\right]$$

with

$$dA_{cl} = \left[\begin{array}{c|c} dA_p & 0 \\ \hline 0 & 0 \end{array}\right]$$

The effect of these changes dA_{cl} on the eigenvalues of A_{cl} and the singular values of C(s), will be computed in the next section, using the designs from Chapter 3.

4.3 Examples

In this section sensitivity studies will be performed on two fictitious plants and the two closed loop systems described in Chapter 3, in order to determine how

these systems will behave with respect to stability and performance, in the face of structured uncertainty.

For each plant a perturbation matrix (as discussed in section 4.2) will be chosen using physical knowledge of the plant and the equations for $d\lambda_i$ and $d\sigma_i$, which were derived in Appendix D. The closed loop systems will then be perturbed, and the effect of these perturbations on the closed loop eigenvalues and singular values will be calculated.

In this section the conjecture will be made that lightly damped stable plant modes give rise to closed loop systems, designed with the H_∞ methodology, which are very sensitive to structured uncertainty. In section 4.3.1.2 the closed loop system for the advanced aircraft is shown to be very sensitive to structured uncertainty. However, when the dutch roll mode damping is increased in section 4.3.1.3, this is no longer the case. Similarly, the closed loop system for the milling circuit is shown to be relatively insensitive to structured uncertainty in section 4.3.2.2. In section 4.3.2.3 a lightly damped pole pair is "introduced" into the reduced order milling circuit of section 3.3.1, and the resulting closed loop system is shown to be sensitive to structured uncertainty.

In section 4.3.3 two fictitious plants with unstable poles and zeros at the same frequency location, are studied. The idea is to determine the effects of near unstable pole zero cancellations on H_∞ designs, and the sensitivity of such designs to structured uncertainty.

4.3.1 Advanced Fighter Aircraft

4.3.1.1 Choice of dA_p

In section 3.2.1 it was mentioned that the dutch roll mode of this aircraft is very lightly damped ($\zeta_d = 0.021$). It is thus conceivable that the controller designed in section 3.2.3 will be sensitive to changes in stability derivatives which determine the dutch roll mode. These derivatives can be found from approximations of the aircraft modes given in [17,19]. They are,

dutch roll mode:

$$\omega_d^2 \approx N'_\beta \tag{4.3.1.1}$$

$$2\zeta_d\omega_d \approx -(Y_v + N'_r) - \frac{L'_\beta}{N'_\beta}(N'_p - \frac{g}{U_0})$$

roll mode:

$$\frac{1}{T_r} \approx -L'_p + \frac{L'_\beta}{N'_\beta}(N'_p - \frac{g}{U_0}) \tag{4.3.1.2}$$

spiral mode:

$$\frac{1}{T_s} \approx T_r \frac{g}{U_0}(\frac{L'_\beta}{N'_\beta} - L'_r) \tag{4.3.1.3}$$

with the characteristic polynomial of the open loop plant,

$$\Delta(s) = (s + \frac{1}{T_s})(s + \frac{1}{T_r})(s^2 + 2\zeta_d\omega_d s + \omega_d)$$

The stability derivatives that have a significant effect on the dutch roll mode for

this plant are L'_β, N'_β, N'_r, and N'_p. As these derivatives depend on the particular flight condition of the aircraft, it is important to know how much of a change in these parameters will result in an unstable closed loop system.

Using the notation established in section 4.2, dA_p can now be chosen to be,

$$dA_p = \epsilon \begin{bmatrix} 0 & 0 & 0 & 0 \\ L'_\beta & 0 & 0 & 0 \\ N'_\beta & N'_p & N'_r & 0 \\ 0 & 0 & 0 & 0 \end{bmatrix} = \epsilon P \qquad ;\epsilon \in \mathbb{R} \qquad (4.3.1.4)$$

with

$$dA_{cl} = \left[\begin{array}{c|c} dA_p & 0 \\ \hline 0 & 0 \end{array}\right] = \epsilon \left[\begin{array}{c|c} P & 0 \\ \hline 0 & 0 \end{array}\right]$$

The range of ϵ, for which the closed loop system is stable, can be determined by using this perturbation matrix dA_{cl} in equation (12) of Appendix D. This equation can be written as follows, for a particular $d\lambda_i$ of the closed loop system:

$$d\lambda_i = \epsilon\gamma_{ii} + \epsilon^2 \sum_{\substack{k=1 \\ k\neq i}}^{n} \frac{\gamma_{ki}\gamma_{ik}}{\lambda_i - \lambda_k} \qquad (4.3.1.5)$$

with $$\gamma_{ij} = w_i^T \left[\begin{array}{c|c} P & 0 \\ \hline 0 & 0 \end{array}\right] v_j$$

Equation 4.3.1.5 shows that the first term will dominate as $\epsilon \to 0$, but that the second term can be large if two or more eigenvalues are close together i.e.

$(\lambda_i - \lambda_k) \rightarrow 0.$

Equation (35) in Appendix D can be used to determine the effect of different values of ϵ on the closed loop frequency response.

4.3.1.2 Plant Perturbations

In this section, the plant will be perturbed using dA_p given in section 4.3.1.1. The idea is to study the effect of this perturbation on the plant model and then on the closed loop system. A question that needs to be answered is: Does a study of the perturbed plant model give an indication as to how sensitive the closed loop system will be to structured uncertainty in the plant model?

Figure 4.3.1.1 shows what happens to the real part of the poles of the plant model for values of ϵ ranging form -0.2 to 0.2 (see equation 4.3.1.4). The plant becomes more unstable as ϵ becomes increasingly negative.

Figure 4.3.1.2 shows the percentage error in the maximum singular value of the plant model G(s) for $\epsilon = -0.05$ and 0.05 . The maximum singular value of the plant seems to be the most sensitive to changes in ϵ near the frequency of the dutch roll mode, which is determined by N'_β according to equation 4.3.1.1. Note that a 5% downward change in the stability derivatives given in equation 4.3.1.4 results in an 78% error in the maximum singular value of the plant at the dutch roll mode frequency!

Figure 4.3.1.3 shows what happens to the real part of four of the ten closed loop poles which are the closest to the $j\omega -$ axis, for values of ϵ ranging form -0.2 to 0.2 (ϵ as defined in equation 4.3.1.4). These four poles correspond to the poles of the plant model and are chosen to study the stability of the closed loop system. The figure shows that the closed loop poles at the mirror image of the spiral mode pole and the roll mode pole do not change much as a function of ϵ. However, the closed loop poles corresponding to the dutch roll mode pole pair change significantly and the closed loop system actually becomes unstable for $\epsilon = -0.059$. Thus a 5.9% downward change in the stability derivatives given in equation 4.3.1.4, results in an unstable closed loop system. *This is of particular concern since the stability derivatives can most likely <u>not</u> be determined to better than within* 5%.

Figure 4.3.1.4 shows the percentage error in the maximum singular value of the closed loop system C(s) for $\epsilon = -0.05$ and 0.05 . The maximum singular value of the closed loop system seems to be the most sensitive to changes in ϵ near the frequency of the dutch roll mode, determined by N'_β according to equation 4.3.1.1. Note that a 5% downward change in the stability derivatives given in equation 4.3.1.4, results in an 400+% error in the maximum singular value of the plant at the dutch roll mode frequency! Figure 4.3.1.5 shows the minimum and maximum singular values of the closed loop system C(s) for $\epsilon = -0.05$ and 0 .

From Figures 4.3.1.4 and 4.3.1.5 it would seem that the closed loop system will be severely affected by disturbances with the same frequency as the dutch roll mode. Figure 4.3.1.6 however shows that a step in the bank angle command results in a closed loop response with $\epsilon = -0.05$, which is almost exactly the same as when

$\epsilon = 0$. This is because the step function does not have significant frequency content at the dutch roll mode frequency. Figure 4.3.1.7 shows that the closed loop system goes unstable for $\epsilon = -0.1$.

4.3.1.3 Plant Perturbations with Increased Dutch Roll Damping

From the previous section it is evident that the H_∞ controller design for the advanced fighter aircraft is very sensitive to plant structured uncertainty. This seems to be largely due to the lightly damped dutch roll mode. The aim of this section is to demonstrate that the lightly damped mode is indeed the culprit. The damping ratio of the dutch roll mode will thus be increased "artificially", and an H_∞ compensator will be designed for this "new" plant. The plant perturbations done in section 4.3.1.2 will then be repeated and, hopefully, the "new" H_∞ controller design will be less sensitive to structured uncertainty.

4.3.1.3.1 The "New" Plant and "New" Compensator

The damping of the dutch roll mode can be increased by using the matrix decomposition given in Appendix A, Theorem 1, i.e. $A = V \Lambda W$. Λ is a diagonal matrix with the eigenvalues of the A matrix along its diagonal. The columns of V are made up of the right eigenvectors of A and $W = V^{-1}$.

The real parts of the dutch roll pole pair are multiplied by a factor of 10.3 in the matrix Λ to give a damping ratio of $\zeta_d = 0.2114$, resulting in a new diagonal matrix conveniently called Λ_{new}. The plant poles associated with the roll and the

spiral modes remain unchanged. The new A matrix, A_{new} is calculated as follows,

$$A_{new} = V \Lambda_{new} W$$

The B, C, and D matrices of the plant were left unchanged.

An H_∞ compensator was designed for this plant using the same weighting functions and γ_{min} given in section 3.2. As the design documentation is similar to what was given in Chapter 3, it will not be repeated here.

4.3.1.3.2 "New" Plant Perturbations

The "new" plant is perturbed using the same dA_p that was used in section 4.3.1.2. Figure 4.3.1.8 shows what happens to the real part of the poles of the "new" plant model for values of ϵ ranging form -0.2 to 0.2 . The plant becomes more unstable as ϵ becomes increasingly negative.

Figure 4.3.1.9 shows the percentage error in the maximum singular value of the "new" plant model $G_{new}(s)$ for $\epsilon = -0.05$ and 0.05 . It is evident from this figure that the damping ratio of the dutch roll mode has been increased significantly. The percentage error in the maximum singular value of $G_{new}(s)$ at the dutch roll mode frequency is now only 5%, instead of 78% as Figure 4.3.1.2 had shown.

Figure 4.3.1.10 shows what happens to the real part of the "new" plant poles as part of the closed loop poles, for values of ϵ ranging form -0.2 to 0.2 . These four poles are the closest to the $j\omega-$ axis and are thus chosen to study the stability of the closed loop system. The figure shows that the pole at the mirror image of the spiral mode pole and the roll mode do not change much as a function of ϵ. The "new" dutch roll mode pole pair changes significantly, as was the case in Figure 4.3.1.3, with the difference being that the closed loop system now only becomes unstable when ϵ reaches -0.43. Thus it takes a 43% downward change in the stability derivatives given in equation 4.3.1.4, to result in an unstable closed loop system, which is a significant improvement over results shown in Figure 4.3.1.3.

Figure 4.3.1.11 shows the singular values of the "new" closed loop system $C_{new}(s)$ for $\epsilon = -0.1$ and 0. The improvement over Figure 4.3.1.5 is evident.

4.3.2 Milling Circuit

4.3.2.1 Choice of dA_p

As far as the milling circuit is concerned, there does not seem to be a specific perturbation matrix to which the controller designed in section 3.3.3, will be particularly sensitive. dA_p is thus chosen to be,

$$dA_p = \epsilon A_p \qquad ;\epsilon \in \mathbb{R} \tag{4.3.2.1}$$

4.3.2.2 Plant Perturbations

The milling circuit given in Appendix C, will be perturbed as described in section 4.2, using dA_p given in section 4.3.2.1. The effect of this perturbation on the 12^{th} order plant and the 21^{th} order closed loop system will be studied.

Figures 4.3.2.1 and 4.3.2.2 show what happens to the real part of the plant poles ($1-7$ and $8-12$ respectively), as ϵ changes form 0.2 to -0.2.

Figure 4.3.2.3 shows the percentage error in the maximum singular value of the plant model G(s) versus frequency, for $\epsilon = -0.1$ and 0.05. The maximum singular value of G(s) is clearly not very sensitive to this particular plant perturbation.

Figure 4.3.2.4 shows the singular values of the closed loop system C(s) for $\epsilon = -0.2$ and 0. Note that a 20% downward change in the elements of the plant A matrix does not have a significant effect on the singular values of the closed loop system. In fact the closed loop system remains stable for $\epsilon > -0.61$.

4.3.2.3 Plant Perturbations with a Lightly Damped Mode

A lightly damped version of the reduced order milling circuit model of section 3.3.1 is used here to show how sensitive such models are to structured uncertainty. The model is 6^{th} order with one complex conjugate pole pair which has a natural frequency $\omega_n = 0.019$ and a damping ratio of $\zeta_d = 0.98$. Using the

same method as described in section 4.3.1.3.1, the pole pair is changed to,

$$-3.4963e{-}04 \pm 7.4962e{-}03i$$

which results in $\omega_n = 0.0075$ and $\zeta_d = 0.047$. The other poles are left intact.

An H_∞ compensator was designed for this "new" plant $G_{new}(s)$, using the weighting functions and γ_{min} of section 3.3.3, and the resulting closed loop system $C_{new}(s)$ will be used for perturbation studies. The perturbation matrix has the same structure as given in equation 4.3.2.1, where A_p is now the "new" A matrix of the plant.

Figure 4.3.2.5 shows the percentage error in the maximum singular value of $G_{new}(s)$ for $\epsilon = -0.05$ and 0.05. The peak at the approximate value of ω_n shows that this plant is now very sensitive to structured uncertainty, when compared to Figure 4.3.2.3.

Figure 4.3.2.6 shows the singular values of the closed loop system $C_{new}(s)$ as a function of frequency for $\epsilon = -0.05$ and 0. It is clear that the closed loop system is severely affected by only a 5% downward change in the elements of A_p. In fact $C_{new}(s)$ actually goes unstable for $\epsilon \leq -0.068$, i.e. a 6.8% downward change in the elements of A_p results in an unstable closed loop system!

4.3.3 Fictitious Plants with Unstable Poles and Zeros

Two fictitious plants were created to show the effects of approximate unstable pole zero cancellations on H_∞ designs and their state space descriptions are given in Appendix E. Both plants have an unstable pole and a transmission zero at the same location s = 1. The directions of this pole and zero are orthogonal to each other in the case of plant I, and nearly in the same direction in the case of plant II. It is well known from [20] that such systems have inherent limitations with respect to achievable performance, independent of the design method used.

The directions of the pole (v_{p1}) and zero (v_{z1}) at s = 1 for plant I are,

$$v_{p1} = \begin{bmatrix} 0 \\ 4.7450e{-}01 \\ 1.0000e{+}00 \end{bmatrix} \qquad v_{z1} = \begin{bmatrix} 1.0000e{+}00 \\ 0 \\ 0 \end{bmatrix}$$

These directions are orthogonal to each other so that this does not represent a pole zero cancellation, despite the fact that the pole and zero have the same location.

The directions of the pole (v_{p2}) and zero (v_{z2}) at s = 1 for plant II are,

$$v_{p2} = \begin{bmatrix} 1.0000e{+}00 \\ 4.7450e{-}04 \\ 1.0000e{-}03 \end{bmatrix} \qquad v_{z2} = \begin{bmatrix} 1.0000e{+}00 \\ 0 \\ 0 \end{bmatrix}$$

These vectors are approximately in the same direction, so that this does represent a near pole zero cancellation.

H_∞ designs were carried out for both plants and the weights used are shown in Appendix E. As expected, the nominal design for plant I gives much better results than the one for plant II as indicated by γ_{min} and $\|S_{fic}(s)\|_\infty$ (infinity norm of the sensitivity transfer function matrix of the fictitious plant and its compensator) of the two plants. For plant I, $\gamma_{min} = 2.7$ and $\|S_{fic}(s)\|_\infty = 2.15$, and for plant II, $\gamma_{min} = 750$ and $\|S_{fic}(s)\|_\infty = 527$. The large value of γ_{min} for plant II is expected due to the inherent limitations of such designs [20].

These plants were perturbed to determine how sensitive H_∞ controllers designed for these plants are to structured uncertainty. For plant I, its A matrix multiplied by ϵ, was used as the perturbation matrix dA_p. Figure 4.3.3.1 shows the singular values of the closed loop system $C_{fic1}(s)$ for values of $\epsilon = 0$ and -0.36. The closed loop system actually goes unstable for $\epsilon = -0.37$.

For plant II, the following perturbation matrix dA_p was used,

$$dA_p = \epsilon \begin{bmatrix} 0 & 0 & 0 \\ .1 & 0 & 0 \\ .1 & 0 & 0 \end{bmatrix}$$

This particular dA_p was chosen because it changes the direction of the pole at $s = 1$, for very small values of ϵ. Figure 4.3.3.2 shows the singular values of the closed loop system $C_{fic2}(s)$ for values of $\epsilon = 0$ and -0.008. The closed loop system actually goes unstable for $\epsilon = -0.009$. As expected, the H_∞ controller for plant II is very sensitive to structured uncertainty, particularly if this uncertainty results in a pole zero cancellation.

4.4 Conclusions

The results shown in section 4.3.1.2 indicate that the nominal H_∞ controller designed for the aircraft in Chapter 3, is totally inadequate when it comes to dealing with plant structured uncertainty. Note that singular value plots prove to be invaluable in detecting this inadequacy which cannot be seen from the time simulation in Figure 4.3.1.6.

When the damping of the dutch roll mode is increased significantly in section 4.3.1.3, the H_∞ controller designed for this "new" plant is shown to be reasonably insensitive to plant structured uncertainty. Some practical way should be found to implement the "artificial" increase in the damping ratio of the lightly damped pole pair. This will be addressed in Chapter 5 where several ways of "desensitizing" a lightly damped plant to structured uncertainty, will be presented.

In section 4.3.2.2 it was shown that the H_∞ controller designed for the milling circuit in Chapter 3, is reasonably robust to structured uncertainty. However, when a lightly damped pole pair is "artificially" introduced into the milling circuit model in section 4.3.2.3, the resulting closed loop system is very sensitive to structured uncertainty, particularly at the natural frequency ω_d of this lightly damped mode.

Results shown in section 4.3.3 agree with the intuitively obvious, i.e. that plants with near unstable pole zero cancellations are sensitive to structured uncertainty and difficult to control. The fact that the controller designed for plant I amplifies disturbances is predicted by [20]. The poor closed loop singular value

shapes for plant II are due to the approximate pole zero cancellation that occurs. This design is also extremely sensitive to structured uncertainty. The direction and location of the nonminimum phase zero could possibly be changed by relocating the actuators and sensors of the plant. The plant should then be easier to control and less sensitive to structured uncertainty.

In section 4.3.1.2 the following question was asked: Does a study of the perturbed plant model give an indication as to how sensitive the closed loop system will be to structured uncertainty in the plant model? From the figures presented here, e.g. Figures 4.3.1.2, 4.3.1.9, 4.3.2.3 and 4.3.2.5, the answer would seem to be a definite *yes*. Large "peaks" with steep slopes (corresponding to lightly damped pole pairs) in the plots of maximum plant singular value error versus frequency, seems to indicate that the corresponding H_∞ closed loop system will be extremely sensitive to structured uncertainty.

From the results shown in this chapter one could conclude that the designer should do the following before an H_∞ design is attempted:

- calculate the poles and zeros plus their direction, of the plant model and look for approximate unstable pole zero cancellations.
- Plot the error in the maximum singular value of the plant, when the plant is perturbed with a well chosen "practical" perturbation, and look for large "peaks" with steep slopes in these plots.

If there are approximate pole zero cancellations in the plant model and/or large

"peaks" with steep slopes in the plot of the maximum singular value error, the plant should be "robustified" by using methods described in Chapter 5, before an H_∞ design is attempted.

From the evidence presented in sections 4.3.1.2 and 4.3.1.3, and sections 4.3.2.2 and 4.3.2.3, it would seem fair to say that the H_∞ methodology should be applied to plants with lightly damped pole pairs as is, only if the plant, and, in particular, the resonant frequencies of the lightly damped pole pairs, is known exactly, which is hardly ever the case. This and any other linear controller design method e.g. LQG/LTR, which cancels the stable part of the plant dynamics –only approximately in real applications–, will have similar problems in dealing with structured uncertainty in the parameters of plants with lightly damped modes. Approximate unstable pole zero cancellations are difficult to deal with, no matter which design method is used.

Figure 4.3.1.1 :eps vs. real part of plant poles G(s)

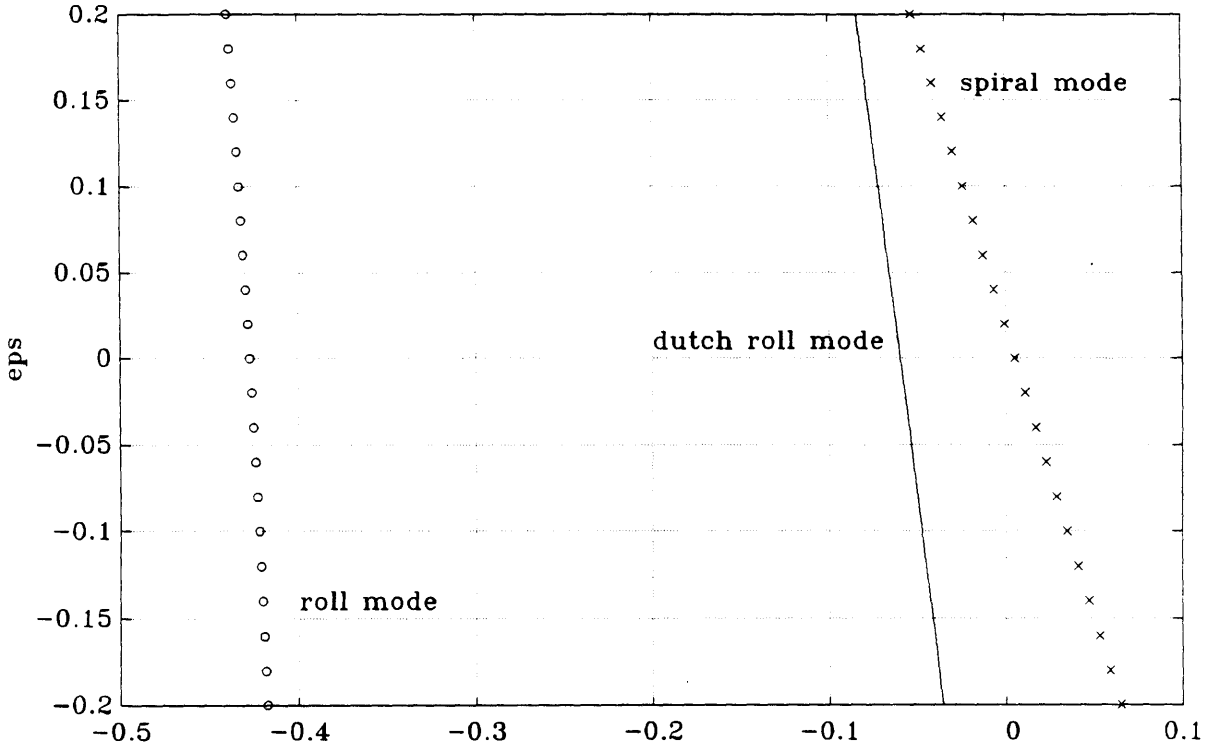

Figure 4.3.1.2 :% error in the maximum singular value of G(s)

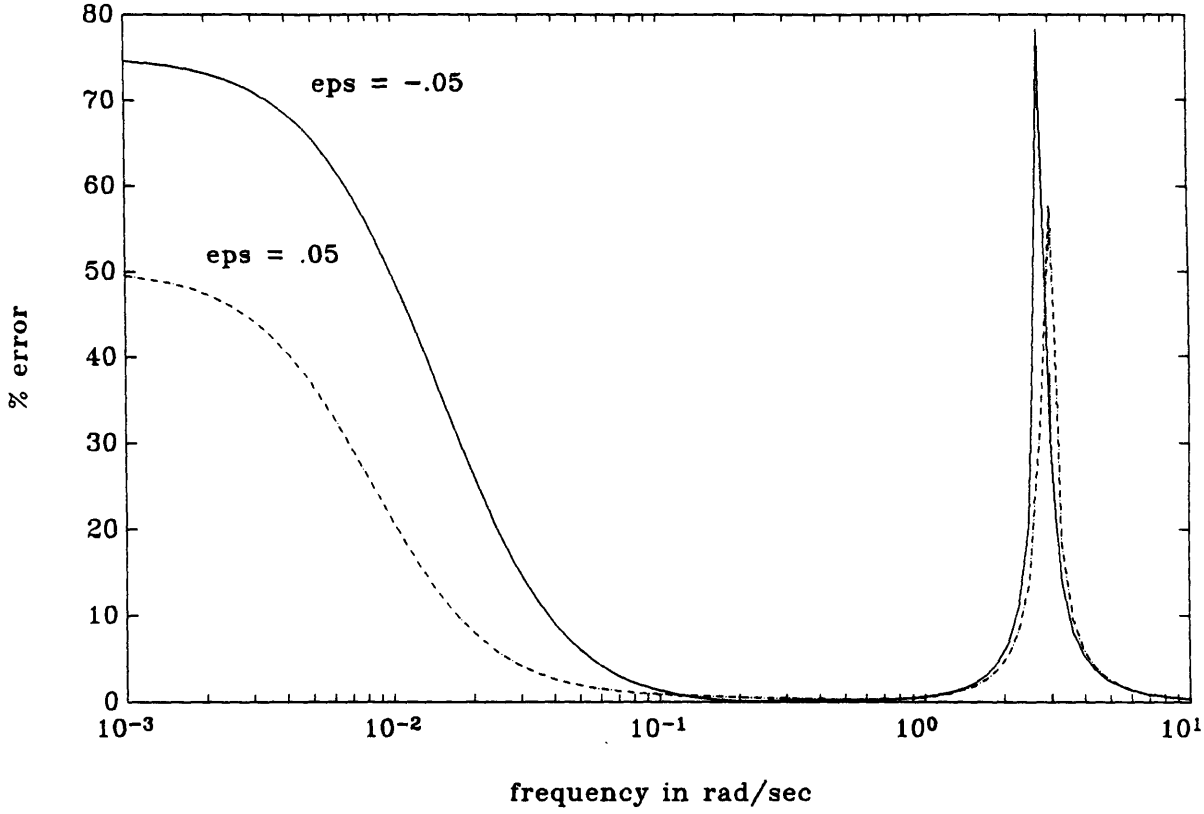

Figure 4.3.1.3 :eps vs. real part of plant poles in C(s)

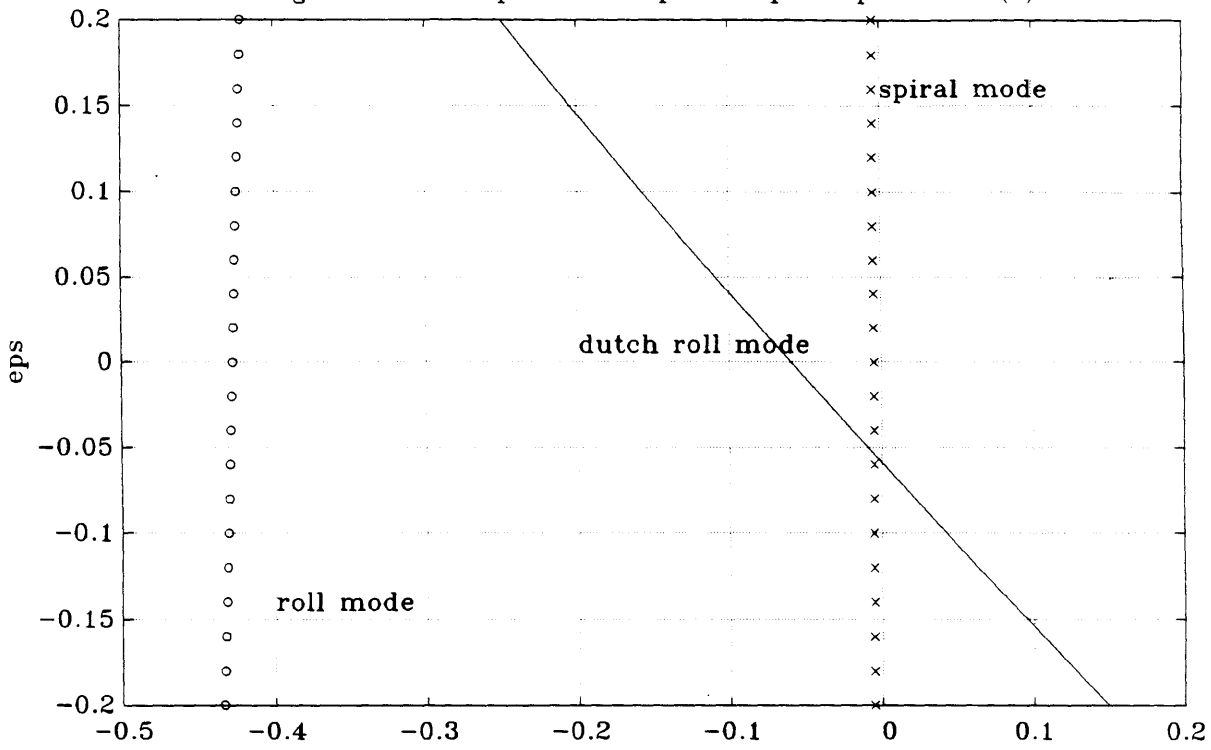

Figure 4.3.1.4 :% error in the maximum singular value of C(s)

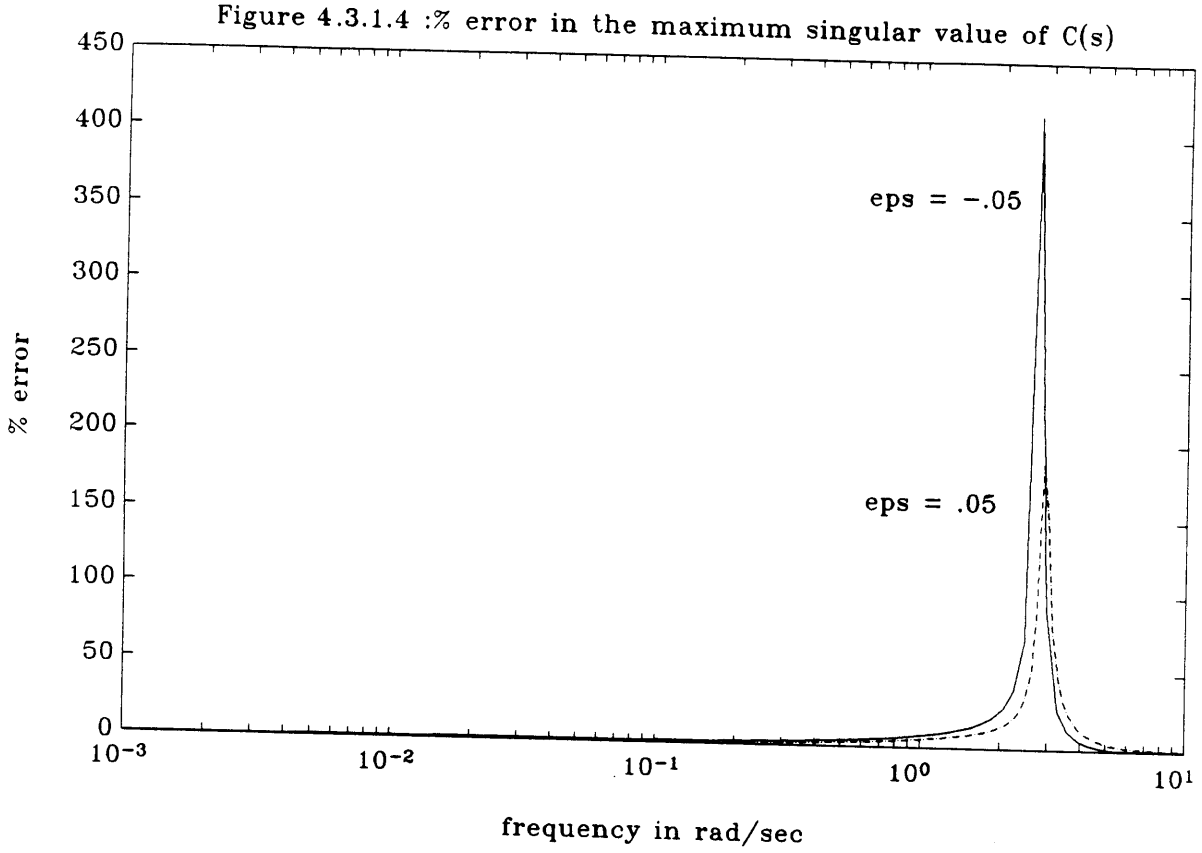

Figure 4.3.1.5 :Singular values of C(s)

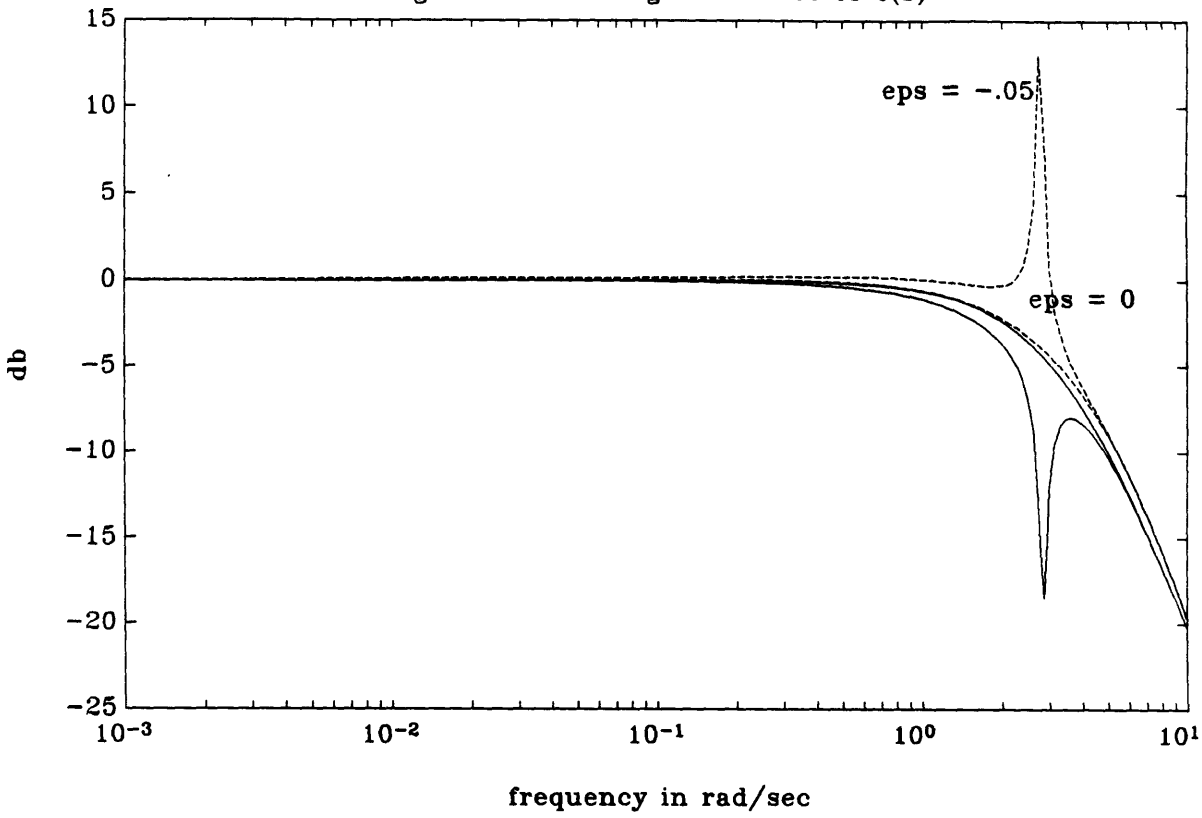

Figure 4.3.1.6 :Response to unit step in bank angle command (eps = −.05)

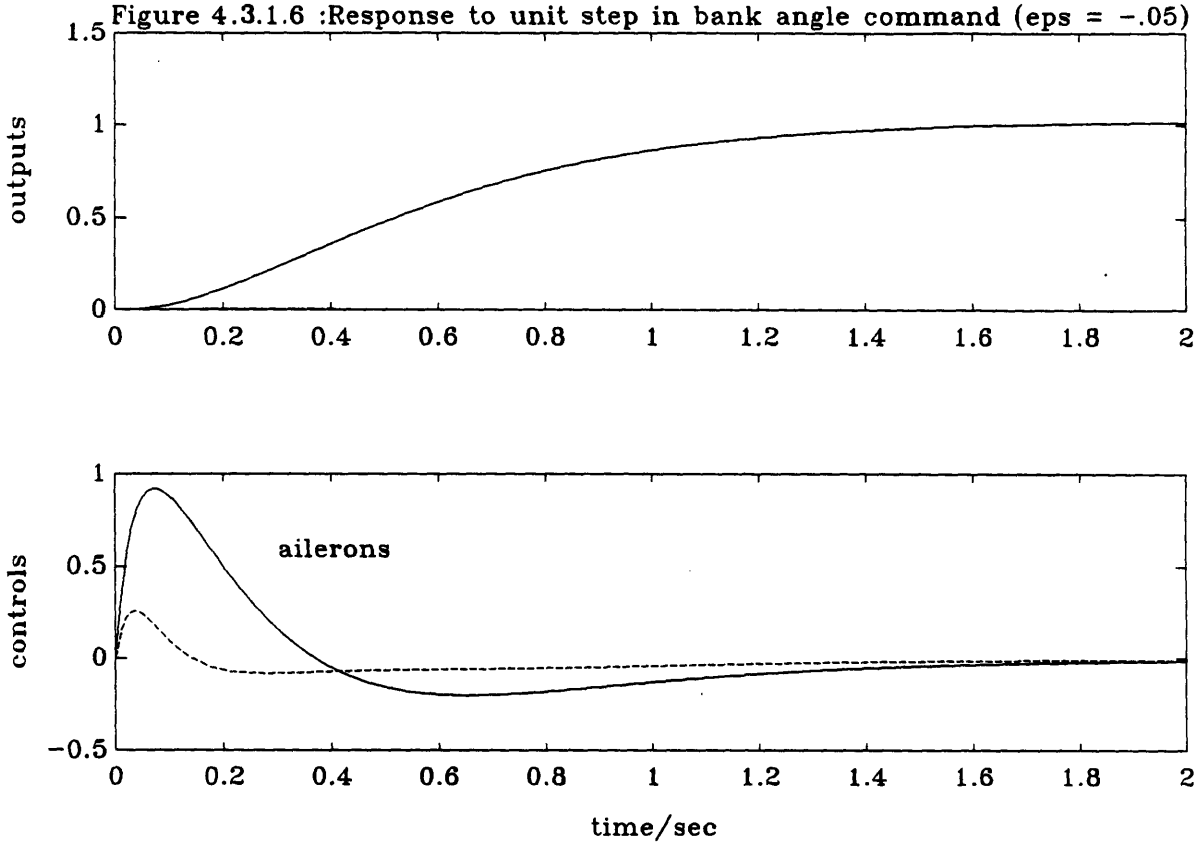

Figure 4.3.1.7 :Response to unit step in bank angle command (eps = −.1)

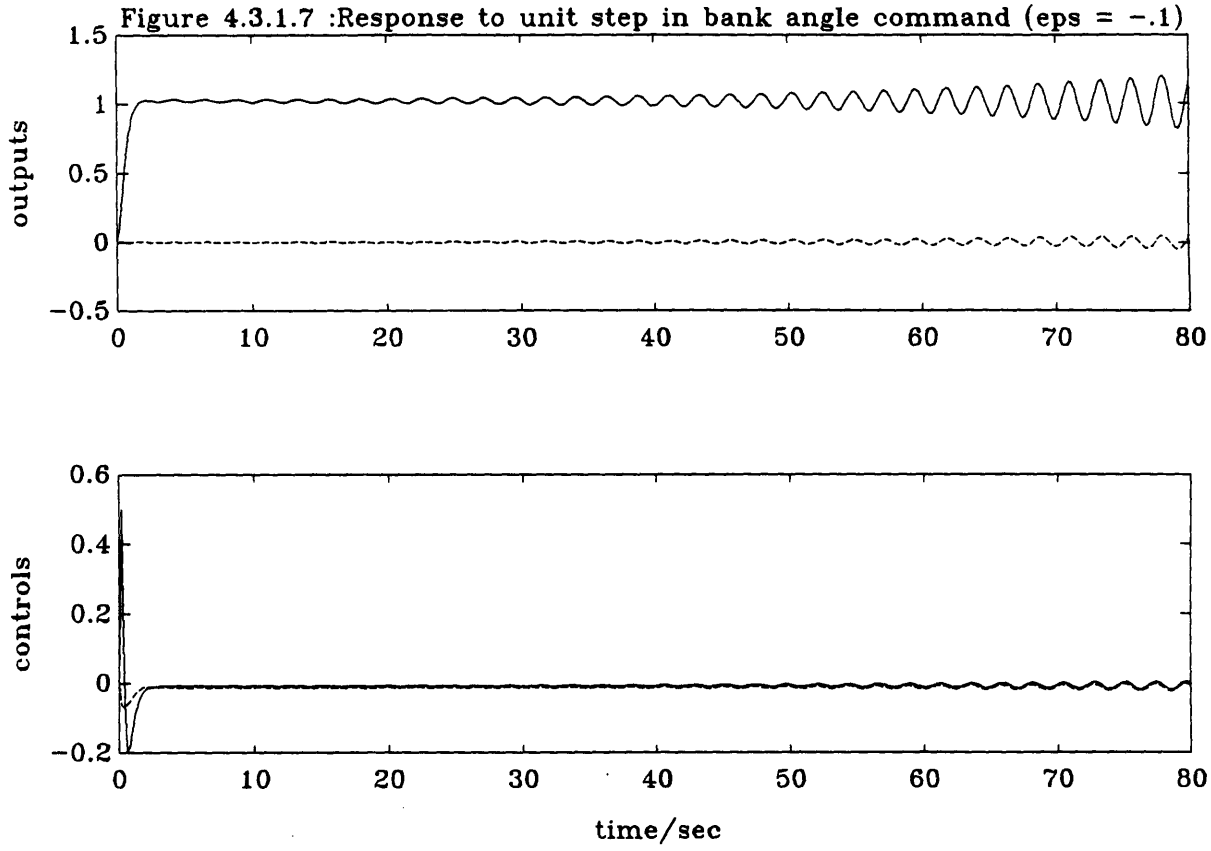

Figure 4.3.1.8 :eps vs. real part of "new" plant poles

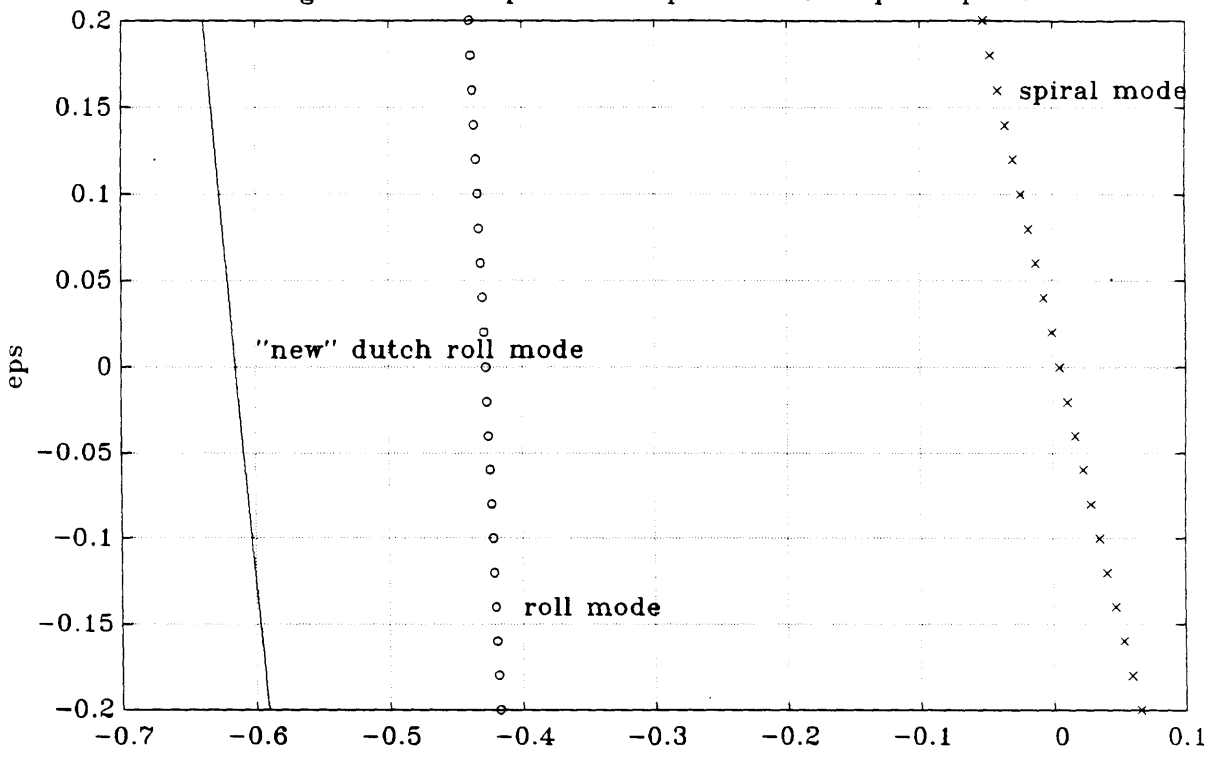

Figure 4.3.1.9 :% error in the maximum singular value of Gnew(s)

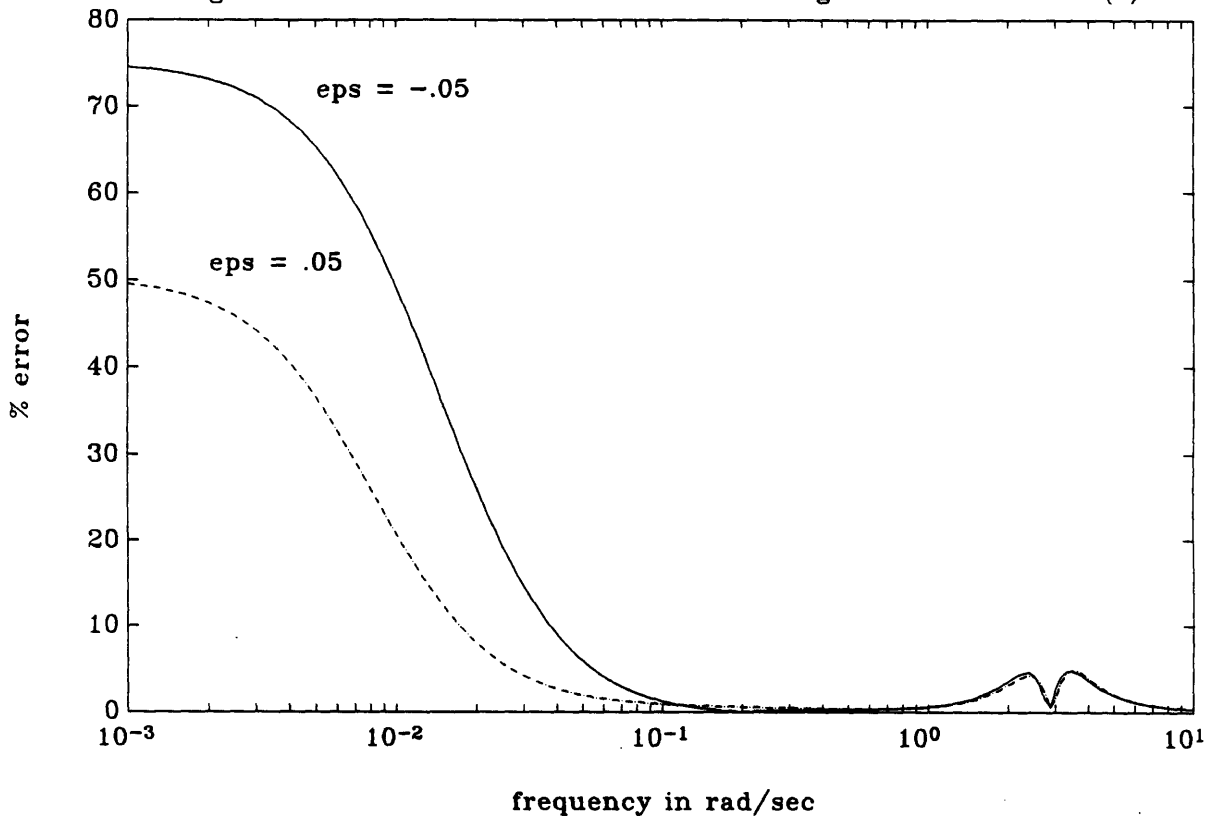

Figure 4.3.1.10 :eps vs. real part of "new" plant poles in Cnew(s)

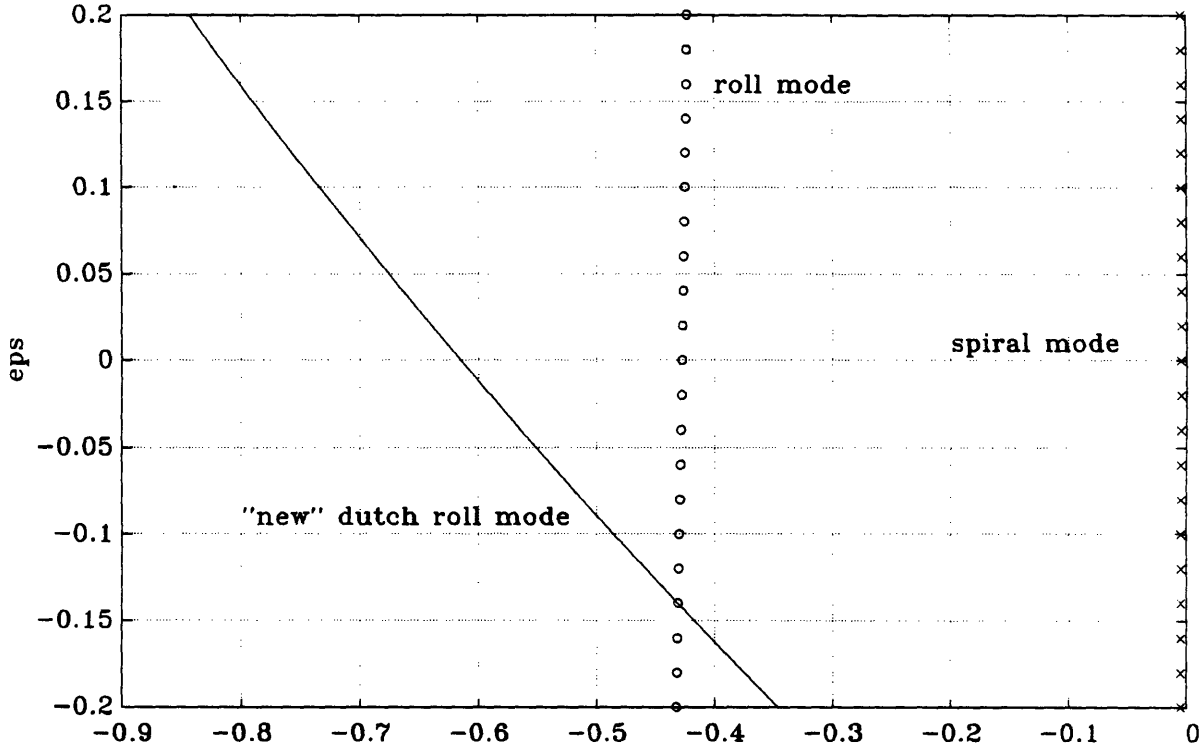

Figure 4.3.1.11 :Singular values of Cnew(s)

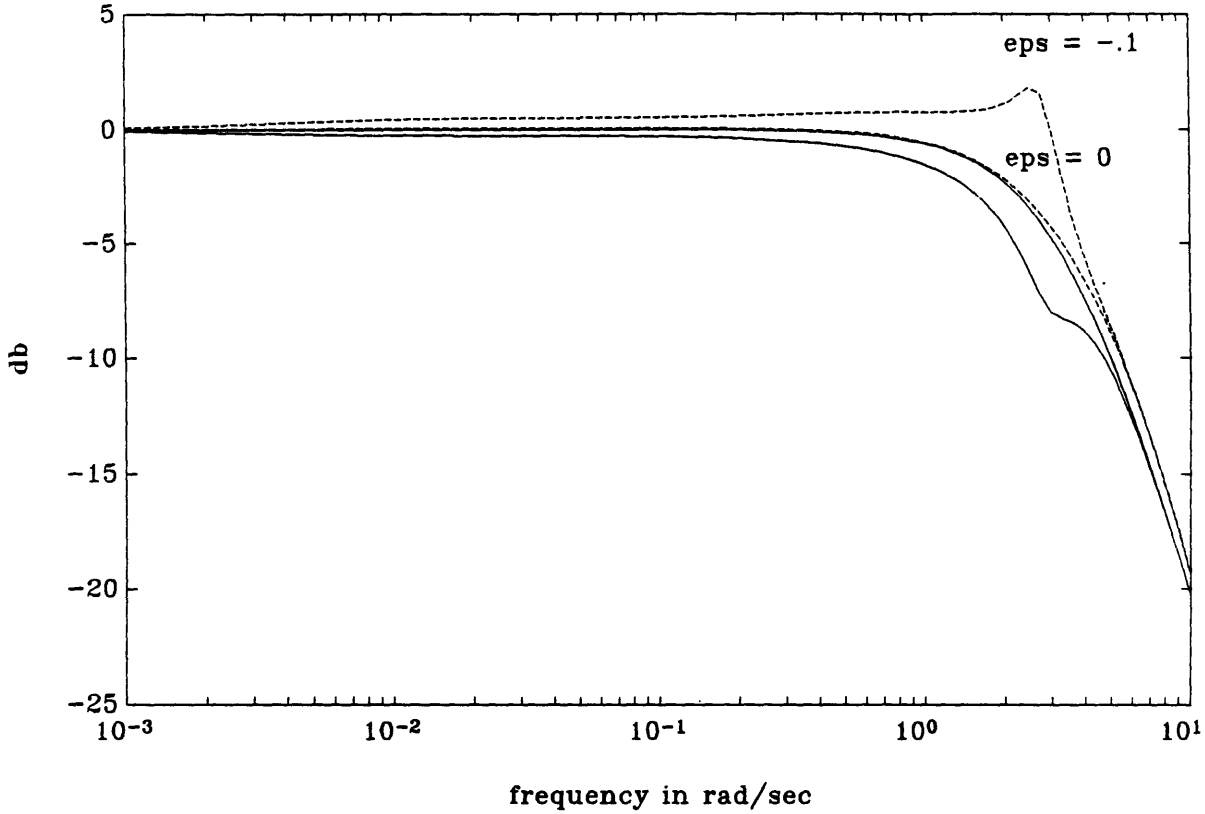

Figure 4.3.2.1 :eps vs. real part of plant poles (1 - 7)

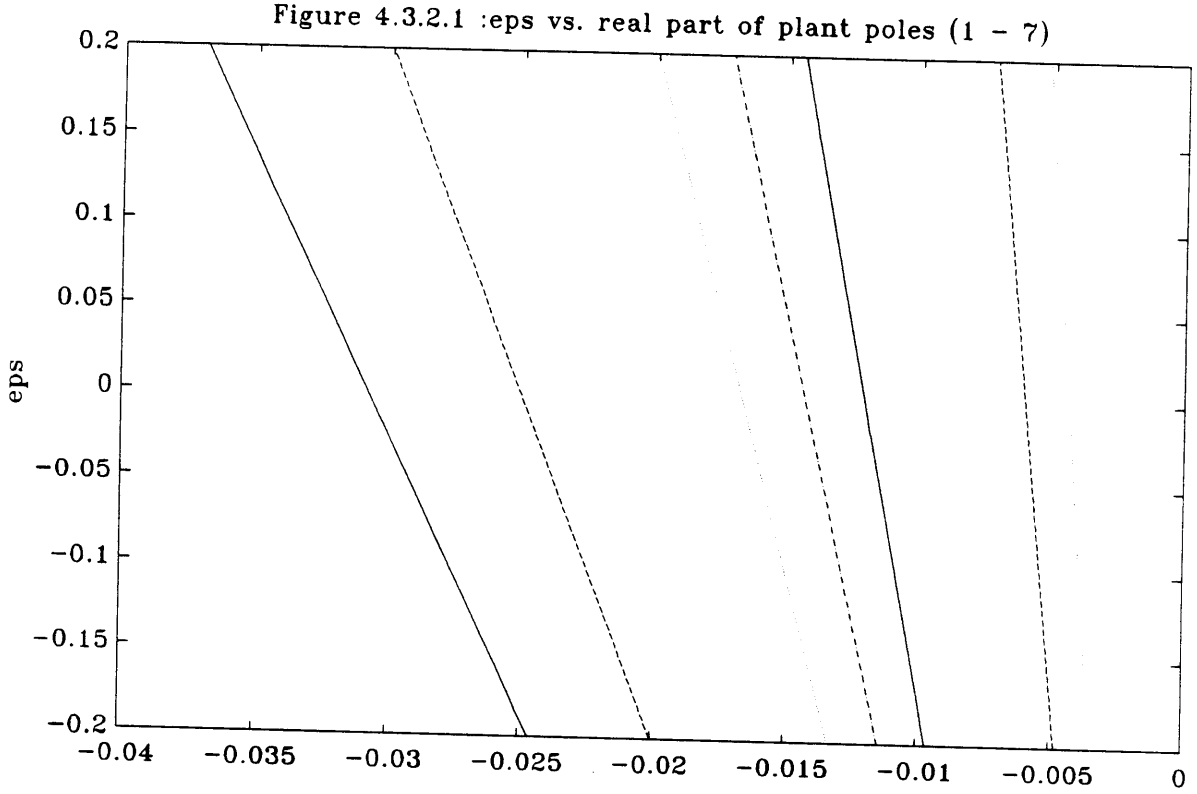

Figure 4.3.2.2 :eps vs. real part of plant poles (8 – 12)

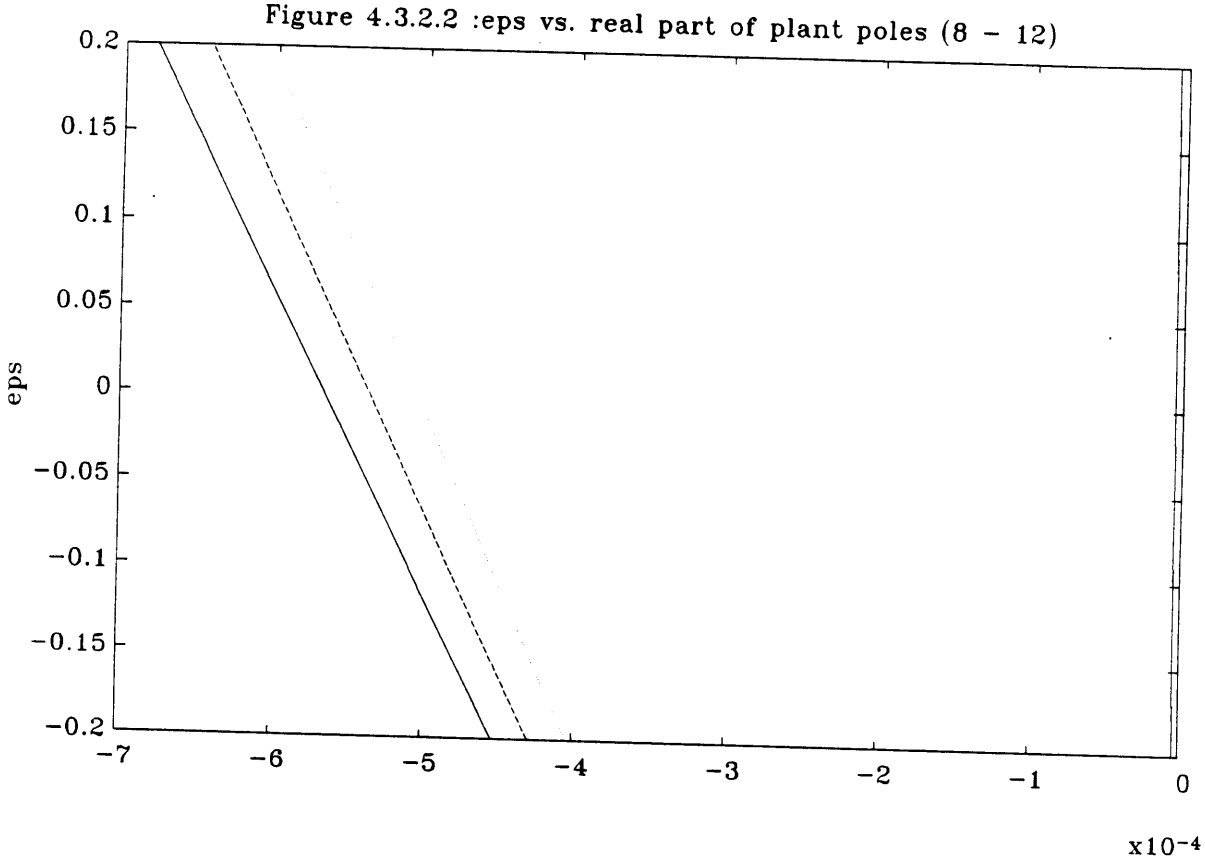

Figure 4.3.2.3 :% error in the maximum singular value of G(s)

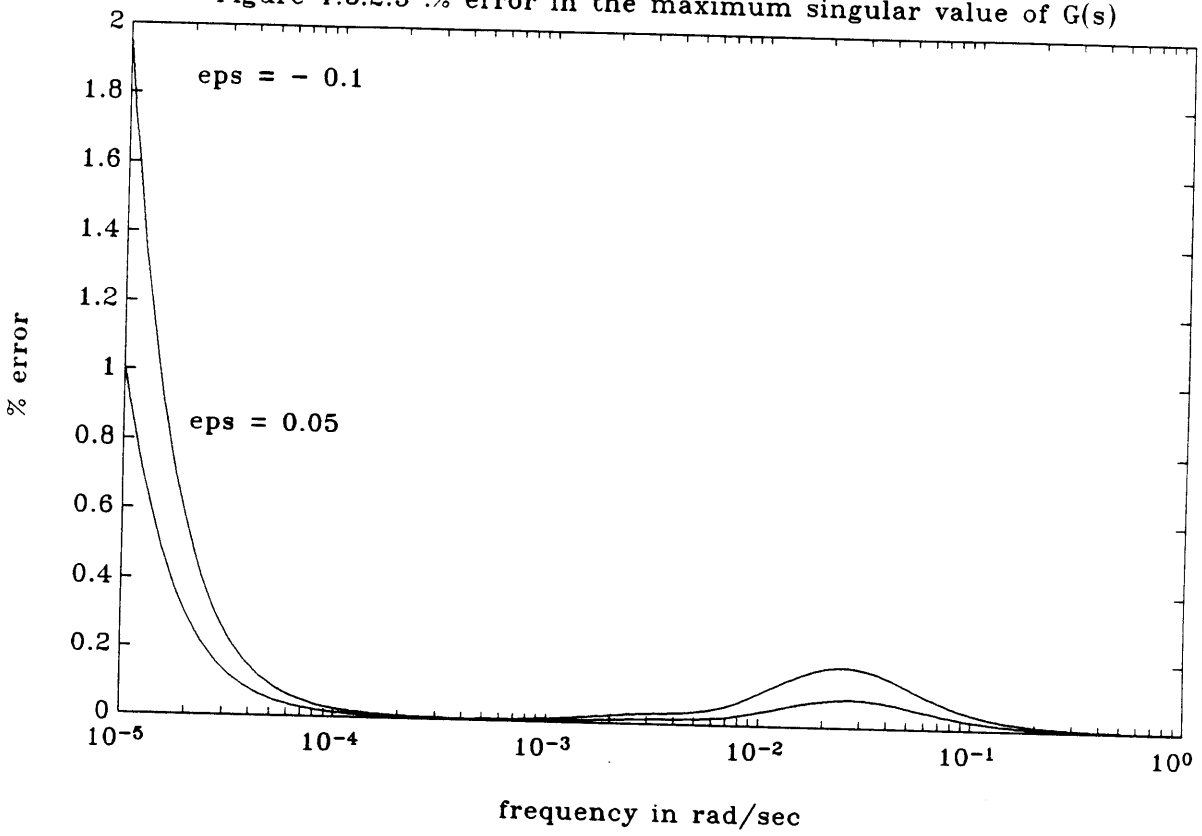

Figure 4.3.2.4 :Singular values of C(s)

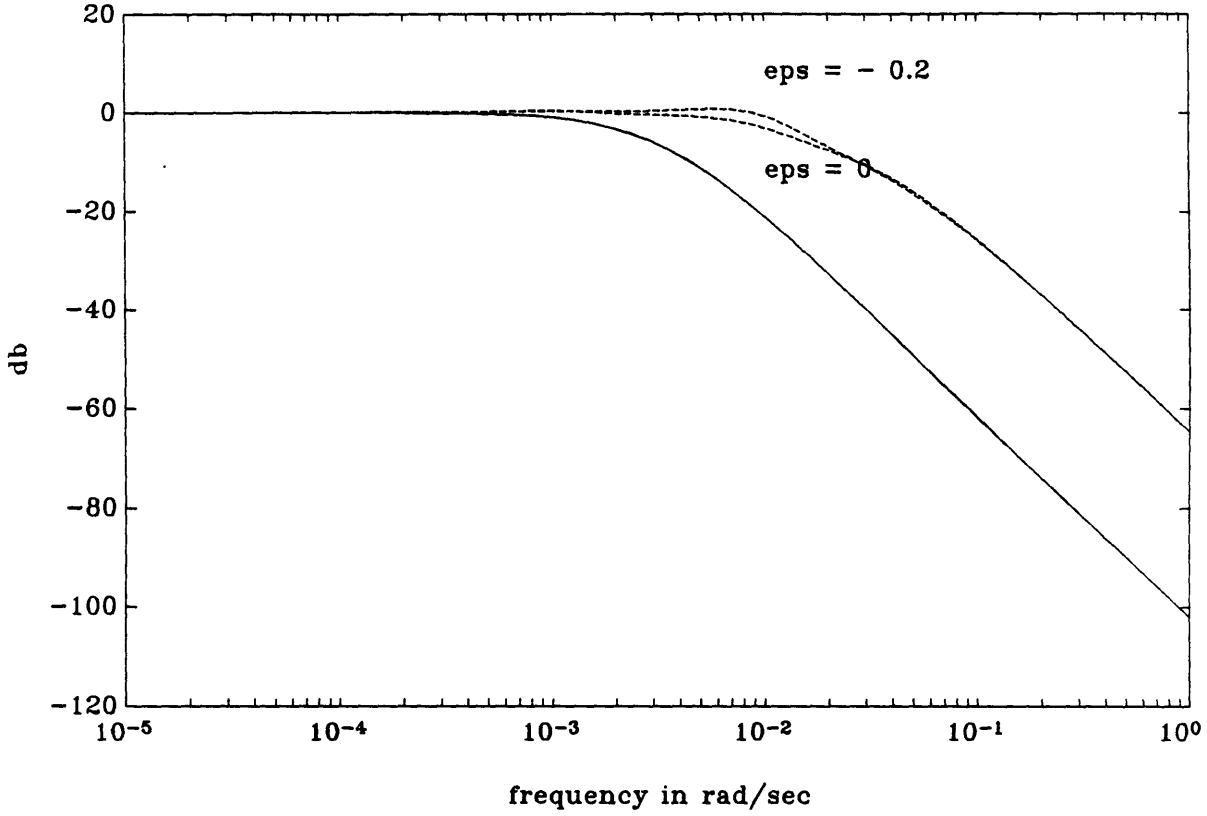

Figure 4.3.2.5 :% error in the maximum singular value of Gnew(s)

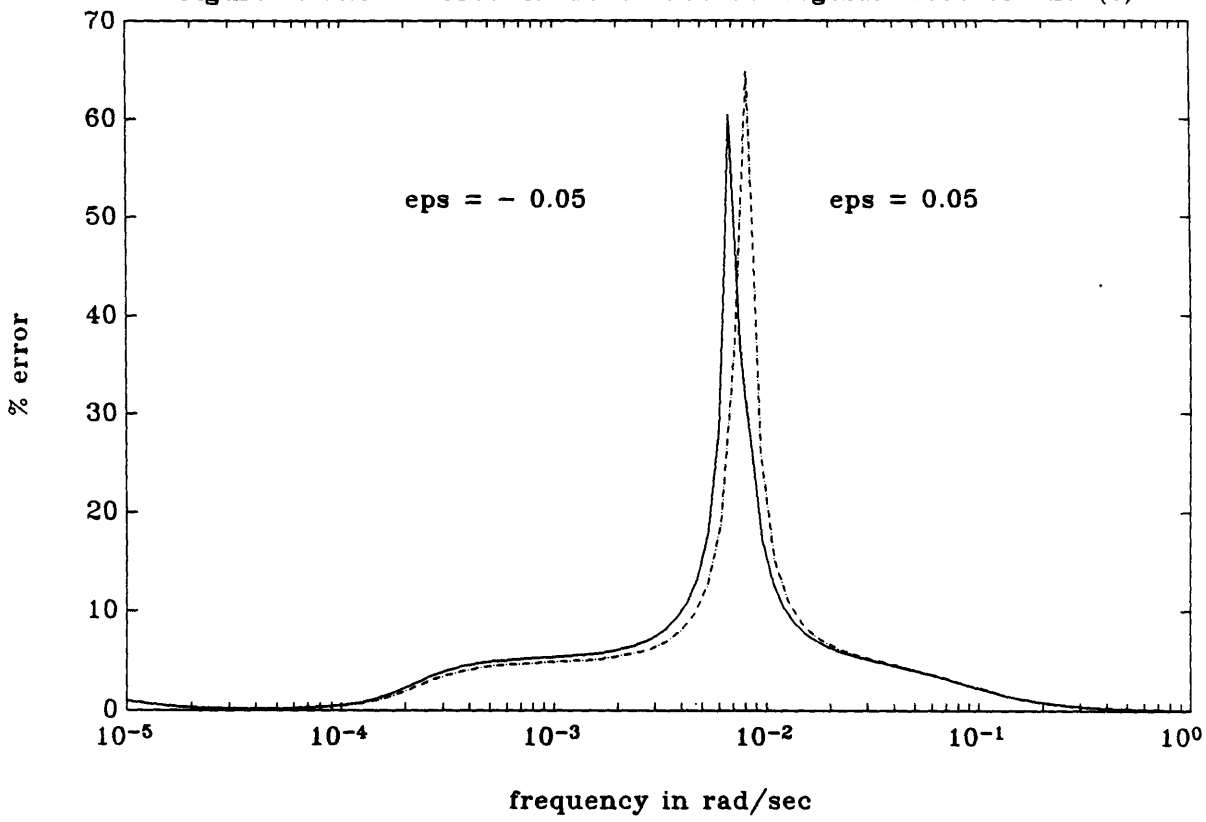

Figure 4.3.2.6 :Singular values of Cnew(s)

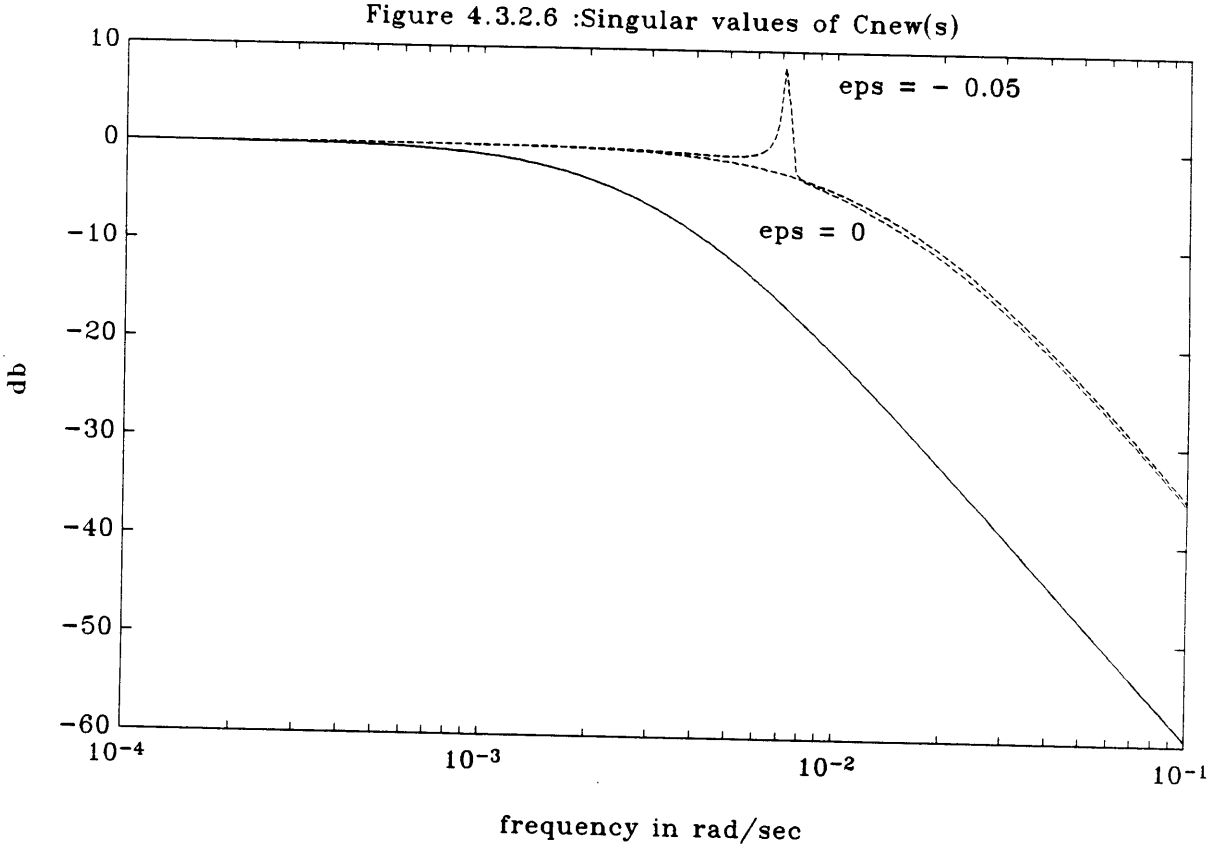

Figure 4.3.3.1 :Singular values of Cfic1(s) for eps = 0 and −.36

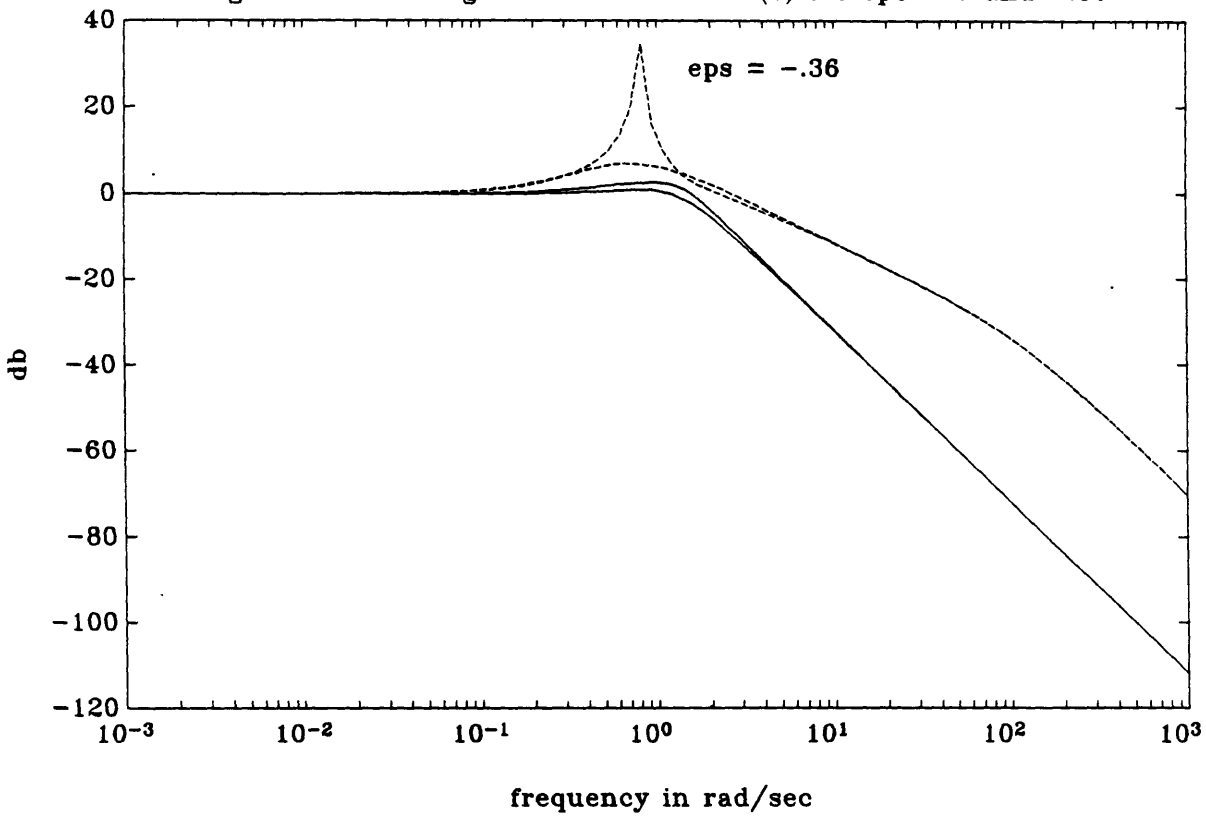

Figure 4.3.3.2 :Singular values of Cfic2(s) for eps = 0 and −.008

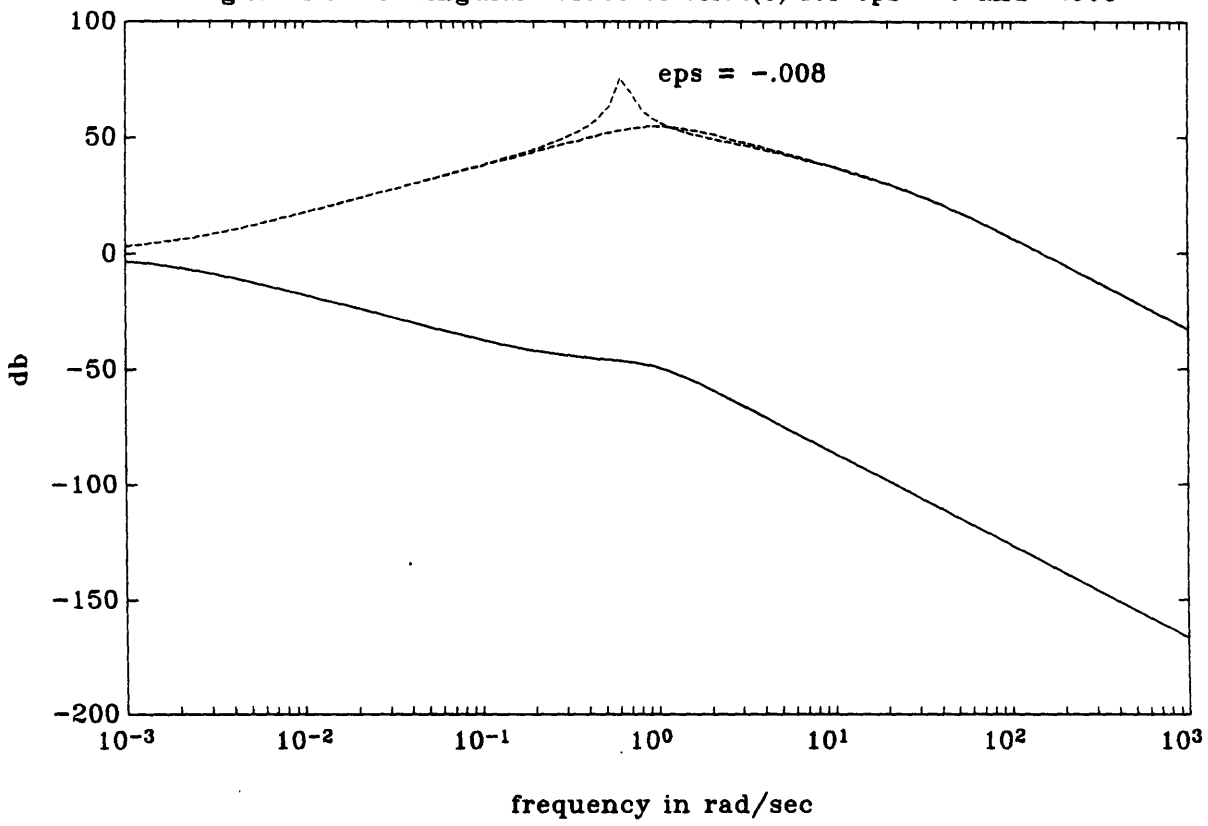

CHAPTER 5

DESENSITIZING H_∞ DESIGNS TO STRUCTURED UNCERTAINTY

5.1 Introduction

In Chapter 4 it was shown that H_∞ controller designs for plants with lightly damped poles are very sensitive to plant structured uncertainty. It was also shown that, by increasing the damping ratio of these lightly damped poles "artificially", the resulting closed loop system can be made relatively insensitive to this type of uncertainty.

This chapter focuses on practical ways of increasing the damping ratio of lightly damped poles of the advanced fighter aircraft, called inner loop compensation. An "inside loop" is closed around the plant to increase the damping of the lightly damped poles. The "new" plant with increased damping is incorporated into the augmented plant P(s) described in Chapter 2, for which an H_∞ compensator is then designed.

In section 5.3 a classical compensator designed for the aircraft described in section 3.2.1, is compared to an inner loop compensated H_∞ controller with respect to performance and robustness. As is well known, classical design methods utilize loop feedback to increase the damping ratio of lightly damped poles, and are traditionally used to design lateral–directional flight control systems for fighter

aircraft.

5.2 Inner Loop Compensation

The type of inner loop compensation used to robustify a particular design, depends on the physics of the problem and the amount of states that are available for measurement. When all plant states can be measured, the control system designer has the freedom to place all the plant poles and to exercise some control over the eigenvectors, using full state feedback eigenstructure assignment ideas [5]. This method will be used in section 5.2.1 to alter the eigenstructure of the aircraft. If all the plant states are not available for measurement or, if only partial state feedback is needed to robustify the design, the method described in section 5.2.2 can be used to increase the damping of the dutch roll mode of the aircraft.

5.2.1 Full State Feedback Inner Loop

In this section a new design plant model for the advanced fighter aircraft will be constructed. In order for this new model to be less sensitive to structured uncertainty, the damping ratio of the lightly damped dutch roll mode needs to be increased. The plant model is controllable and all the states are assumed available for measurement, so that full state feedback pole placement techniques can be applied to achieve an increase in damping. This method was previously applied to the design of pitch pointing flight control systems [21].

The assumption that all the states of the advanced fighter aircraft are available for measurement is, strictly speaking, only valid under test flight conditions. Normally, the sideslip angle β is not measured and measurements of yaw and roll rates (r_b and p_b) are provided by yaw and roll rate gyros. The bank angle (ϕ) measurement is provided by a vertical gyro. Inner loop compensation can be successfully applied to the aircraft without the need for additional sensors, as shown in section 5.2.2. For plants in general, additional sensors may be needed to accommodate this type of compensation.

5.2.1.1 Inner Loop Design

Following the notation used in previous chapters, let the open loop plant dynamics be described by,

$$\dot{x}_p(t) = A_p x_p(t) + B_p u_p(t)$$

Now define the following full state feedback law,

$$u_p(t) = -G\, x_p(t) + u_2(t)$$

with $u_2(t)$ as shown in Figure 2.3.1. The closed loop dynamics are,

$$\dot{x}_p(t) = [A_p - B_p G]\, x_p(t) + B_p u_2(t)$$

The freedom exists to place all four of the plant poles and to retain two out of the four entries of each eigenvector of A_p. G was chosen such that the dominant eigenvector values remain the same, i.e. A_p and $[A_p - B_pG]$ have approximately the same eigenvectors. The dutch roll mode pole pair was changed to be the same as the "artificial" pole pair that was chosen in section 4.3.1.3.1 ($\zeta_d = .2114$). The other two poles were left as is. In choosing G this way, the matrix $[A_p - B_pG]$ is as close to the matrix A_{new} of section 4.3.1.3.1 as possible. The numerical values of the full state feedback gain matrix G and the old and new eigenvalues and eigenvectors, are given in Appendix B, section B.6.

Figure 5.2.1 shows the singular values of $G_{new}(s)$ and its condition number versus frequency. Comparing Figure 5.2.1 to Figure 3.2.1.1, it is evident that the damping ratio of the dutch roll mode has been increased significantly.

The zeros of the plant remain at their open loop locations, as full state feedback does not change the location of these zeros. They can, however, become uncontrollable or unobservable if pole zero cancellations result from pole placement.

The state space description of the new plant with increased damping, is given by,

$$G_{new}(s) = \left[\begin{array}{c|c} A_p - B_pG & B_p \\ \hline C_p & D_p \end{array}\right]$$

In choosing the full state feedback gain matrix G, the objective was not to achieve "good" performance or even nominal stability but, rather, to make the final

H_∞ controller design less sensitive to structured uncertainty. The pole placement technique is used to increase the damping ratio of the dutch roll mode and to maintain the directional properties of the matrix A_p. Performance and stability issues are addressed by the H_∞ compensator.

5.2.1.2 H_∞ Compensator Design and Evaluation

In this section an H_∞ compensator will be designed for the new plant $G_{new}(s)$ described in section 5.2.1.1. The design specifications and weighting functions used are as given in section 3.2.2.

Using the γ – iteration procedure described in section 2.5.1, the minimum value of γ, which does not give rise to excessive control action, was found to be $\gamma_{min} = 1.3$. The poles and transmission zeros of the 6^{th} order compensator are,

$\lambda_i(A_k) =$ – 9.4829e+00 ± 4.3262e+00i
– 3.5603e+01
– 6.6843e+00
2 @ – 1.0000e–04

zeros =	– 6.1480e–01 ± 2.8437e+00i	(damped dutch roll mode)
	– 4.2730e–01	(roll subsidence mode)
	– 4.8717e–01	(mirror image of spiral mode)

Figures 5.2.2, 5.2.3 and 5.2.4 show the singular values of the loop $T_{new}(s)$, sensitivity $S_{new}(s)$, and closed loop $C_{new}(s)$ transfer function matrices respectively. From Figure 5.2.3, k can be found to be k = 1.231, according to equation 2.2.2.1. This gives the controller the following gain and phase margins in each loop simultaneously and independently,

$$GM\uparrow \geq 5.33$$

$$GM\downarrow \leq 0.55$$

$$PM \geq 47.93 \text{ deg}$$

It would seem that the controller designed here exhibits good nominal performance characteristics. The question that remains to be asked is : Will the new H_∞ controller design be "less" sensitive to structured uncertainty than the one designed in Chapter 3? This question will be answered in the next section.

5.2.1.3 Sensitivity Studies

In this section perturbation studies will be performed in the same manner as was described in section 4.3. The perturbation matrix dA_p used here is the one described in section 4.3.1.1, and the A matrix of the "true" plant, including the structured uncertainty is given by,

$$A_{newt} = A_p + dA_p - B_p G$$

where G is the full state feedback gain matrix.

Figure 5.2.5 shows the percentage error in the maximum singular value of the new plant $G_{new}(s)$, for $\epsilon = -0.05$ and 0.05 (see state space description in section 5.2). This figure is almost exactly the same as Figure 4.3.1.9, which portrays the error in the maximum singular value of the "artificial" plant. The effect of the dutch roll mode damping is evident when Figure 5.2.5 is compared to Figure 4.3.1.2.

Figure 5.2.6 shows what happens to the real part of the four closed loop poles which are at the same location as the poles of $G_{new}(s)$, for values of ϵ ranging from -0.2 to 0.2. Again, the damped dutch roll mode pole pair changes significantly –compare with Figure 4.3.1.10–, but the closed loop system goes unstable only when ϵ reaches -0.51. Thus, the closed loop system remains stable even when the stability derivatives in equation 4.3.1.4 are simultaneously reduced by 50%.

Figure 5.2.7 shows the singular values of $C_{new}(s)$ for $\epsilon = -0.1$ and 0, and the improvement over Figure 4.3.1.5 is evident.

5.2.2 One State Feedback Inner Loop

In this section a new design plant model for the advanced fighter aircraft will be constructed. In the design of classical flight control systems (FCS), it is standard practice [17] to feed back the yaw rate measurement (r_s) to the rudder (δ_r) in order to increase the damping of the dutch roll mode. This will be done here and the feedback will consist of a constant gain represented as a "sparse" matrix G shown in equation 5.2.1.

5.2.2.1 Inner Loop Design

Following the notation established before, let the open loop plant dynamics be described by:

$$\dot{x}_p(t) = A_p x_p(t) + B_p u_p(t)$$

Now define the following feedback law:

$$u_p(t) = -G\, x_p(t) + u_2(t)$$

with $u_2(t)$ as shown in Figure 2.3.1. The inner loop closed loop dynamics are:

$$\dot{x}_p(t) = [A_p - B_p G]\, x_p(t) + B_p u_2(t)$$

Consequently, the state space description of the new plant with increased damping, is given by:

$$G_{new}(s) = \left[\begin{array}{c|c} A_p - B_p G & B_p \\ \hline C_p & D_p \end{array}\right]$$

The feedback gain matrix G, is given by:

$$G = \begin{bmatrix} 0 & 0 & 0 & 0 \\ 0 & 0 & -g_{23} & 0 \end{bmatrix} \qquad 5.2.1$$

where g_{23} will determine the damping increase of the dutch roll mode.

Figure 5.2.8 shows the singular values of $G_{new}(s)$ and its condition number versus frequency, for $g_{23} = 0.4$ which corresponds to a dutch roll mode damping ratio of 0.206. Comparing Figure 5.2.8 to Figure 3.2.1.1, it is evident that the damping ratio of the dutch roll mode has been increased significantly.

5.2.2.2 H_∞ Compensator Design and Design Evaluation

In this section an H_∞ compensator will be designed for the plant $G_{new}(s)$ described in section 5.2.2.1 with $g_{23} = 0.4$. The design specifications and weighting functions used are as given in section 3.2.2.

Using the γ – iteration procedure described in section 2.5.1, the minimum value of γ, which does not give rise to excessive control action, was found to be $\gamma_{min} = 1.3$. The poles and transmission zeros of the 6^{th} order compensator are,

$\lambda_i(A_k) =$ $-9.2811e+00 \pm 4.2951e+00i$
$-3.5637e+01$
$-6.6046e+00$
$2\ @ -1.0000e-04$

zeros = $-5.7158e-01 \pm 2.7102e+00i$ ← new plant poles
$-2.1592e-01 \pm 2.0054e-01i$

Figures 5.2.9, 5.2.10 and 5.2.11 show the singular values of the loop $T_{new}(s)$, sensitivity $S_{new}(s)$, and closed loop $C_{new}(s)$ transfer function matrices respectively.

The figures presented here show that the controller exhibits good nominal performance characteristics. Again the question that remains to be asked is : Will the new H_∞ controller design be "less" sensitive to structured uncertainty than the one designed in Chapter 3? This question will be answered in the next section.

5.2.2.3 Sensitivity Studies

In this section perturbation studies will be performed in the same manner as was described in section 4.3. The perturbation matrix dA_p used here is the one described in section 4.3.1.1, and the A matrix of the inner loop modified actual plant is given by:

$$A_{newt} = A_p + dA_p - B_p G$$

where G is the feedback gain matrix of section 5.2.2.1.

Figure 5.2.12 shows the percentage error in the maximum singular value of the new plant $G_{new}(s)$ for $\epsilon = -0.05$. The effect of the dutch roll mode damping is evident when Figure 5.2.12 is compared to Figure 4.3.1.2. The percentage error at low frequencies –below the dutch roll mode frequency– has also decreased, but this is not a factor in determining the robustness of the H_∞ controller to structured uncertainty, as the controller for the full state feedback inner loop compensated

plant –see section 5.2.1.3–, indicates.

The closed loop system goes unstable only when ϵ reaches -0.46. Thus, the closed loop system remains stable even when the stability derivatives in equation 4.3.1.4 are simultaneously reduced by 46%.

Figure 5.2.13 shows the singular values of $C_{new}(s)$ for $\epsilon = -0.1$ and 0, and the improvement over Figure 4.3.1.5 is evident.

The H_∞ controller becomes more robust as g_{23} is increased. Column 2 of Table 5.2 shows how the damping ratio (ζ_d) of the dutch roll mode changes for different values of g_{23}. Column 3 shows for which value of ϵ the closed loop system $C_{new}(s)$ will go unstable.

Table 5.2 seems to indicate that g_{23} should be made as large as possible to achieve a robust closed loop design. This can be misleading; as g_{23} increases the other two poles of $[A_p - B_pG]$ become lightly damped for values greater than 1.6. Hence, $g_{23} = 1.1$ is a good choice for this particular plant, i.e. the closed loop system will remain stable even if the stability derivatives in dA_p are reduced by 106% ($-\epsilon$ x 100). g_{23} was chosen to be 0.4 in section 5.2.2.1, such that the resulting H_∞ design could be compared to the one designed for the "artificial" plant of section 4.3.1.3.1 ($\zeta_d \approx 0.21$).

Table 5.2 :Robustness of the H_∞ controller as a function of g_{23}

g_{23}	ζ_d	$-\epsilon$
0	0.0210	0.060
0.01	0.0255	0.075
0.05	0.0434	0.12
0.1	0.0661	0.18
0.2	0.1119	0.28
0.3	0.1587	0.38
0.4	**0.2064**	**0.46**
0.5	0.2550	0.55
0.6	0.3047	0.64
0.7	0.3550	0.72
0.8	0.4070	0.80
0.9	0.4596	0.88
1.0	0.5128	0.97
1.1	**0.5665**	**1.06**
1.2	0.6204	1.15
1.3	0.6740	1.24
1.4	0.7269	1.35
1.5	0.7787	1.46
1.6	0.8292	1.60
1.7	0.8780	1.25

5.3 Other Possible Desensitizing Measures

5.3.1 Classical Compensator

Classical design methods are traditionally used to design lateral–directional flight control systems (FCS) for fighter aircraft [17]. These designs, although somewhat ad hoc in a multivariable sense, are popular because of their robustness to structured uncertainty, i.e. uncertainty in the relevant stability derivatives, in the plant model. The aim of the classical compensator is to meet specifications similar to those presented in section 3.2.2 and, in particular, feedback is used to increase the damping of the dutch roll mode in order to make the closed loop dutch roll characteristics robust to structured uncertainty.

5.3.1.1 Compensator Design and Evaluation

A classical compensator designed for the aircraft [17] is shown in Figure 5.3.1. The plant model is controllable and three of the states (p_s, r_s and ϕ_s) can be measured.

The transfer function matrix for a (3 x 2) classical compensator is given by,

$$\begin{bmatrix} \delta_a \\ \delta_r \end{bmatrix} = K_c(s) \begin{bmatrix} -p_b \\ \phi_c - \phi_b \\ -r_s \end{bmatrix}$$

with ϕ_c the bank angle command and

$$K_c(s) = \begin{bmatrix} \dfrac{.3(.2s + 1)}{.04s + 1} & .66 & 0 \\ 0 & 0 & \dfrac{-.8s}{s + 1.5} \end{bmatrix}$$

$K_c(s)$ is 2^{nd} order and its state space description is given in Appendix B, section B.7.

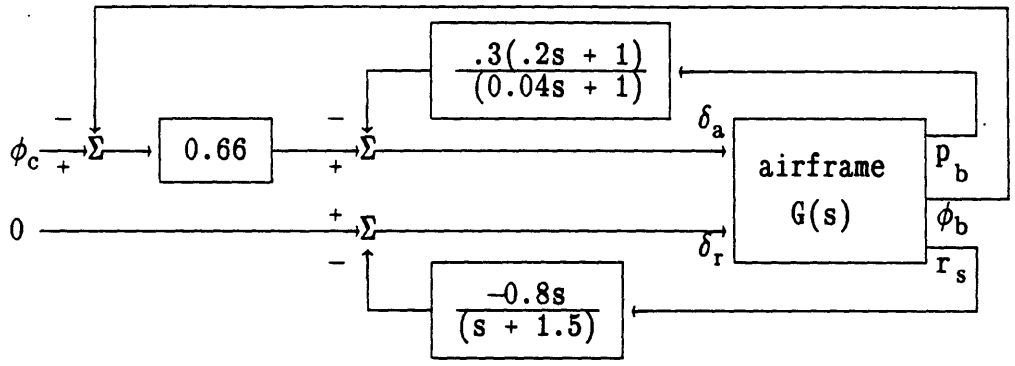

Figure 5.3.1 : Plant and Classical Compensator

5.3.1.2 Comparison — Classical versus the Inner Loop Compensated H_∞ Controller

In this section, a comparison will be made between the classical controller designed in section 5.3.1.1, and the inner loop compensated H_∞ controller of section 5.2.1.2. The classically compensated system goes unstable with $\epsilon = -1.01$ (see equation 4.3.1.4). In order to make a fair comparison, $g_{23} = 1.1$ is chosen from Table 5.2, the value for which the H_∞ controller with inner loop compensation goes

unstable for $\epsilon = -1.06$.

Figure 5.3.2 shows the Bode plot of the closed loop transfer function between the bank angle command ϕ_c and the bank angle ϕ_b, and the singular values of the H_∞ closed loop system $C_{new}(s)$. The two systems have more or less the same bandwidth.

Figure 5.3.3 shows the response of the classical system to a step in ϕ_c. Figure 5.3.4 shows the response of the H_∞ controller to the same command. The step response of the classical system is slightly oscillatory and is also somewhat slower than the step response of the H_∞ controller.

Figure 5.3.5 shows the response of the classical and H_∞ system to a rapidly changing bank angle command with $\epsilon = 0$. Figure 5.3.7 shows the response of the two systems to the same command with $\epsilon = -0.5$ and gives an indication of the performance robustness of the two systems. The systems are perturbed using the perturbation matrix given in equation 4.3.1.4 with $\epsilon = -0.5$, i.e. the relevant stability derivatives are reduced by 50%. When unperturbed, both controllers do a reasonable job of following the command, but the classical system overshoots and lags the H_∞ controller's response by a small amount. The H_∞ controller follows the shape of the command better than the classical system. Both systems seem to handle the perturbation well, with the H_∞ controller doing slightly better than the classical system.

The response of the controls that correspond to Figures 5.3.5 and 5.3.7, are shown in Figures 5.3.6 and 5.3.8 respectively. The H_∞ controller seems to use the controls more efficiently than the classical compensator. The controls commanded by the classical compensator shows a significantly increase when the plant is perturbed, whereas the controls used by the H_∞ controller are approximately the same.

Figure 5.3.9 shows the response of the classical and H_∞ system to a sinusoidal bank angle command with $\epsilon = 0$. Figure 5.3.11 shows the response of the two systems to the same command with $\epsilon = -0.5$. The corresponding controls are shown in Figures 5.3.10 and 5.3.12 respectively. The frequency of the sinusoidal command corresponds to the dutch roll mode frequency ($\omega = 2.83$ rad/sec). Both controllers do a reasonable job of following the command, but the classically compensated system response lags the H_∞ compensated system response and the command by a significant amount. The outputs of both controllers are attenuated, as one would conclude by looking at Figure 5.3.2.

5.3.2 Frequency Shifting

The basic idea with frequency shifting is to regard the lightly damped poles as unstable poles, by shifting the $j\omega$–axis in the s–plane to the left. The H_∞ design methodology then "thinks" that the lightly damped poles are unstable and, as a result, the compensator will not try to cancel these poles with zeros. This method is equivalent to having an exponential weight in the cost function of a Linear Quadratic –LQ– regulator [22], and is illustrated in Figure 5.3.13.

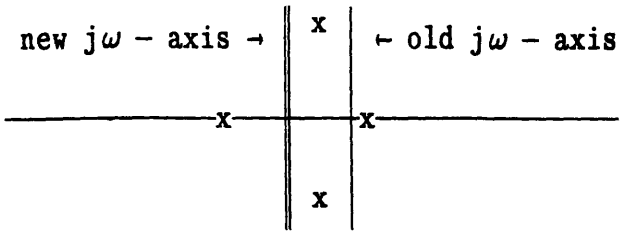

Figure 5.3.13 : Frequency Shifting

This method in conjunction with inner loop compensation should result in a controller which is very robust, but which performs relatively poorly due to the fact that the damping ratios of lightly damped pole pairs are not increased. There is, thus, a trade off between robustness and performance.

5.4 Conclusions

Chapter 4 stressed the need for increasing the damping ratio of the lightly damped dutch roll mode of the advanced aircraft before designing an H_∞ compensator for it, such that the resulting closed loop system will be robust to structured uncertainty.

In this chapter some practical methods were presented to achieve this increase in damping ratio. The method presented in section 5.2.2, where only one state is fed back in an inner loop, seems to work well for this particular plant. The increase in damping is achieved with a gain matrix G, without increasing the dimensionality of the design plant model. The H_∞ controller designed in section 5.2.2.2 for this design plant model is reasonably insensitive to structured uncertainty, as was shown in section 5.2.2.3.

In section 5.3 a traditional classical compensator was designed for the advanced aircraft. A comparison between this design and the H_∞ controller of section 5.2.2 showed that the H_∞ design can be made to perform at least as well as the classical design as far as robustness to structured uncertainty is concerned. The performance of the H_∞ controller, however, is slightly better than that of the classical controller –especially in the upper part of the controller bandwidth–, which could make all the difference in combat situations.

The classical compensator has in its favor the fact that it is of low order –two states–, and that it performs adequately under most circumstances. However, the design of such a compensator is more of an art than a science, as SISO techniques are used to design a compensator for a multivariable plant. As these designs are somewhat ad hoc in a multivariable sense, they can be difficult to reproduce for a different but similar plant. Usually, time consuming parameter "tuning" is undertaken to get a satisfactory design.

The H_∞ compensator, on the other hand, is more complex –six states– and performs slightly better than the classical compensator. The big advantage that the H_∞ design method has over the classical design method, is that it has a strong theoretical base and that it is a truly multivariable design technique. With the complexity of the H_∞ design also comes design flexibility. Frequency specifications are "built" into the design method, and nominal stability is guaranteed. The H_∞ design methodology is easily reproducible, i.e. it is applied the same way to all FDLTI plants and the tediousness of a lengthy trial and error design procedure, as in classical control, is avoided. However, "robustifying" steps should be taken when

required as was discussed in this chapter.

The frequency shifting technique does not address the question of increased damping. The only guarantee that it provides is that the lightly damped pole pair of the plant will not be canceled by H_∞ compensator zeros. This technique, however, in conjunction with inner loop compensation could lead to very robust designs, at the expense of very sluggish performance.

Figure 5.2.1 :Singular values and condition no. of Gnew(s)

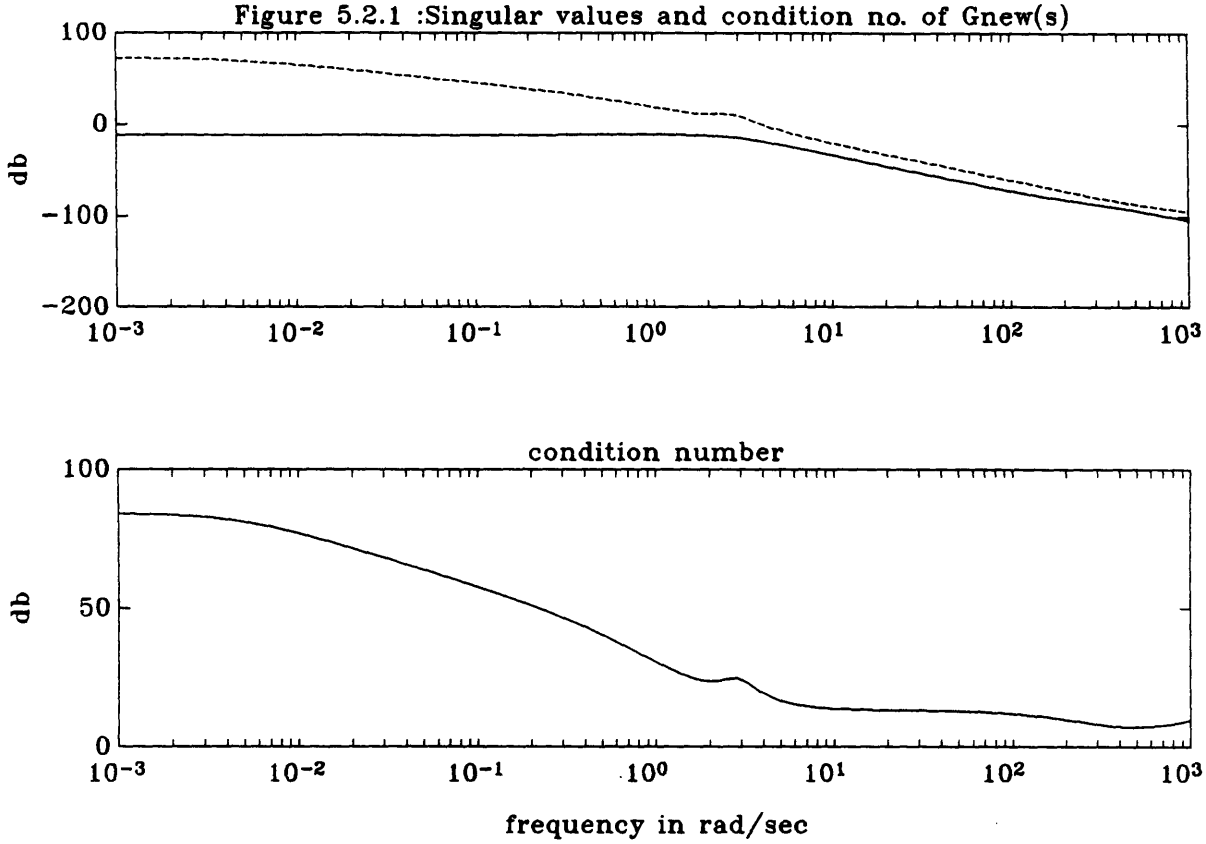

Figure 5.2.2 :Singular values of Tnew(s) = Gnew(s)Knew(s)

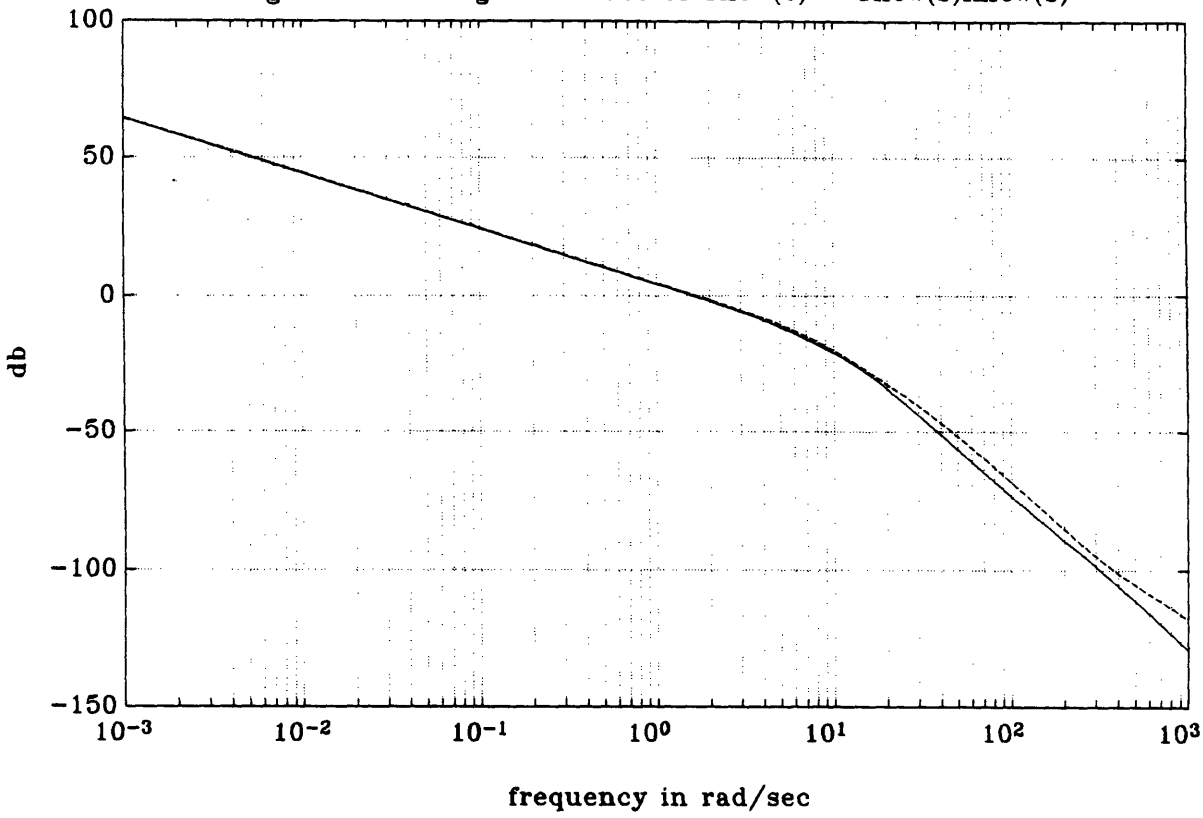

Figure 5.2.3 :Singular values of Snew(s)

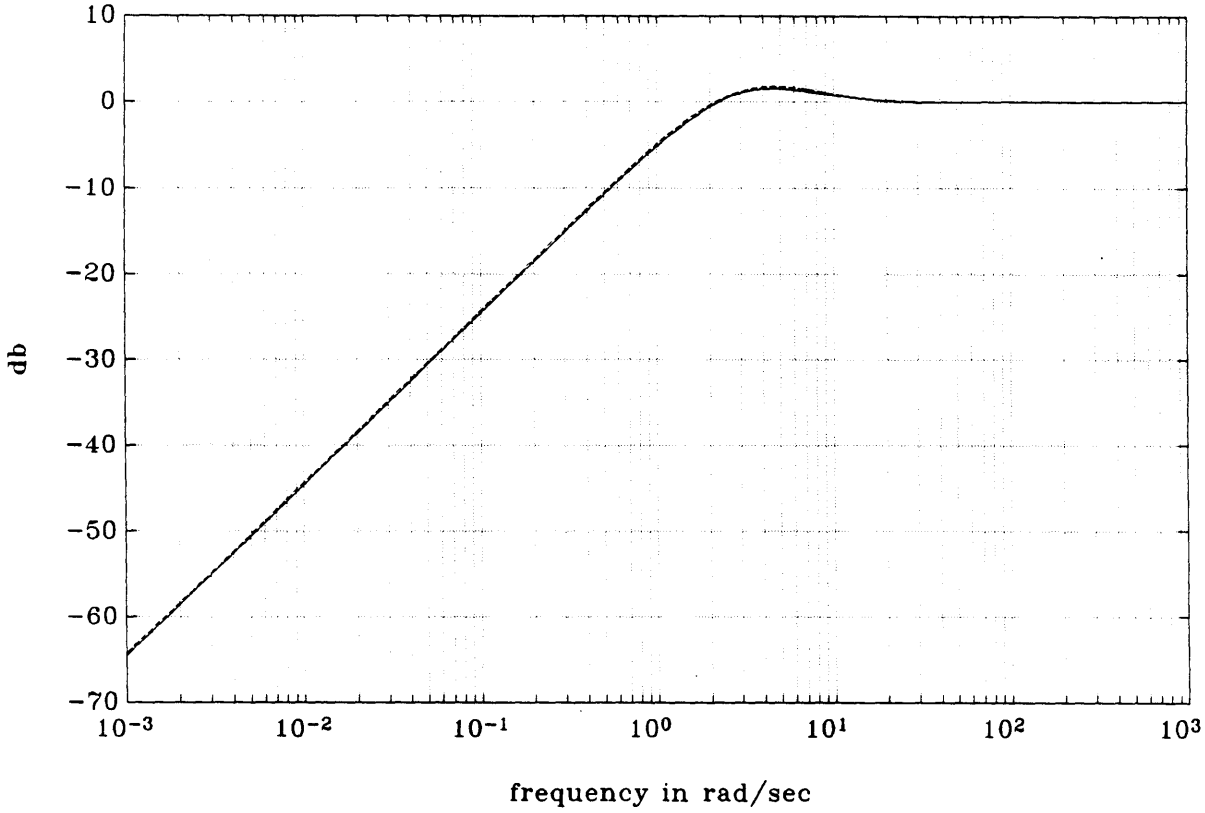

Figure 5.2.4 :Singular values of Cnew(s)

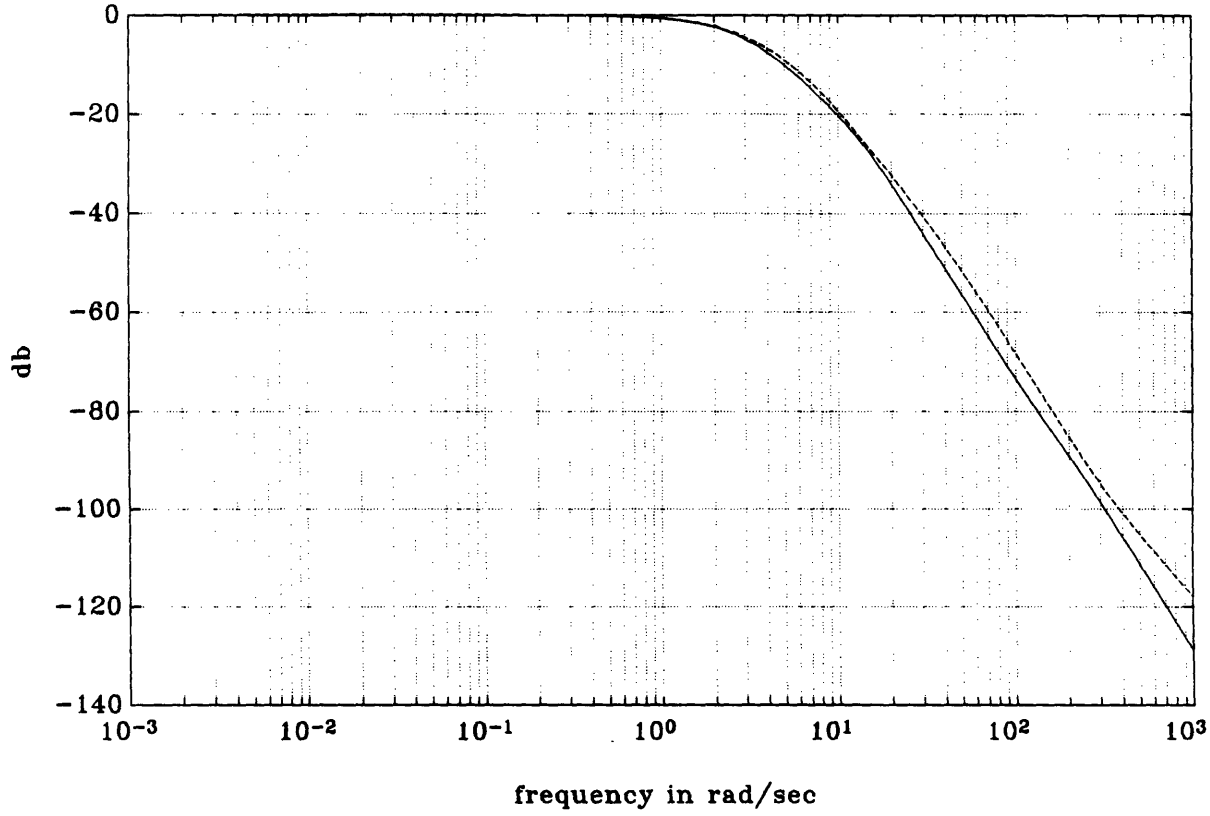

Figure 5.2.5 :% error in the maximum singular value of Gnew(s)

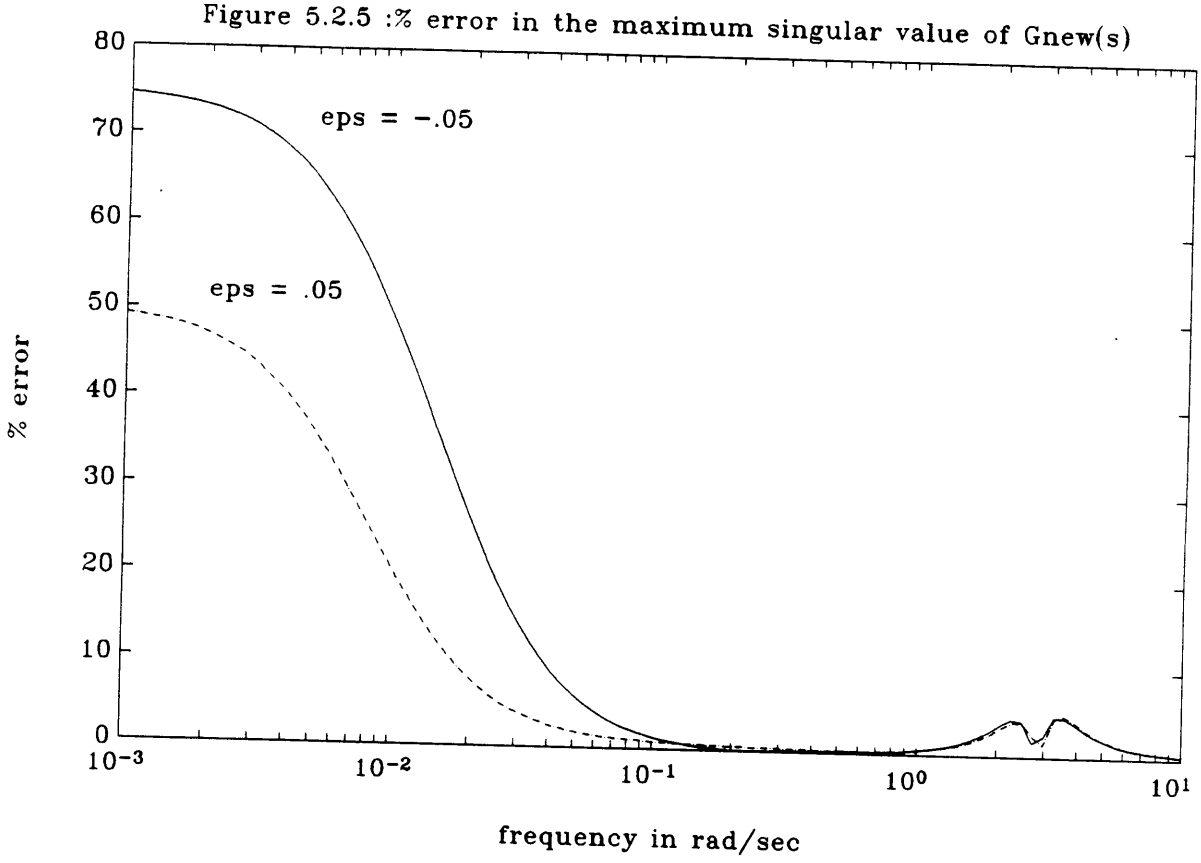

Figure 5.2.6 :eps vs. real part of Gnew(s)'s poles in Cnew(s)

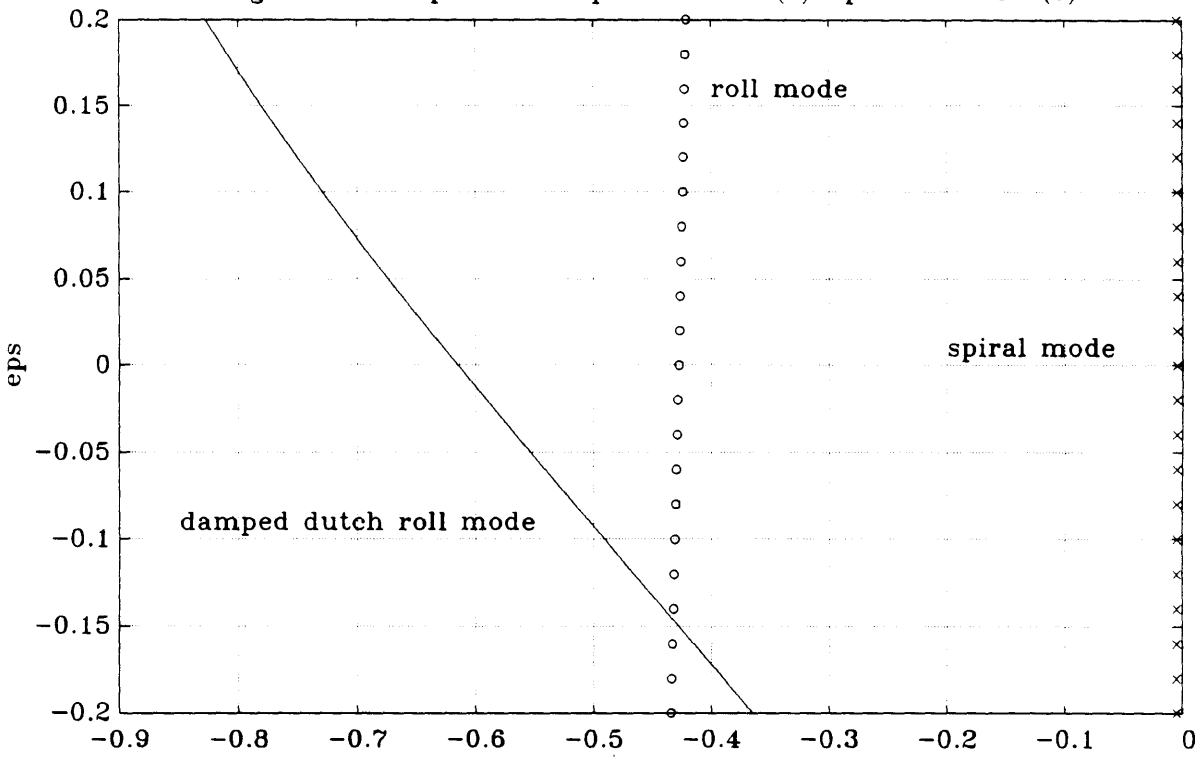

Figure 5.2.7 :Singular values of Cnew(s)

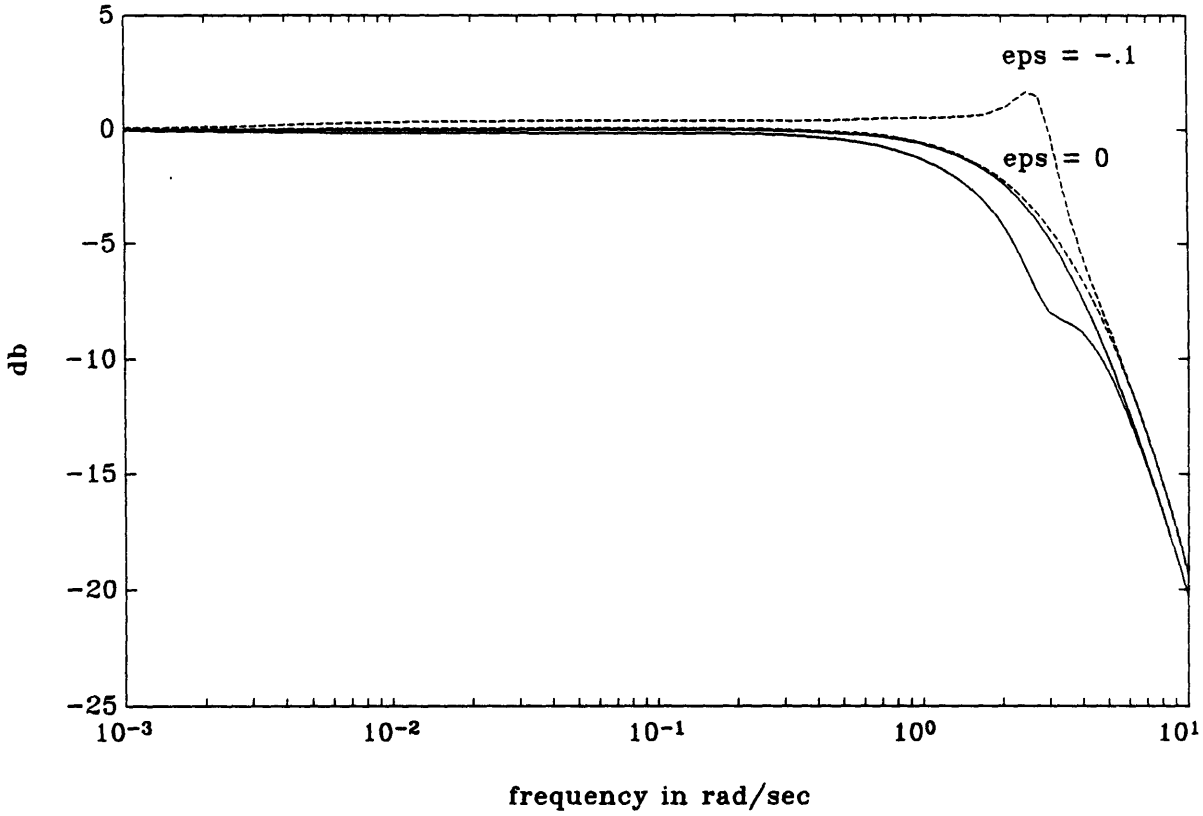

Figure 5.2.8 :Singular values and condition no. of Gnew(s)

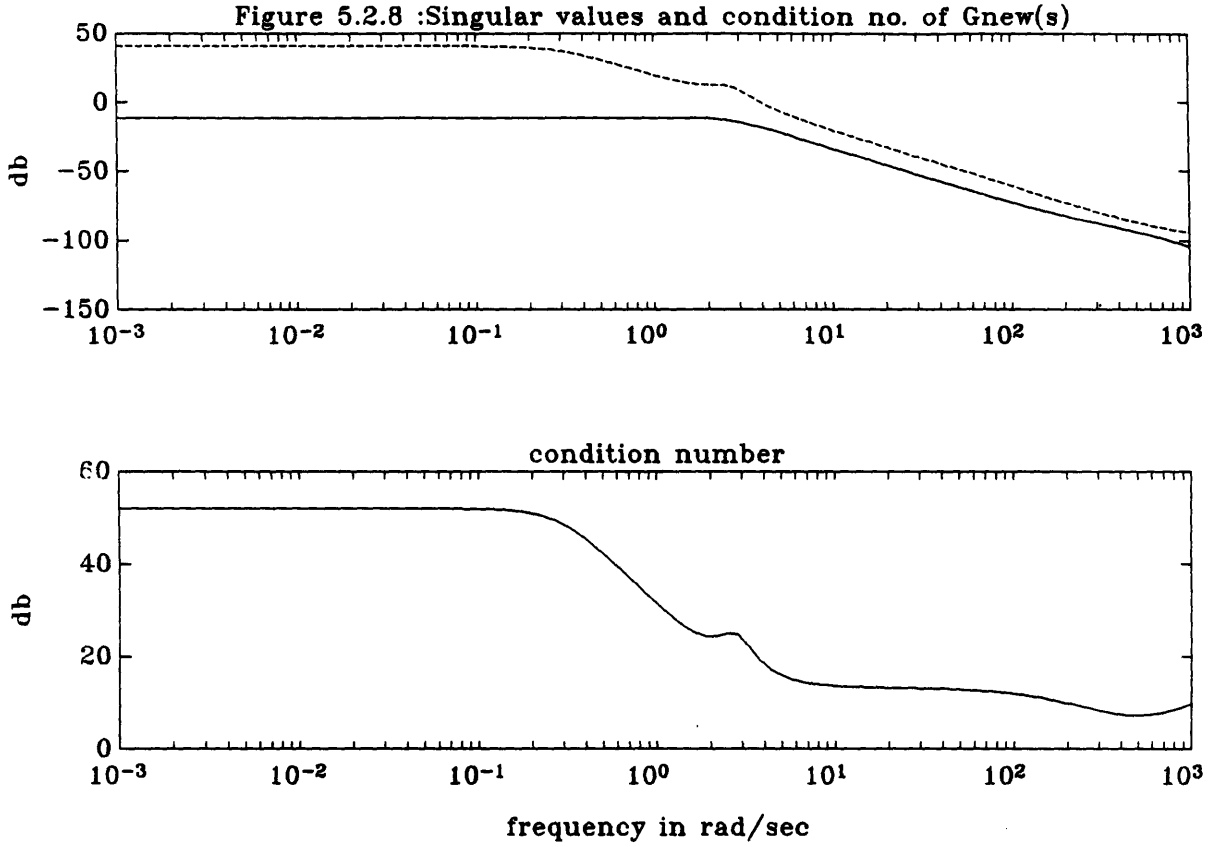

Figure 5.2.9 :Singular values of Tnew(s) = Gnew(s)Knew(s)

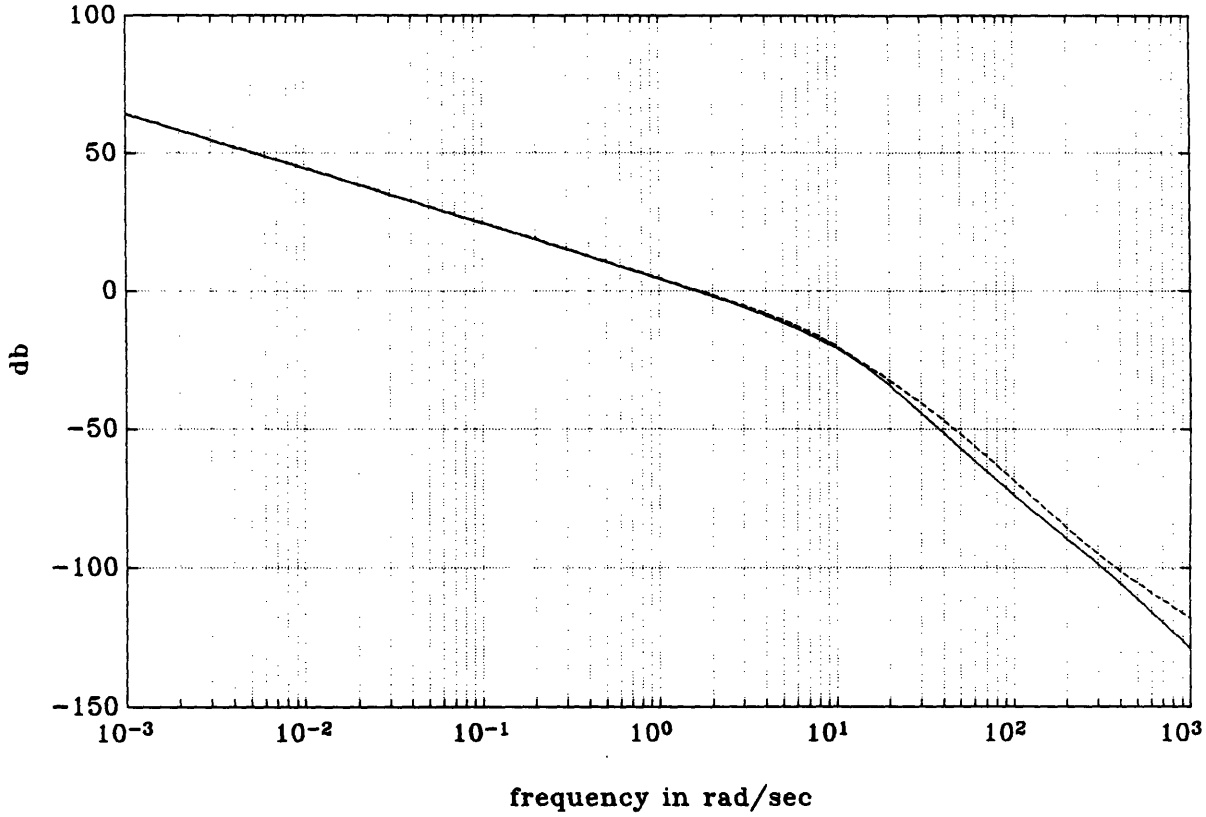

Figure 5.2.10 :Singular values of Snew(s)

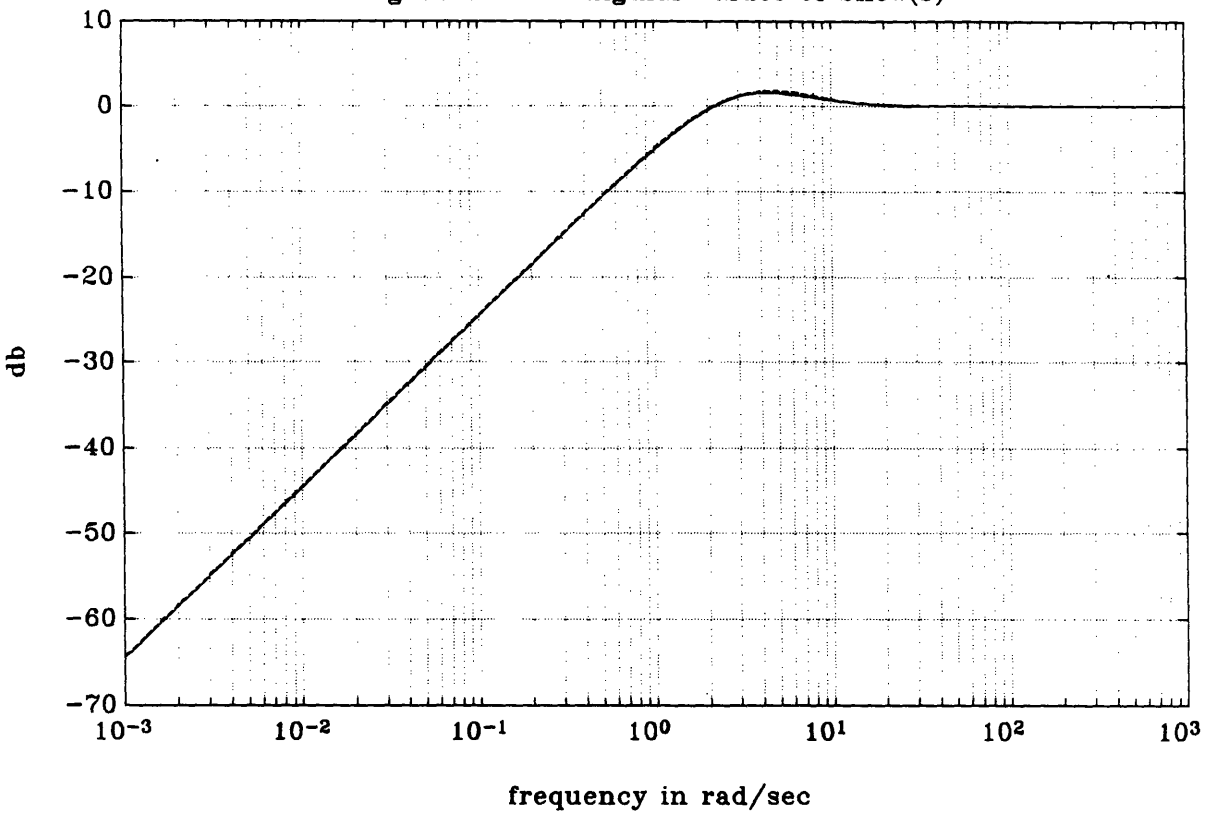

Figure 5.2.11 :Singular values of Cnew(s)

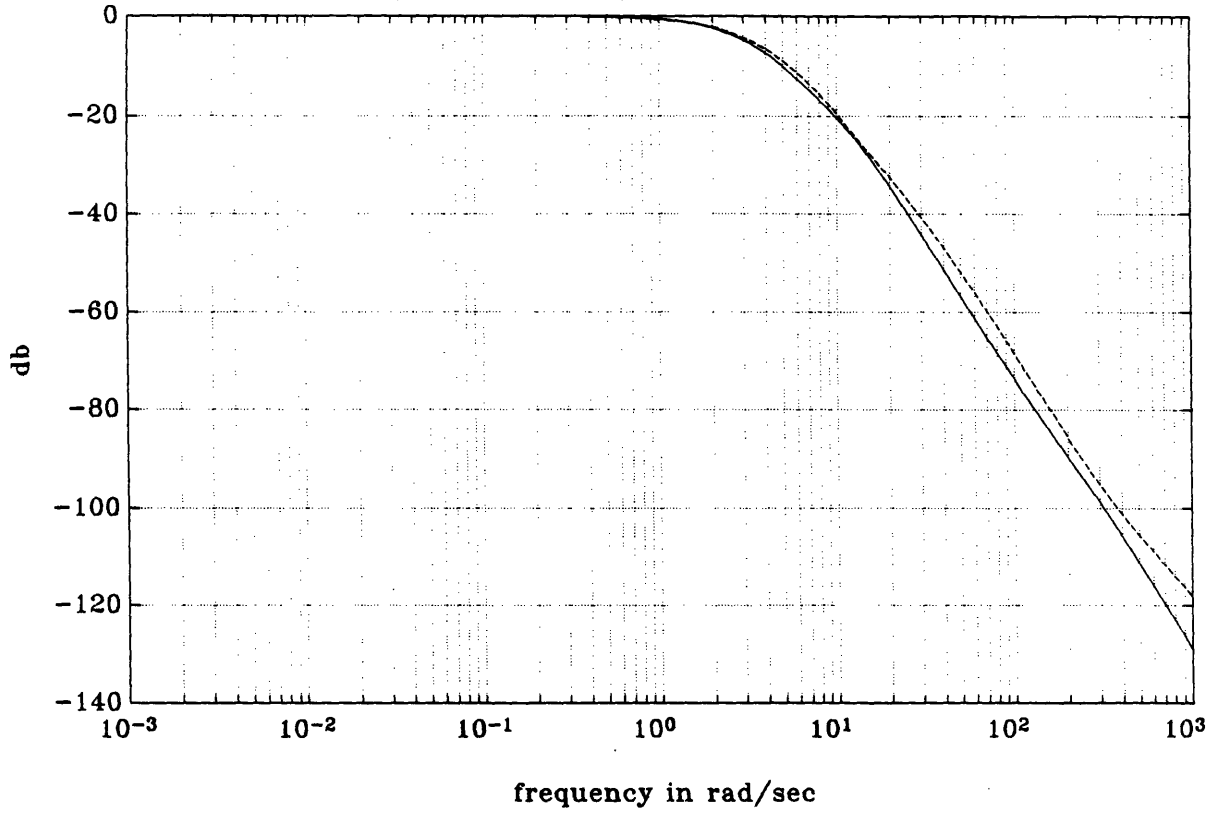

Figure 5.2.12 :% error in the maximum singular value of Gnew(s)

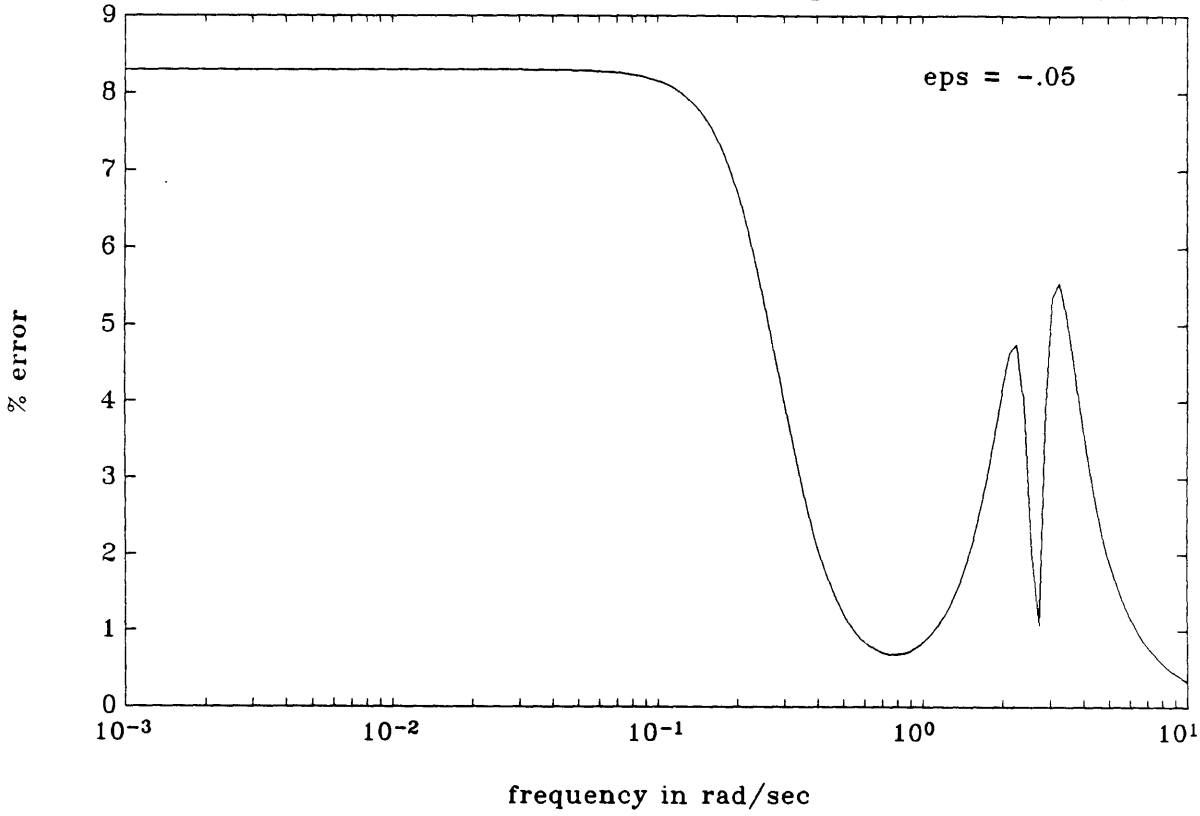

Figure 5.2.13 :Singular values of Cnew(s)

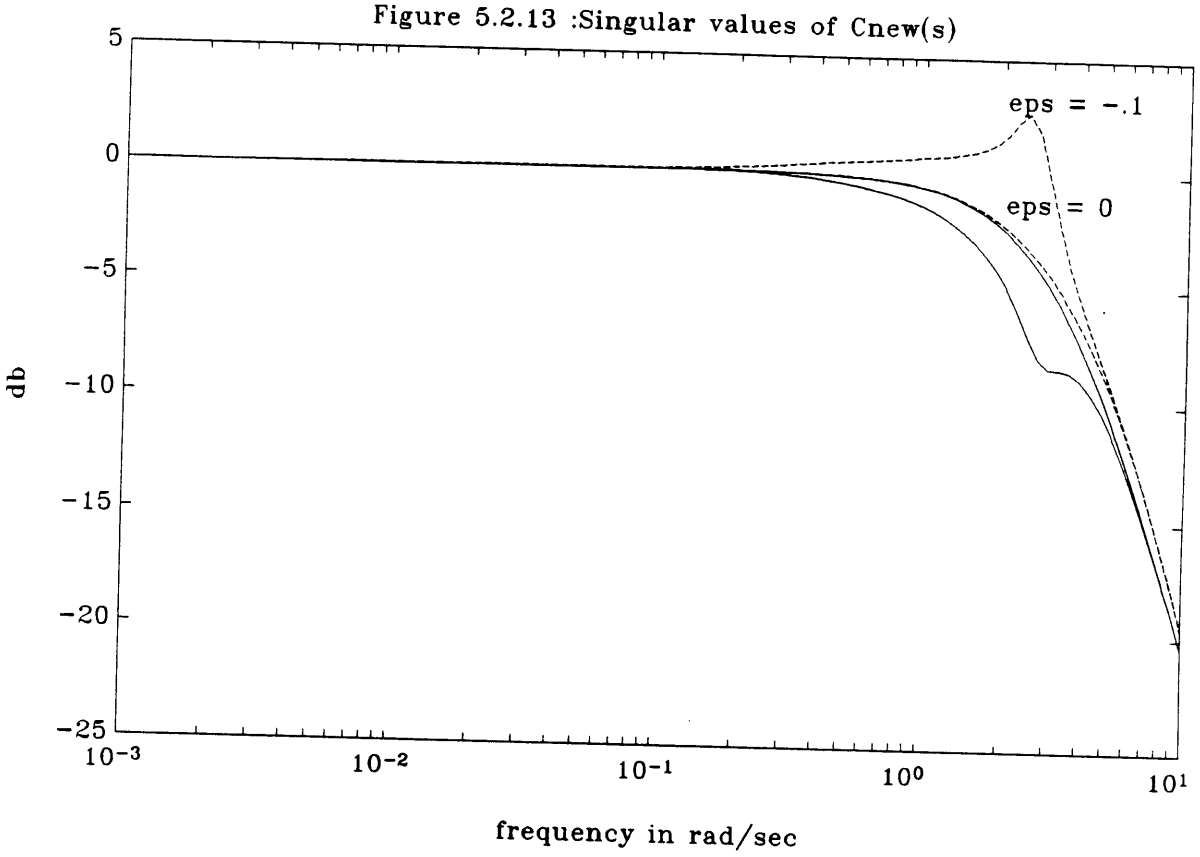

Figure 5.3.2 :Closed loop frequency response of the 2 compensators

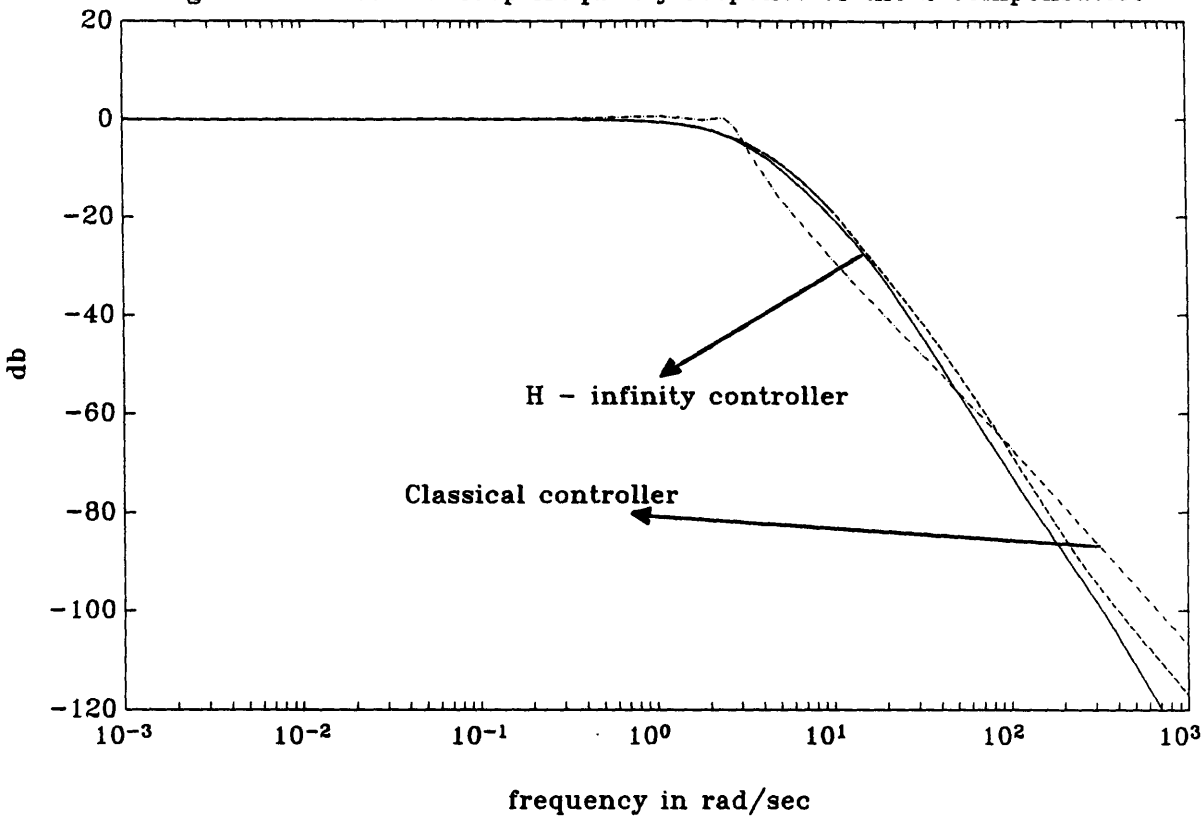

Figure 5.3.3 :Response to unit step in bank angle – classical comp.

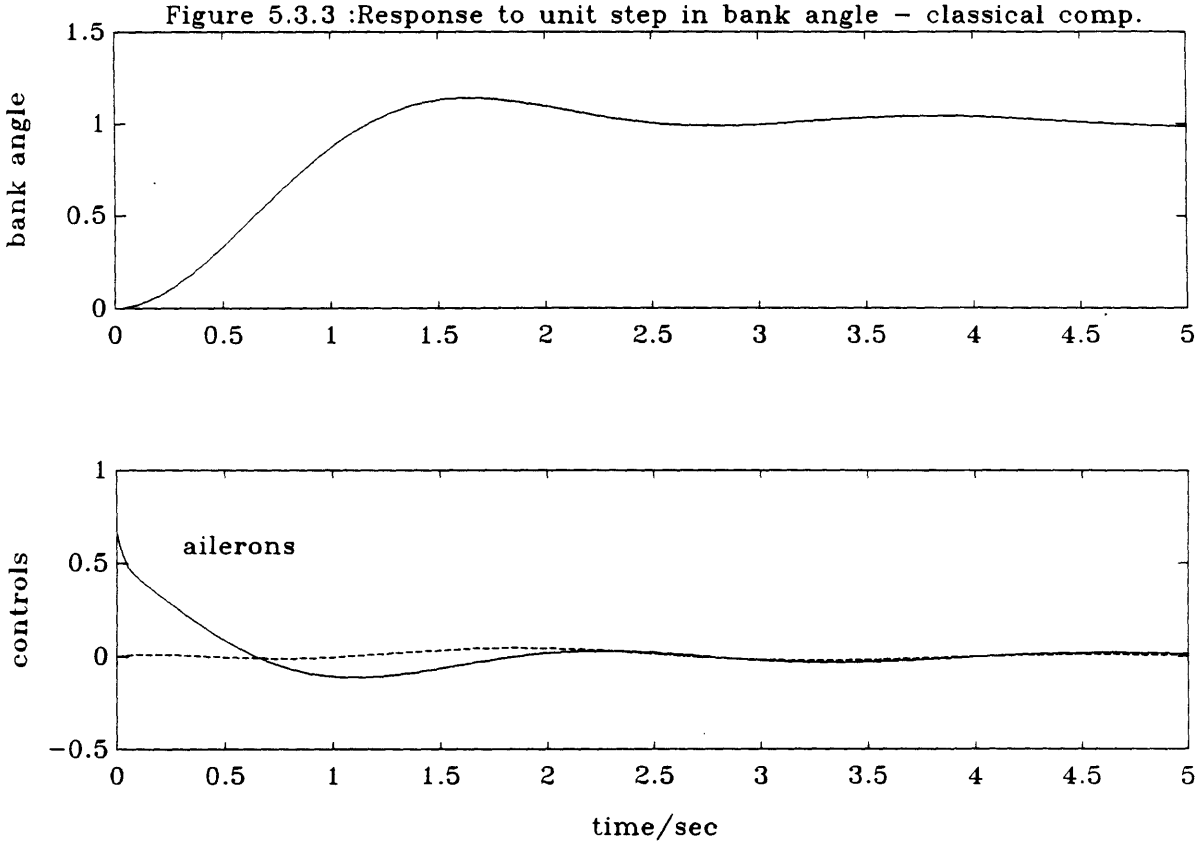

Figure 5.3.4 :Response to unit step in bank angle - H-inf comp.

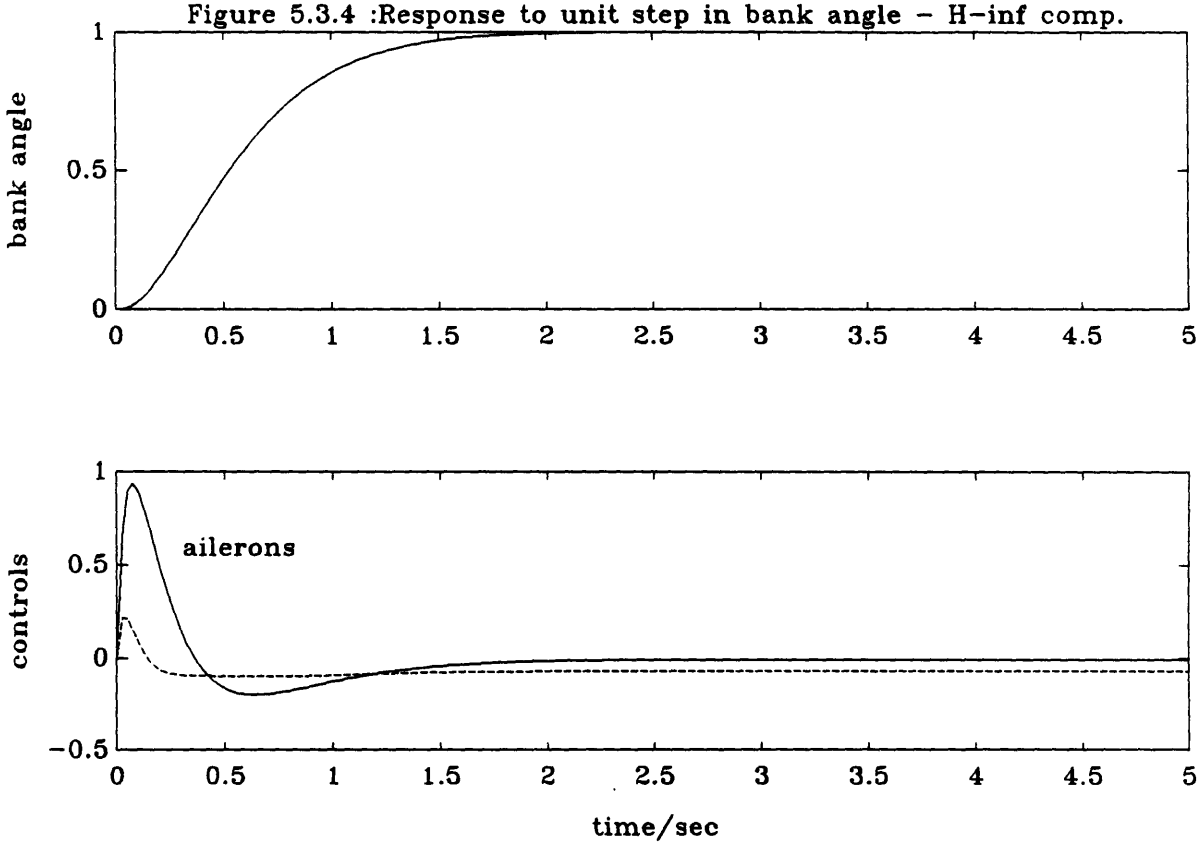

Figure 5.3.5 :Command following capabilities of the 2 controllers

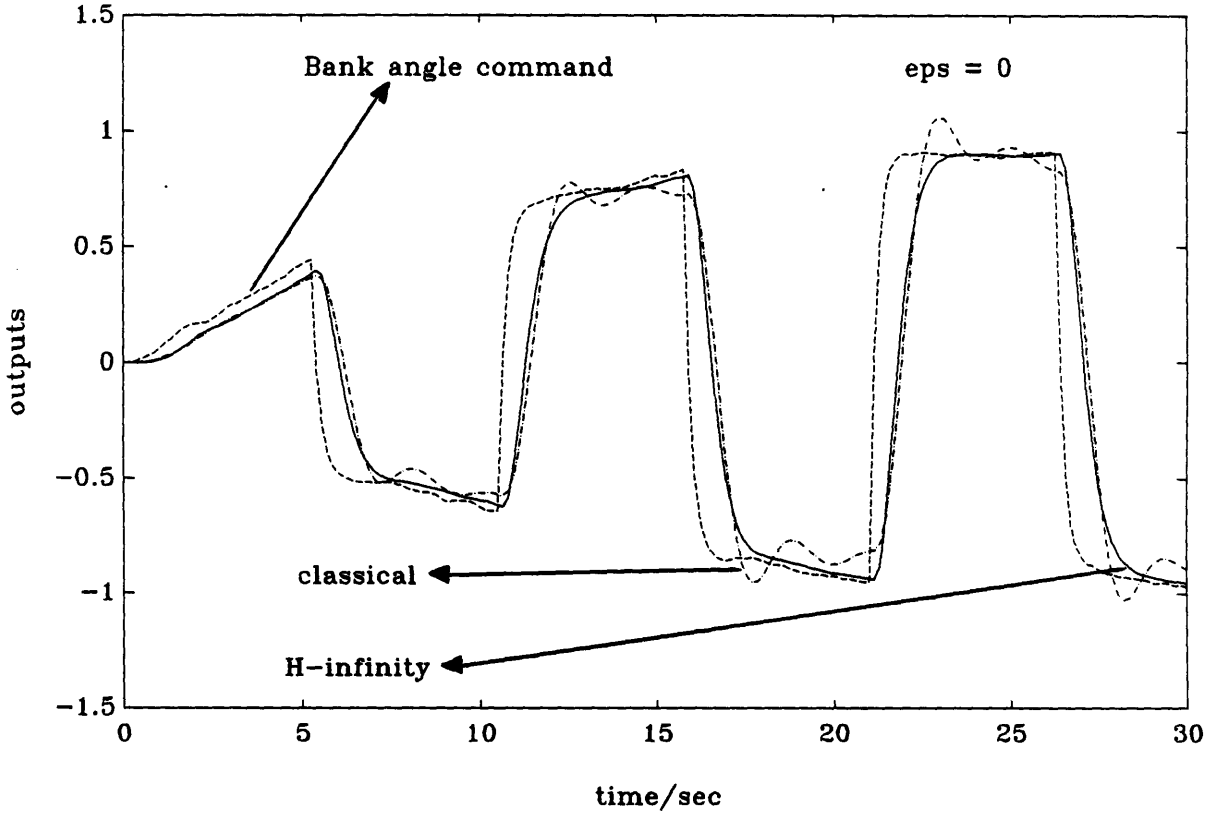

Figure 5.3.6 :Response of controls to command input: H−inf controller

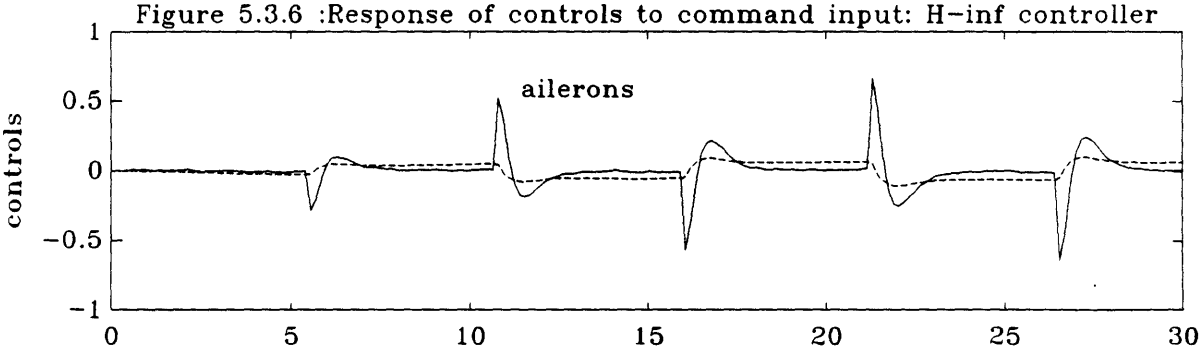

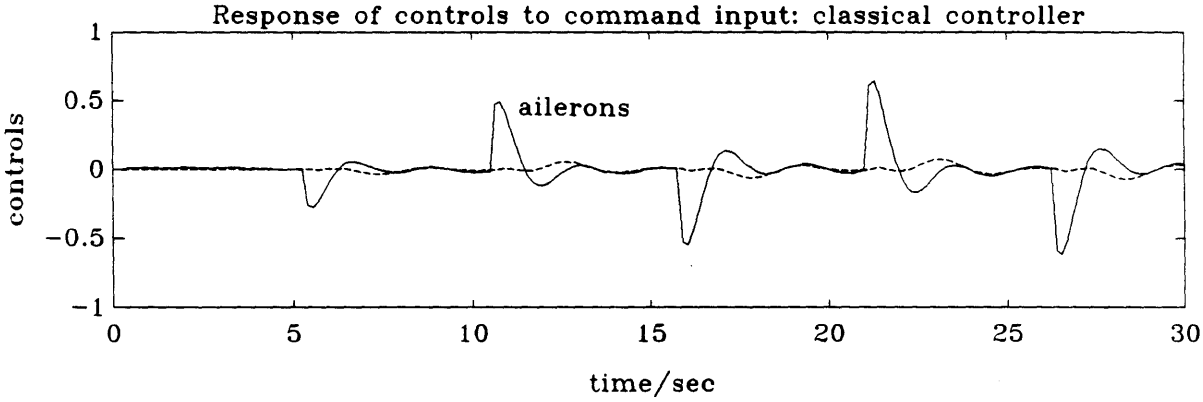

Figure 5.3.7 :Command following capabilities of the 2 controllers

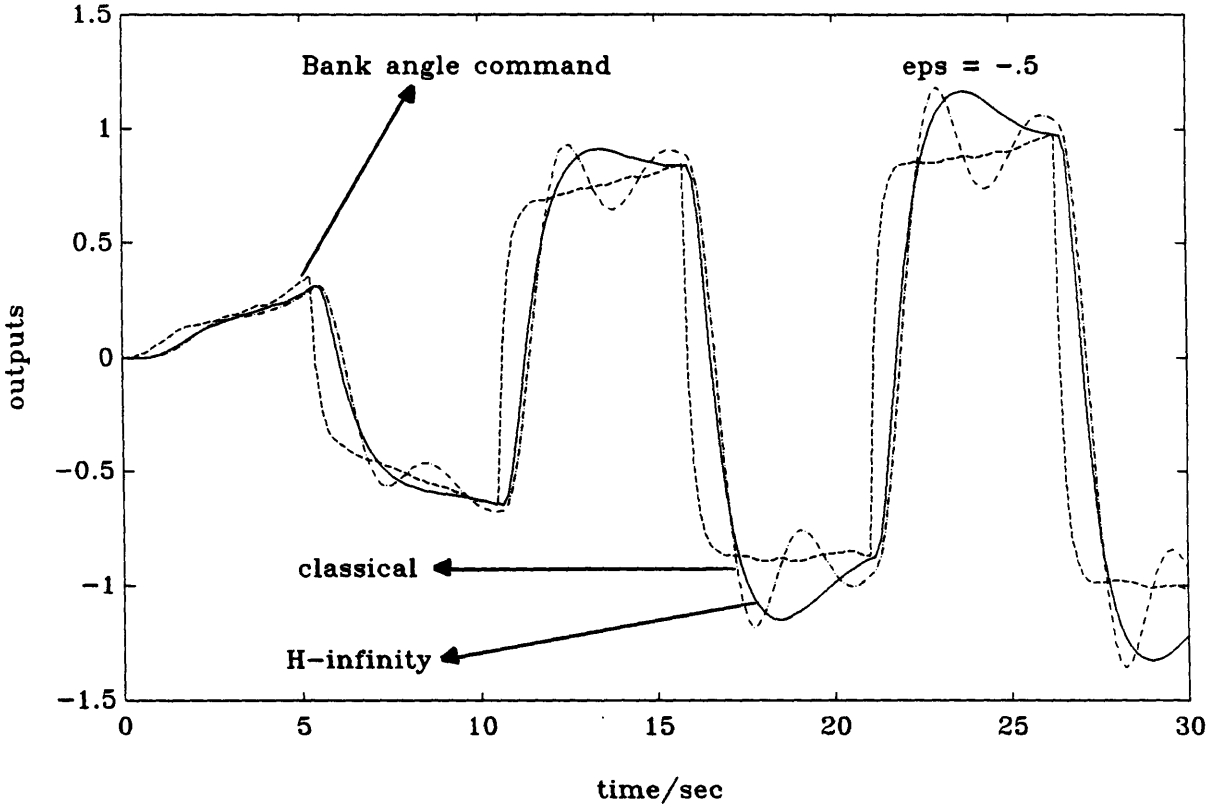

Figure 5.3.8 :Response of controls to command input: H−inf controller

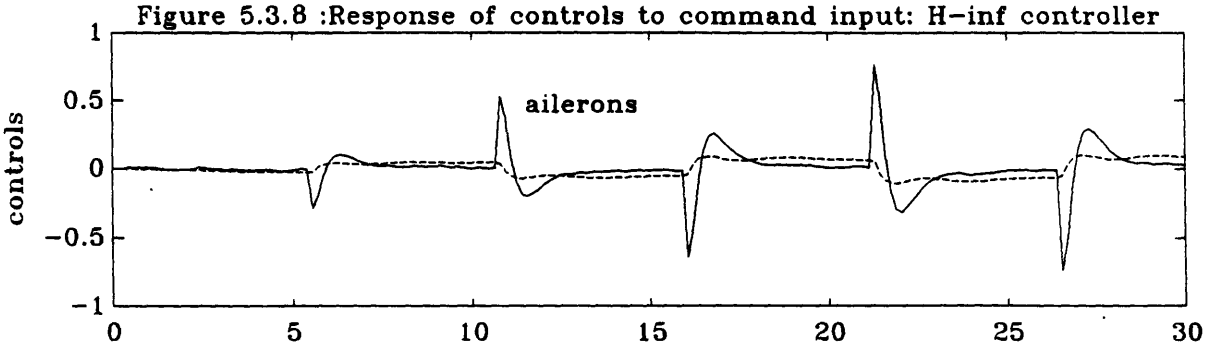

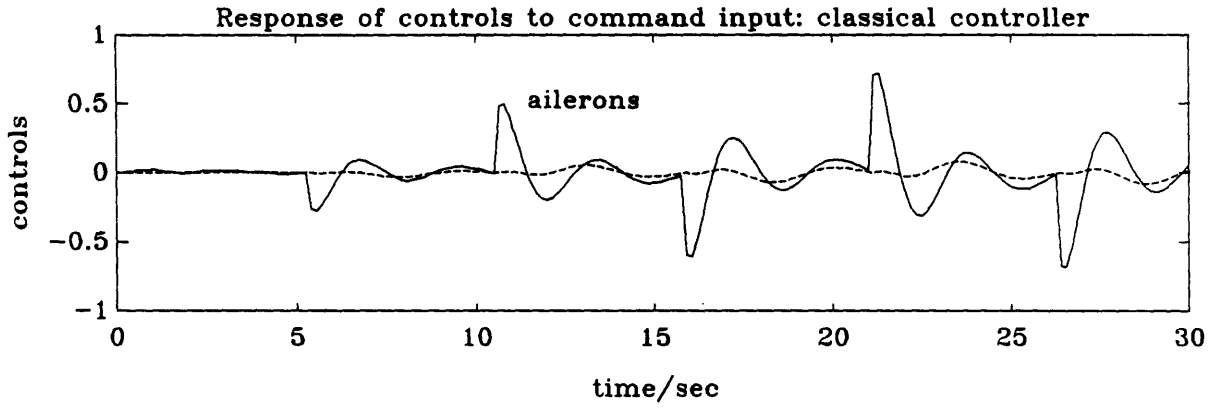

Figure 5.3.9 :Command following capabilities of the 2 controllers

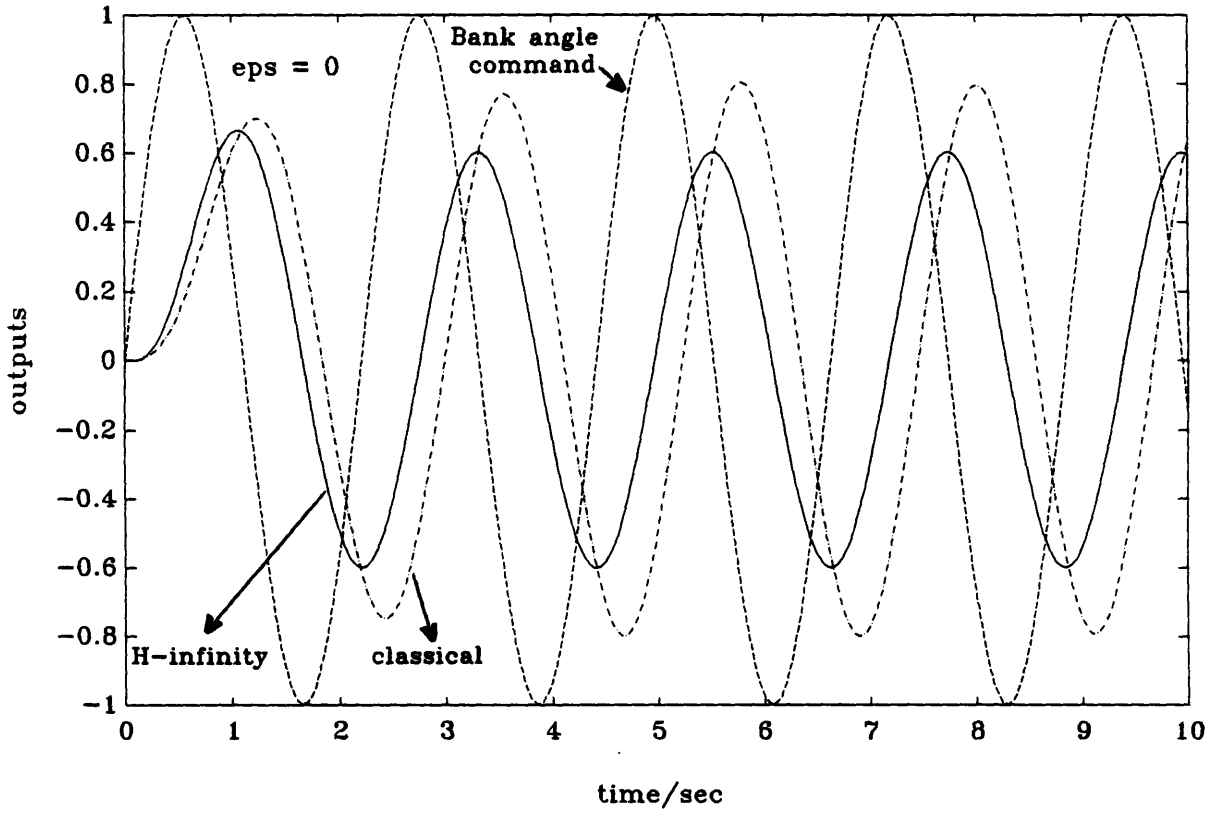

Figure 5.3.10:Response of controls to command input: H−inf controller

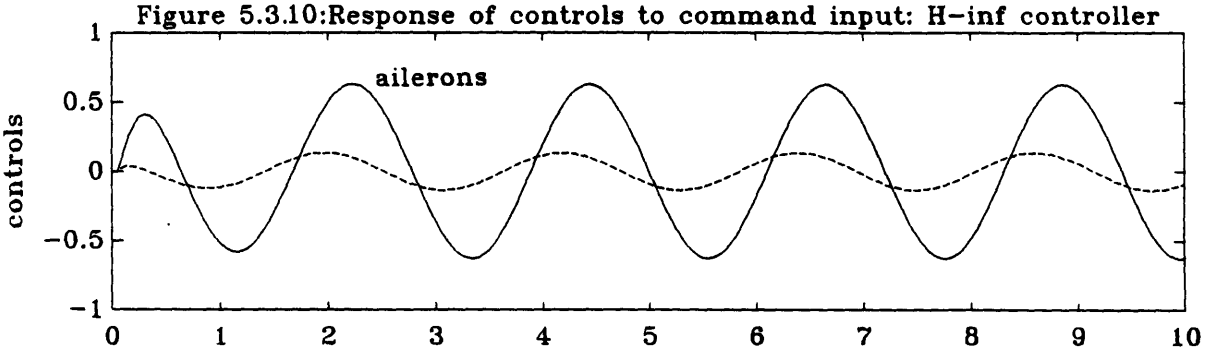

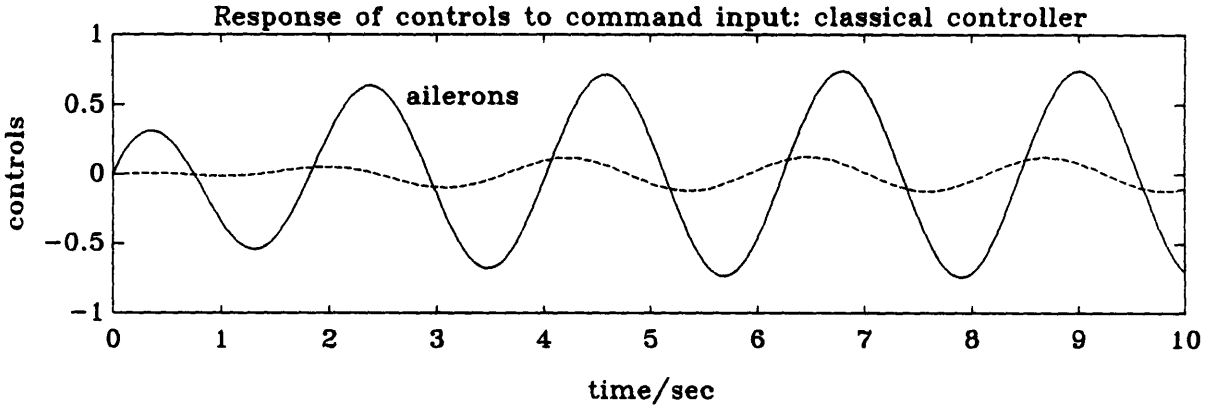

Figure 5.3.11 :Command following capabilities of the 2 controllers

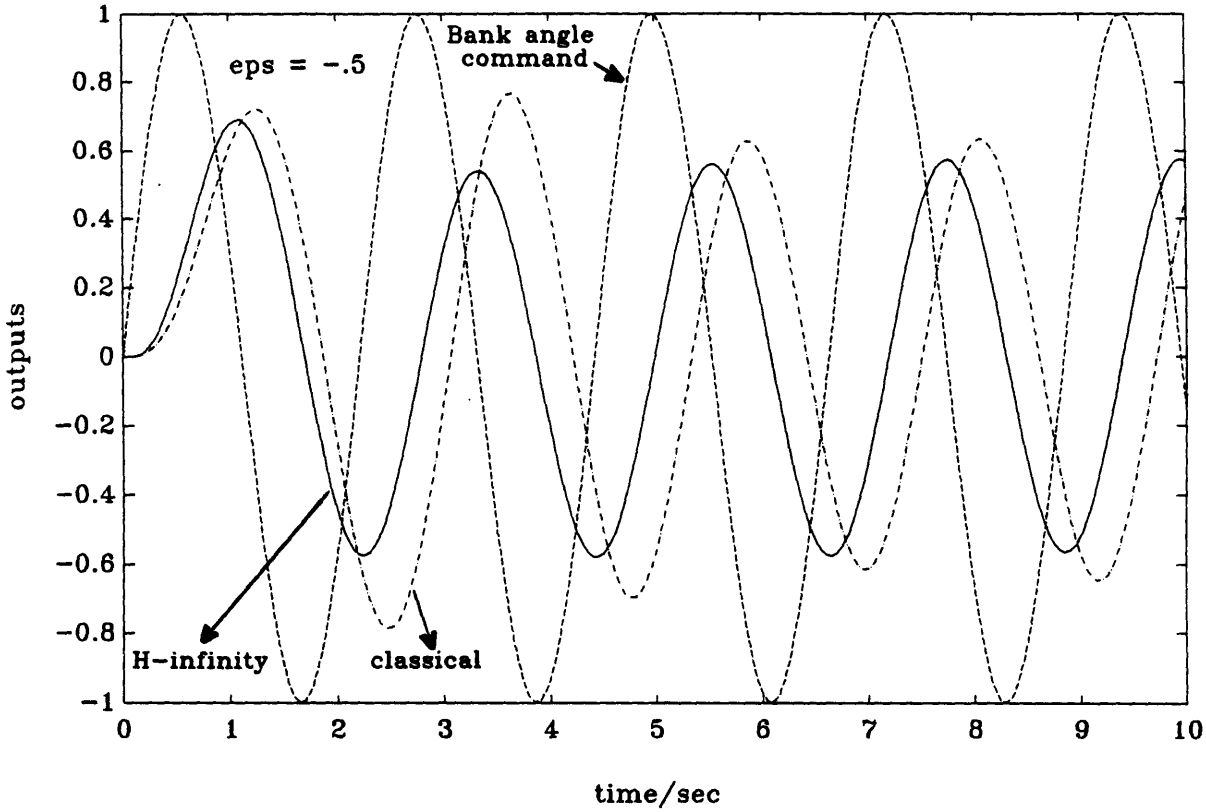

Figure 5.3.12 :Response of controls to command input: H-inf controller

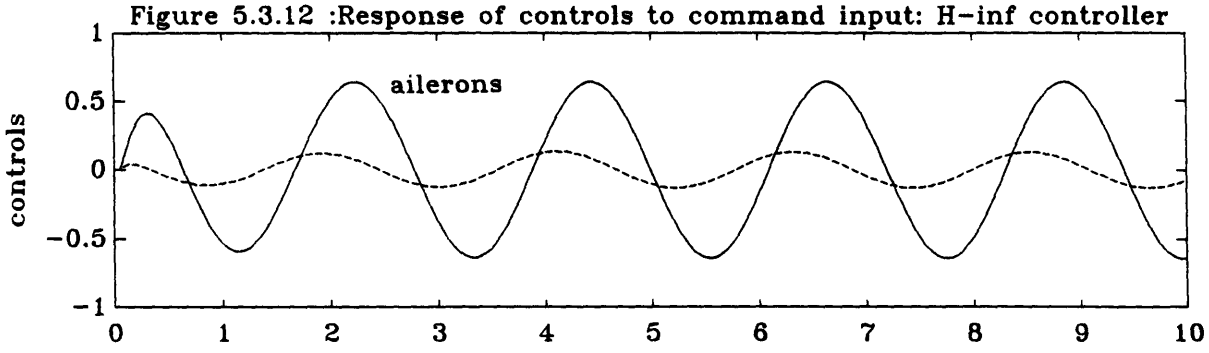

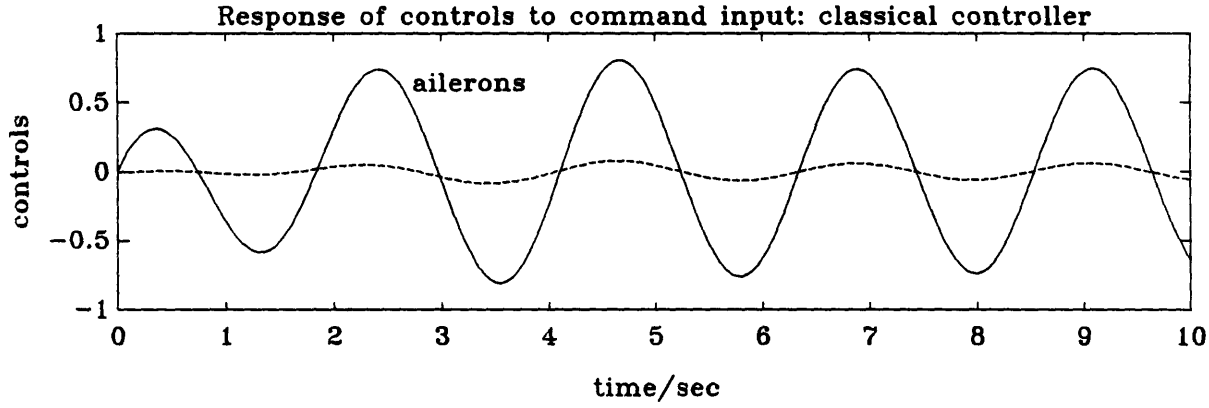

CHAPTER 6

CONCLUSIONS AND FUTURE RESEARCH

6.1 Conclusions

In this thesis the H_∞ design methodology was applied to two "realistic" plants, an advanced fighter aircraft and a milling circuit. It was shown that, while the milling circuit closed loop system is robust to structured uncertainty, the aircraft closed loop system is extremely sensitive to such uncertainty due to the very lightly damped dutch roll mode of the plant. The reason for this is that the H_∞ compensator cancels the lightly damped pole pair with zeros to make them unobservable. When structured uncertainty is present, the lightly damped poles are not canceled exactly and thus become observable, causing performance degradation and, in addition, due to the fact that they are so close to the $j\omega$ – axis, instability can result for relatively small perturbations of the plant A matrix.

It was shown that H_∞ designs for plants with unstable poles and nonminimum phase zeros, are reasonably insensitive to structured uncertainty, unless there is an approximate unstable pole zero cancellation. In the latter case, H_∞ designs delivered very bad performance and were extremely sensitive to structured uncertainty. A relocation of plant sensors and actuators is a possible solution to this problem.

It was shown that the control system designer can determine, before an actual H_∞ design is done, whether the resulting closed loop system will be sensitive to structured uncertainty by studying the singular values of the design plant model.

A practical way of desensitizing H_∞ designs to structured uncertainty, called inner loop compensation, was given in Chapter 5. The idea is to close an inner loop around the plant to increase the damping of lightly damped pole pairs. This inner loop compensated plant acts as the new design plant model for which an H_∞ compensator is then designed. Resulting designs were shown to be robust to structured uncertainty.

A classical controller for the aircraft was compared to an H_∞ controller with inner loop compensation. Classical methods have traditionally been used for the design of flight control systems for fighter aircraft, largely because such controllers deliver adequate performance and are very robust to structured uncertainty. In this thesis, it was shown that H_∞ controllers with inner loop compensation can be made as robust to structured uncertainty as their classical counterparts, while delivering slightly better performance. LQG/LTR controllers with inner loop compensation should give similar results.

Furthermore, the H_∞ design methodology was shown to be a very powerful multivariable design technique. The ease with which frequency specifications can be accommodated in the design procedure, and the fact that H_∞ controllers can be made robust to structured uncertainty, makes this design method a tool that every control engineer should have in his/her toolbox.

6.2 Directions for Future Research

In this thesis structured uncertainty was indirectly incorporated in the H_∞ design methodology. Research should be done on how to include this uncertainty into the design methodology directly. The structured singular value introduced by Doyle [23,12] is a step towards this goal.

The H_∞ compensator design for the advanced fighter aircraft addressed only one operating point in the lateral control problem. H_∞ compensators should be designed for different flight conditions and a global controller could be constructed using gain scheduling ideas [24].

In the design of an H_∞ controller for the milling circuit, weighting functions were chosen which gave rise to different time responses for the milling circuit outputs. Research could be done to find a way to incorporate time domain specifications directly into the H_∞ design framework.

The ultimate success of a design methodology lies in its acceptance by the control engineering community. To this end, the H_∞ design methodology should be applied to many more practical problems such that the "average" control engineer becomes familiar with its use.

APPENDIX A

ABSORBING THE IMPROPER WEIGHT $W_3(s)$ INTO THE PLANT G(s)

In this appendix, the state space description of the transfer function matrix $W_3(s)$ G(s), will be derived. $W_3(s)$ is assumed to be an improper diagonal weighting function, and G(s) a strictly proper transfer function.

A.1 Mathematical Preliminaries

1 **Theorem :** Suppose that the n x n matrix A has n distinct eigenvalues λ_i and n linearly independent eigenvectors v_i. Now if v_i make up the columns of a matrix V, the matrix A can be expressed in terms of V, a diagonal matrix Λ, and V^{-1} as follows,

2 $$A = V \Lambda W$$

with

3 $$W = V^{-1}$$

The rows of W contains the left eigenvectors (w_i^T) of A and the eigenvalues of A can be found along the diagonal of Λ.

Proof see [13] page 190

4 **Remark :** From (1) it is evident that $A = \sum_{i=1}^{n} \lambda_i v_i w_i^T$

5 **Theorem :** For the same matrix A as described in (1), where A is assumed to be nonsingular, the following equations hold,

6 $$\sum_{i=1}^{n} v_i w_i^T = I_n$$

7 $$v_i w_i^T = A^{-1} \lambda_i v_i w_i^T$$

Proof From the definition of an eigenvector and an eigenvalue follows that

8 $$A\, v_i = \lambda_i v_i$$

now multiply (8) from the right with w_i and summing over i,

$$A \sum_{i=1}^{n} v_i w_i^T = \sum_{i=1}^{n} \lambda_i v_i w_i^T$$

9 $$= A$$

(9) follows from (4) and implies that (6) is true.

To prove (7), just multiply (8) from the left by A^{-1} and from the right by w_i^T.

A.2 The State Space Description Of $W_3(s)\ G(s)$

The m x m transfer function G(s) can be expressed as

10 $$G(s) = C\ (sI_n - A)^{-1}\ B$$

with

$$A\ v_i = \lambda_i v_i$$

$$w_i^T\ A = \lambda_i w_i^T$$

as described in section A.1. G(s) can also be written in a residue expansion form as follows,

11 $$G(s) = \sum_{i=1}^{n} \frac{R_i}{s - \lambda_i}$$

with

$$R_i = C\ v_i w_i^T\ B$$

With $W_3(s) = \frac{s}{k} I_m$, the product $W_3(s)\ G(s)$ becomes,

12 $$W_3(s)\ G(s) = \frac{1}{k} \sum_{i=1}^{n} \frac{R_i\ s}{s - \lambda_i}$$

Applying partial fraction expansion to each term in the sum in (12) gives,

$$W_3(s)\,G(s) = \frac{1}{k}\sum_{i=1}^{n}\left[\frac{\lambda_i\, R_i}{s-\lambda_i} + R_i\right]$$

13
$$= \frac{1}{k}C\left[\sum_{i=1}^{n}\frac{\lambda_i v_i w_i^T}{s-\lambda_i} + \sum_{i=1}^{n} v_i w_i^T\right]B$$

now letting results (7) and (6) from (5) act on the first and second summations of (13) respectively, it follows that,

14
$$W_3(s)\,G(s) = \frac{1}{k}\left[CA\sum_{i=1}^{n}\frac{v_i w_i^T}{s-\lambda_i}B + CB\right]$$

15
$$= \frac{1}{k}\left[CA\,(sI_n - A)^{-1}B + CB\right]$$

The new C and D matrices of the state space description for the transfer function shown in (15), are given by,

$$C_{new} = \frac{1}{k}CA$$

$$D_{new} = \frac{1}{k}CB$$

The A and B matrices of the plant stay intact. This concludes the derivation of the state space description of $W_3(s)\,G(s)$.

APPENDIX B

AIRCRAFT EXAMPLE

In this appendix the aircraft's equations of motion are given in terms of the flight condition and aircraft stability derivatives. Nomenclature used, is given in section B.3. State space descriptions for the augmented plant and the H_∞ compensator, are given in section B.4. Section B.5 contains a controllability/observability study of the closed loop system of section 3.3.3. Numerical data that relates to the full state feedback inner loop design of section 5.2.1.1 is given in section B.6. The state space description of the classical compensator of section 5.3.1.1 is given in section B.7.

B.1 Flight Conditions

The flight condition used in this example is given by straight and level flight at,

mach number $M = 0.6$

altitude $= 35{,}000$ ft

true speed $V_{T_0} = 584$ fps

trim angle of attack $\alpha_0 = 12.4$ deg (body axis)

flight path angle $\gamma_0 = 0$ deg

load factor $n_0 = 1$ g

B.2 Equations Of Motion

The lateral equations of motion given here are for straight, wing level, horizontal flight. The equations are expressed in arbitrary body fixed axis and results in the following state space description.

$$\dot{x} = A\,x + B\,u$$

$$y = C\,x$$

with

$$x = (\beta,\ p_s,\ r_s,\ \phi_s)^T$$

$$u = (\delta_a,\ \delta_r)^T$$

$$y = (\phi_b,\ \beta)^T$$

and

$$A = \begin{bmatrix} Y_v \sin\alpha_o & -\cos\alpha_o & \dfrac{g\cos\theta_o}{V_{To}} \\ L'_\beta & L'_p & L'_r & 0 \\ N'_\beta & N'_p & N'_r & 0 \\ 0 & 1 & \tan\theta_o & 0 \end{bmatrix}$$

$$B = \begin{bmatrix} Y^*_{\delta_a} & Y^*_{\delta_r} \\ L'_{\delta_a} & L'_{\delta_r} \\ N'_{\delta_a} & N'_{\delta_r} \\ 0 & 0 \end{bmatrix}$$

$$C = \begin{bmatrix} 0\ 0\ 0 & \dfrac{1}{\cos\theta_{ob}} \\ 1\ 0\ 0 & 0 \end{bmatrix}$$

With $\alpha_o = \theta_o = 0$, and $\theta_{ob} = 12.4$ deg, the state space matrices for the stability axis are given by,

$$A = \begin{bmatrix} -.0868 & 0 & -1 & .055 \\ -31.31 & .1340 & 2.352 & 0 \\ 7.971 & -.0879 & -.5890 & 0 \\ 0 & 1 & 0 & 0 \end{bmatrix}$$

$$B = \begin{bmatrix} 0 & .0179 \\ 6.569 & 6.251 \\ .3064 & -2.583 \\ 0 & 0 \end{bmatrix}$$

$$C = \begin{bmatrix} 0 & 0 & 0 & 1.024 \\ 1 & 0 & 0 & 0 \end{bmatrix}$$

B.3 Nomenclature

s	stability axis
b	body axis
β	side slip angle (deg)
p	roll rate (deg/sec)
r	yaw rate (deg/sec)
ϕ	roll angle (deg)
δ_a	aileron deflection from trim (deg)
δ_r	rudder deflection from trim (deg)
Y_v	resultant aerodynamic force (1/sec)
L	rolling moment

N	yawing moment
α_o	trim angle–of–attack (deg)
θ_o	trim pitch angle (deg)

B.4 State Space Descriptions

Let the plant and weights have state space descriptions as given in equation 3.4.4 (section 3.4). The augmented plant can then be described as follows.

$$A = \begin{bmatrix} A_p & 0 \\ -B_{w1}C_p & A_{w1} \end{bmatrix}$$

$$[B1 \mid B2] = \left[\begin{array}{c|c} 0 & B_p \\ B_{w1} & -B_{w1}D_p \end{array}\right]$$

$$\left[\frac{C1}{C2}\right] = \left[\begin{array}{cc} -D_{w1}C_p & C_{w1} \\ 0 & 0 \\ C_{new} & 0 \\ \hline -C_p & 0 \end{array}\right]$$

$$\left[\begin{array}{c|c} D_{11} & D_{12} \\ \hline D_{21} & D_{22} \end{array}\right] = \left[\begin{array}{c|c} D_{w1} & -D_{w1}D_p \\ 0 & D_{w2} \\ 0 & D_{new} \\ \hline I & -D_p \end{array}\right]$$

with C_{new} and D_{new} as derived in Appendix A.

The state space description of the H_∞ compensator is,

$$K(s) = \left[\begin{array}{c|c} A_k & B_k \\ \hline C_k & D_k \end{array}\right]$$

with

$$A_{k1} = \begin{bmatrix} -6.8404e{-}01 & -3.7683e{-}02 & -8.8967e{-}01 \\ -2.6972e{+}01 & -4.1531e{+}01 & 4.2523e{+}00 \\ 1.0408e{+}02 & 4.0203e{+}00 & -1.8219e{+}01 \\ -3.8345e{-}05 & 1.0000e{+}00 & -2.3657e{-}08 \\ 0 & 0 & 0 \\ 0 & 0 & 0 \end{bmatrix}$$

$$A_{k2} = \begin{bmatrix} -1.5726e{-}01 & 3.4197e{-}01 & 1.1150e{+}00 \\ -2.3326e{+}02 & 3.7680e{+}02 & 4.9125e{+}01 \\ 2.3199e{+}01 & -3.7342e{+}01 & -1.7676e{+}02 \\ -9.7435e{-}03 & 1.2278e{-}08 & 4.0030e{-}08 \\ 0 & -1.0000e{-}04 & 0 \\ 0 & 0 & -1.0000e{-}04 \end{bmatrix}$$

$$A_k = \begin{bmatrix} A_{k1} & A_{k2} \end{bmatrix}$$

$$B_k = \begin{bmatrix} -3.9238e{-}05 & -1.5801e{-}07 \\ -4.6361e{-}05 & -1.8670e{-}07 \\ -5.1979e{-}04 & -2.0932e{-}06 \\ -9.5161e{-}03 & -3.8322e{-}05 \\ 1.0000e{+}00 & 0 \\ 0 & 1.0000e{+}00 \end{bmatrix}$$

$$C_{k1} = \begin{bmatrix} 3.2411e{+}01 & -4.3393e{+}00 & -5.5762e{+}00 \\ -3.3365e{+}01 & -2.1052e{+}00 & 6.1638e{+}00 \end{bmatrix}$$

$$C_{k2} = \begin{bmatrix} -2.4228e{+}01 & 3.9180e{+}01 & -5.1795e{+}01 \\ -1.1856e{+}01 & 1.9104e{+}01 & 6.2288e{+}01 \end{bmatrix}$$

$$C_k = \begin{bmatrix} C_{k1} & C_{k2} \end{bmatrix}$$

$$D_k = \begin{bmatrix} 0 & 0 \\ 0 & 0 \end{bmatrix}$$

B.5 Controllability/Observability Study

An eigenstructure analysis [5] is done to determine if the closed loop system of section 3.3.3 is observable and controllable. Let D be a vector containing the poles of A_{cl} with V and W as defined in Appendix A, theorem (1). D is given by,

$$D = \begin{bmatrix} D_1 \\ D_2 \end{bmatrix}$$

with

$$D_1 = \begin{bmatrix} -3.5995e+01 \\ -8.7283e+00 \\ -6.3733e+00 \\ -5.9686e-02 \pm 2.8437e+00i \\ -3.1521e+00 \pm 1.0167e+00i \end{bmatrix}$$

$$D_2 = \begin{bmatrix} -4.2730e-01 \\ -3.0328e+00 \\ -4.8718e-03 \end{bmatrix}$$

Note that rows 4, 5, and 8 of D represent the closed loop poles which are at the same location as the stable plant poles.

Let B_{cl} and C_{cl} be the B and C matrices of the closed loop system respectively. To determine if the closed loop system is controllable and/or observable, the absolute values of each entry of the matrices $C_{cl}V$ and WB_{cl}, will be studied:

$$\text{abs}(C_{cl}V) = [\ Ob_1\ \ Ob_2\ ]$$

$$Ob_1 = \begin{bmatrix} 2.8446e{-}02 & 2.0192e{-}02 & 2.6290e{-}02 & 3.5998e{-}01 & 3.5998e{-}01 \\ 3.3951e{-}03 & 1.0938e{-}01 & 1.5232e{-}01 & 8.9704e{-}02 & 8.9704e{-}02 \end{bmatrix}$$

$$Ob_2 = \begin{bmatrix} 3.0915e{-}01 & 3.0915e{-}01 & 2.4492e{-}01 & 6.7429e{-}02 & 2.9568e{-}03 \\ 7.5553e{-}02 & 7.5553e{-}02 & 3.5771e{-}03 & 3.2928e{-}01 & 1.3169e{-}05 \end{bmatrix}$$

$$\text{abs}(WB_{cl}) = \begin{bmatrix} Co_1 \\ Co_2 \end{bmatrix}$$

$$Co_1 = \begin{bmatrix} 1.2470e{+}01 & 2.6467e{+}00 \\ 1.8144e{+}01 & 1.0590e{+}02 \\ 2.3993e{+}01 & 1.3166e{+}02 \\ 7.6802e{-}14 & 1.3160e{-}13 \\ 7.6396e{-}14 & 1.3149e{-}13 \end{bmatrix}$$

$$Co_2 = \begin{bmatrix} 1.8479e{+}01 & 3.0589e{+}00 \\ 1.8479e{+}01 & 3.0589e{+}00 \\ 6.4726e{-}13 & 7.5298e{-}13 \\ 7.4854e{+}00 & 2.5053e{+}01 \\ 9.5437e{-}03 & 3.8432e{-}05 \end{bmatrix}$$

The closed loop system will be fully observable if the 2x10 matrix $C_{cl}V$ has full column rank. This is indeed the case. For the closed loop system to be fully controllable the 10x2 matrix WB_{cl} must have full row rank. This is not the case as rows 4, 5, and 8 of this matrix have zero entries for all practical purposes. These rows correspond to the closed loop poles which are at the same location as the stable plant poles. The entries in row 10 of WB_{cl} are relatively small which indicate that the closed loop pole at the mirror image of the unstable open loop pole, is only weakly controllable.

B.6 Full State Feedback Eigenstructure Assignment

The gain matrix G of the full state feedback design described in section 5.2.1.1, is given by:

$$G = \begin{bmatrix} 1.9444e{-}03 & -2.1413e{-}03 & -2.2787e{-}01 & 1.1344e{-}02 \\ 1.3075e{-}01 & -6.6904e{-}03 & -4.7757e{-}01 & 2.3292e{-}02 \end{bmatrix}$$

The full state inner loop closed loop A matrix is given by:

$$[A_p - B_p G] = \begin{bmatrix} -8.9140e{-}02 & 1.1976e{-}04 & -9.9145e{-}01 & 5.4583e{-}02 \\ -3.2140e{+}01 & 1.8989e{-}01 & 6.8341e{+}00 & -2.2012e{-}01 \\ 8.3081e{+}00 & -1.0453e{-}01 & -1.7527e{+}00 & 5.6688e{-}02 \\ 0 & 1.0000e{+}00 & 0 & 0 \end{bmatrix}$$

The eigenvalues of A_p and $[A_p - B_p G]$ are given by:

$$[\ \lambda_i(A_p)\ |\ \lambda_i(A_p - B_p G)\ ] =$$

$$\left[\begin{array}{l|l} -5.9686e{-}02 \pm 2.8437e{+}00i & -6.1480e{-}01 \pm 2.8437e{+}00i \\ -4.2730e{-}01 & -4.2730e{-}01 \\ 4.8718e{-}03 & 4.9000e{-}03 \end{array}\right]$$

The eigenvectors of A_p and $[A_p - B_p G]$ are given by:

$$v_i(A_p) = \begin{bmatrix} -1.2902e{-}02 \pm 8.9337e{-}02i & -3.6213e{-}03 & 4.1233e{-}03 \\ 1.0000e{+}00 \pm 2.5479e{-}17i & -4.2730e{-}01 & 4.8718e{-}03 \\ -2.5410e{-}01 \pm 1.9778e{-}02i & 5.3767e{-}02 & 5.4622e{-}02 \\ -7.3778e{-}03 \pm 3.5150e{-}01i & 1.0000e{+}00 & 1.0000e{+}00 \end{bmatrix}$$

$$v_i(A_p - B_p G) = \begin{bmatrix} -2.8497e{-}02 \pm 8.1972e{-}02i & -3.6213e{-}03 & 4.7895e{-}03 \\ 1.0000e{+}00 \pm 1.8702e{-}17i & -4.2730e{-}01 & 4.9000e{-}03 \\ -2.5410e{-}01 \pm 1.9778e{-}02i & 5.3767e{-}02 & 5.4600e{-}02 \\ -7.2632e{-}02 \pm 3.3595e{-}01i & 1.0000e{+}00 & 1.0000e{+}00 \end{bmatrix}$$

B.7 Classical Compensator State Space Description

The state space description of the classical compensator described in section 5.3.1.1, is given by,

$$K(s) = \left[\begin{array}{c|c} A_k & B_k \\ \hline C_k & D_k \end{array}\right]$$

with

$$A_k = \begin{bmatrix} -1.5000e{+}00 & 0 \\ 0 & -2.5000e{+}01 \end{bmatrix}$$

$$B_k = \begin{bmatrix} 0 & 0 & -5.2144e{-}02 \\ -7.2369e{-}01 & 0 & 0 \end{bmatrix}$$

$$C_k = \begin{bmatrix} 0 & 4.1454e{+}01 \\ -2.3013e{+}01 & 0 \end{bmatrix}$$

$$D_k = \begin{bmatrix} -1.5000e{+}00 & 6.6000e{-}01 & 0 \\ 0 & 0 & -8.0000e{-}01 \end{bmatrix}$$

APPENDIX C

MILLING CIRCUIT EXAMPLE

In this appendix a transfer function mathematical model is given for a typical milling circuit that processes gold bearing ore. The state space description for the plant is derived in section C.2. Nomenclature used, and a short description of how the plant operates, are given in section C.3. The plant need to be scaled to reflect the relative importance of the inputs and outputs, and this is done in section C.4. Plant model reduction is discussed in section C.5 and a state space description for the augmented plant is given in section C.6.

C.1 The Transfer Function Mathematical Model

The transfer function model given here was derived from "step–tests" done on an actual milling circuit. The G(s) of the plant is as follows,

$$y(s) = G(s)\, u(s)$$

with

$$y = [\text{PSM LOAD LEVEL}]^T$$

$$u = [\text{SFW SLF CFF}]^T$$

and

$$G(s) = \begin{bmatrix} g_{11}(s) & g_{12}(s) & g_{13}(s) \\ g_{21}(s) & g_{22}(s) & g_{23}(s) \\ g_{31}(s) & g_{32}(s) & g_{33}(s) \end{bmatrix}$$

$$g_{11}(s) = \frac{0.105\ e^{-65s}}{83s + 1}$$

$$g_{12}(s) = \frac{-0.082\ e^{-80s}}{1766s + 1}$$

$$g_{13}(s) = \frac{-0.0575\ e^{-460s}}{167s + 1}$$

$$g_{21}(s) = \frac{-0.0468\ e^{-140s}}{1864s + 1}$$

$$g_{22}(s) = \frac{0.0001217}{s}$$

$$g_{23}(s) = \frac{0.1148\ e^{-120s}}{1981s + 1}$$

$$g_{31}(s) = \frac{.00253}{s}$$

$$g_{32}(s) = 0$$

$$g_{33}(s) = \frac{-.00299}{s}$$

A first order Pade approximation was used for the time delays, using the following equation,

$$e^{-\tau s} \cong \frac{1 - \frac{\tau s}{2}}{1 + \frac{\tau s}{2}}$$

Using this Pade approximation, G(s) can be written in partial fraction expansion form as,

$$g_{11}(s) = \frac{2.8934e{-}03}{s + 1/83} + \frac{{-}4.1584e{-}03}{s + 2/65}$$

$$g_{12}(s) = \frac{{-}4.8585e{-}05}{s + 1/1766} + \frac{9.5017e{-}05}{s + 2/80}$$

$$g_{13}(s) = \frac{2.1697e{-}03}{s + 1/167} + \frac{{-}1.8254e{-}03}{s + 2/460}$$

$$g_{21}(s) = \frac{{-}2.7067e{-}05}{s + 1/1864} + \frac{5.2174e{-}05}{s + 2/140}$$

$$g_{22}(s) = \frac{1.2170e{-}04}{s}$$

$$g_{23}(s) = \frac{6.1571e{-}05}{s + 1/1981} + \frac{{-}1.1952e{-}04}{s + 2/120}$$

$$g_{31}(s) = \frac{2.5300e{-}03}{s}$$

$$g_{32}(s) = 0$$

$$g_{33}(s) = \frac{-2.9900e{-}03}{s}$$

C.2 Deriving The State Space Description

The state space description of the G(s) given in section C.1, is derived using Gilbert's diagonal realization [25]. Let the p x m plant G(s) be written in a residue expansion form as in section A.2, with r distinct roots and a denominator polynomial,

$$d(s) = \prod_{i=1}^{r} (s - \lambda_i) \quad ; \lambda_i \neq \lambda_j$$

$$G(s) = \sum_{i=1}^{r} \frac{R_i}{s - \lambda_i}$$

with

$$R_i = \lim_{s \to \lambda_i} (s - \lambda_i)\, G(s)$$

$$\rho_i = \text{rank}(R_i)$$

and $R_i = C_i B_i$ $\qquad C_i - p \times \rho_i$

$B_i - \rho_i \times m$

The state space description is then given by,

$$A = \text{block diagonal} \{ \lambda_i I_{\rho_i}, i = 1, ..., r \}$$

$$B^T = [B_1^T, ..., B_r^T]$$

$$C = [C_1, ..., C_r]$$

with $$G(s) = C (sI - A)^{-1} B$$

The minimum order of this or any other state space realization is given by,

$$n = \sum_{i=1}^{r} \rho_i$$

The state space description for the milling circuit G(s) as given in partial fraction expansion form has n = 12, and can now be found to be,

$$A = \text{diag} \{ dd \}$$

with

$$dd = \begin{bmatrix} dd_1 \\ dd_2 \end{bmatrix}$$

$$dd_1 = \begin{bmatrix} -1.2048e{-}02 \\ -3.0769e{-}02 \\ -5.6625e{-}04 \\ -2.5000e{-}02 \\ -5.9880e{-}03 \\ -4.3478e{-}03 \end{bmatrix}$$

$$dd_2 = \begin{bmatrix} -5.3648e{-}04 \\ -1.4286e{-}02 \\ -5.0480e{-}04 \\ -1.6667e{-}02 \\ -5.0000e{-}06 \\ -5.0000e{-}06 \end{bmatrix}$$

The three integrators in G(s) were approximated by $s = -5.0e{-}06$ in the A matrix given above, so as to keep the Riccati equation solvers needed to compute the H_∞ compensator, "happy". The B matrix is,

$$B = \begin{bmatrix} B_1 \\ B_2 \end{bmatrix}$$

with

$$B_1 = \begin{bmatrix} 1.0000e{+}00 & 0 & 0 \\ 1.0000e{+}00 & 0 & 0 \\ 0 & 1.0000e{+}00 & 0 \\ 0 & 1.0000e{+}00 & 0 \\ 0 & 0 & 1.0000e{+}00 \\ 0 & 0 & 1.0000e{+}00 \end{bmatrix}$$

$$B_2 = \begin{bmatrix} 1.0000e{+}00 & 0 & 0 \\ 1.0000e{+}00 & 0 & 0 \\ 0 & 1.0000e{+}00 & 1.0000e{+}00 \\ 0 & 1.0000e{+}00 & 1.0000e{+}00 \\ 2.5300e{-}03 & 2.9900e{-}03 & -2.9900e{-}03 \\ -8.4401e{-}01 & 2.5300e{-}03 & 9.9747e{-}01 \end{bmatrix}$$

$$C = [\, C_1 \;\; C_2 \;\; C_3 \;\; C_4 \,]$$

with C_i (i = 1, ..., 4) 3x3 matrices given by,

$$\begin{bmatrix} C_1 \\ C_3 \end{bmatrix} = \begin{bmatrix} 2.8934e{-}03 & -4.1584e{-}03 & -4.8585e{-}05 \\ 0 & 0 & 0 \\ 0 & 0 & 0 \\ 0 & 0 & 0 \\ -2.7067e{-}05 & 5.2174e{-}05 & 6.1571e{-}05 \\ 0 & 0 & 0 \end{bmatrix}$$

$$\begin{bmatrix} C_2 \\ C_4 \end{bmatrix} = \begin{bmatrix} 9.5017e{-}05 & 2.1697e{-}03 & -1.8254e{-}03 \\ 0 & 0 & 0 \\ 0 & 0 & 0 \\ 0 & 0 & 0 \\ -1.1952e{-}04 & 4.0599e{-}02 & 1.2170e{-}04 \\ 0 & 2.5300e{-}03 & -2.9900e{-}03 \end{bmatrix}$$

$$D = \begin{bmatrix} 0 & 0 & 0 \\ 0 & 0 & 0 \\ 0 & 0 & 0 \end{bmatrix}$$

The poles and zeros of the state space description given above are,

$\lambda_i(A)$ = poles are the elements of dd.

zeros = 4.7582e–02 ← nonminimum phase zero

– 2.4870e–02

– 1.6875e–02

– 1.4241e–02

– 7.9281e–03

– 1.1474e–03 ± 2.7639e–04i

– 2.8806e–04

– 5.7060e–04

C.3 Plant Description and Nomenclature

C.3.1 Plant description

The milling circuit is shown in Figure C.3.1.1, and its operation can briefly be described as follows:

Gold bearing ore is fed into the mill via a conveyor belt, after which water is added. The turning motion of the mill lifts rocks and when it falls down, it breaks itself and other rocks beneath it into smaller pieces. At the outlet of the mill there is a grid which only lets small pieces of ore through into a sump. More water is added, and the mixture of water and ore (called "slurry"), is pumped to a hydrocyclone. The cyclone separates fine and course slurry. The fine slurry leaves the milling circuit as product, and the coarse slurry is returned back to the mill inlet.

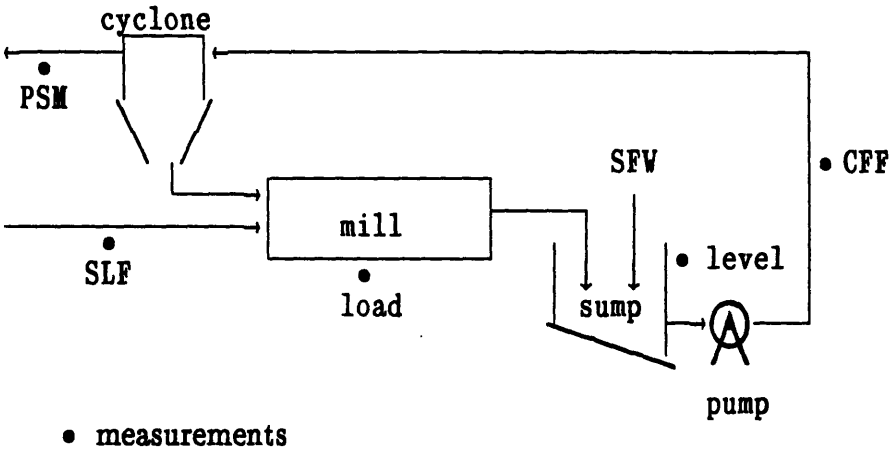

Figure C.3.1.1 : The Milling Circuit

The variables that need to be controlled in the milling circuit are:
The PSM which is a measure of the "fineness" of the product, the mill load, and the sump level. The mill load and sump level act as integrators and are thus open loop unstable.

The control variables are:
The rate of ore fed into the mill, the rate of water added to the sump, and the the rate of slurry pumped to the cyclone.

C.3.2 Nomenclature

PSM	particle size measurement – output size (% –75 μm)
LOAD	mill load (% of capacity up to axis level)
LEVEL	sump level (% of capacity)
SFW	sump feed water rate (m^3/hour)
SLF	solids feed rate (metric tons/hour)
CFF	cyclone feed flow rate (m^3/hour)

C.4 Scaling

In MIMO systems the control and the output variables have different units and, thus, it is usually necessary to scale the plant in order to reflect the relevant importance of commands or outputs. A compensator is designed for the scaled plant, and then the scaling matrices are absorbed into the compensator. The

eigenvalues and eigenvectors of the A matrix do not change with scaling but the singular values and singular vectors, i.e. the plant transmission zeros, do.

The solids feed rate input is first scaled to be in m^3/hour. With the average density of the ore 2700 kg/m^3, this scaling can be accomplished by multiplying the second column of the B matrix by 2.7.

In order to reflect the relative importance of the outputs, the following relationships are established:

- 1% PSM error is as serious as a 1% error in mill load
- 1% PSM error is 10 times as serious as a 1% error in sump level

These relationships and the range of the outputs, lead to the output scaling matrix Q_y given by,

$$Q_y = \begin{bmatrix} 1/5 & 0 & 0 \\ 0 & 1/5 & 0 \\ 0 & 0 & 1/50 \end{bmatrix}$$

The controls are scaled, using their saturation levels. The control scaling matrix Q_u that results is,

$$Q_u = \begin{bmatrix} 1/125 & 0 & 0 \\ 0 & 1/34 & 0 \\ 0 & 0 & 1/125 \end{bmatrix}$$

The scaled plant $G_s(s)$ is given by,

$$G_s(s) = Q_y \, G(s) \, Q_u^{-1}$$

After a compensator $K_s(s)$ has been designed for the scaled plant augmented as shown in section C.6, the scaling matrices are absorbed into the compensator, to give

$$K(s) = Q_u^{-1} \, K_s(s) \, Q_y$$

C.5 Plant Model Reduction

The order of the H_∞ compensator is equal to the order of the augmented plant, which in this case is 15. If a reduced order milling circuit model can be found that gives an adequate representation of the milling circuit, this reduced order model can be used for compensator design. In this section the order of the scaled milling circuit model will be reduced by 50%, i.e. six states will be removed. Schur balanced model reduction will be used, as described in [26].

Let the milling circuit model be given by G(s), and the reduced order model by $G_m(s)$. The accuracy of the reduced order model can be expressed by,

$$\| G(j\omega) - G_m(j\omega) \|_\infty \leq \text{bnd}$$

When six states are removed, bnd = 0.889. Figures C.5.1 to C.5.6 show that the outputs of G(s) and $G_m(s)$ in response to steps in each of the three milling circuit

inputs, are more or less the same. The singular value plots of G(s) and $G_m(s)$ are shown in Figures C.5.7 and C.5.8.

The state space description of the reduced order plant is as follows,

$$A = [\, A_1 \;\; A_2 \,]$$

with

$$A_1 = \begin{bmatrix} -5.0502e{-}06 & -3.4292e{-}06 & 1.4925e{-}05 \\ -4.0717e{-}06 & -6.0542e{-}04 & 5.3080e{-}04 \\ 1.6341e{-}05 & 5.7029e{-}04 & -8.8664e{-}03 \\ 7.1548e{-}06 & 5.0717e{-}04 & -6.9803e{-}03 \\ 2.6505e{-}05 & 4.1073e{-}04 & -1.1130e{-}02 \\ -6.1984e{-}05 & -4.5121e{-}04 & 2.0616e{-}02 \end{bmatrix}$$

$$A_2 = \begin{bmatrix} 2.0953e{-}06 & 2.2336e{-}05 & -6.4768e{-}07 \\ 3.2246e{-}04 & 1.7722e{-}03 & -3.6808e{-}05 \\ -2.3118e{-}03 & -9.9893e{-}03 & -3.6029e{-}03 \\ -3.5567e{-}03 & -7.7426e{-}03 & -6.5040e{-}03 \\ -9.0770e{-}04 & -1.5275e{-}02 & 5.2946e{-}04 \\ -3.1866e{-}03 & 2.1212e{-}02 & -8.5897e{-}03 \end{bmatrix}$$

$$B = \begin{bmatrix} 1.0542e{+}02 & -2.5069e{-}01 & -1.2418e{+}02 \\ -3.4921e{+}01 & -6.3706e{+}00 & 1.0030e{+}02 \\ -1.0720e{+}02 & -2.3154e{+}01 & -6.2767e{+}01 \\ -1.3399e{+}02 & -3.3715e{+}01 & -7.0415e{+}01 \\ -9.1434e{+}01 & 1.7352e{-}01 & 6.0475e{+}01 \\ 5.6788e{+}01 & 5.0151e{+}00 & -2.3873e{+}01 \end{bmatrix}$$

$$C = [\, C_1 \;\; C_2 \,]$$

$$\begin{bmatrix} C_1 \\ C_2 \end{bmatrix} = \begin{bmatrix} -1.0315e{-}06 & 4.5504e{-}06 & 2.2226e{-}04 \\ -6.3698e{-}06 & 9.3679e{-}04 & 5.3167e{-}03 \\ 5.9911e{-}05 & 5.4447e{-}06 & 3.3111e{-}05 \\ -1.6704e{-}04 & 5.5722e{-}05 & -3.2488e{-}04 \\ -3.9591e{-}03 & -3.5120e{-}04 & 7.4653e{-}04 \\ -2.4606e{-}05 & -2.0896e{-}06 & 4.5892e{-}06 \end{bmatrix}$$

$$D = \begin{bmatrix} 0 & 0 & 0 \\ 0 & 0 & 0 \\ 0 & 0 & 0 \end{bmatrix}$$

From Figures C.5.1 to C.5.8, it is evident that the reduced order model gives an adequate representation of the milling circuit.

C.6 State Space Descriptions

Let the plant and weights have state space descriptions as given in equation 3.4.4 (section 3.4). The augmented plant can then be described as follows.

$$A = \begin{bmatrix} A_p & 0 \\ -B_{w1}C_p & A_{w1} \end{bmatrix}$$

$$[B1 \mid B2] = \left[\begin{array}{c|c} 0 & B_p \\ B_{w1} & -B_{w1}D_p \end{array}\right]$$

$$\left[\frac{C1}{C2}\right] = \left[\begin{array}{cc} -D_{w1}C_p & C_{w1} \\ 0 & 0 \\ C_{new} & 0 \\ \hline -C_p & 0 \end{array}\right]$$

$$\left[\begin{array}{c|c} D_{11} & D_{12} \\ \hline D_{21} & D_{22} \end{array}\right] = \left[\begin{array}{c|c} \begin{matrix} D_{w1} \\ 0 \\ 0 \end{matrix} & \begin{matrix} -D_{w1}D_p \\ 0 \\ D_{new} \end{matrix} \\ \hline I & -D_p \end{array}\right]$$

with C_{new} and D_{new} as derived in Appendix A.

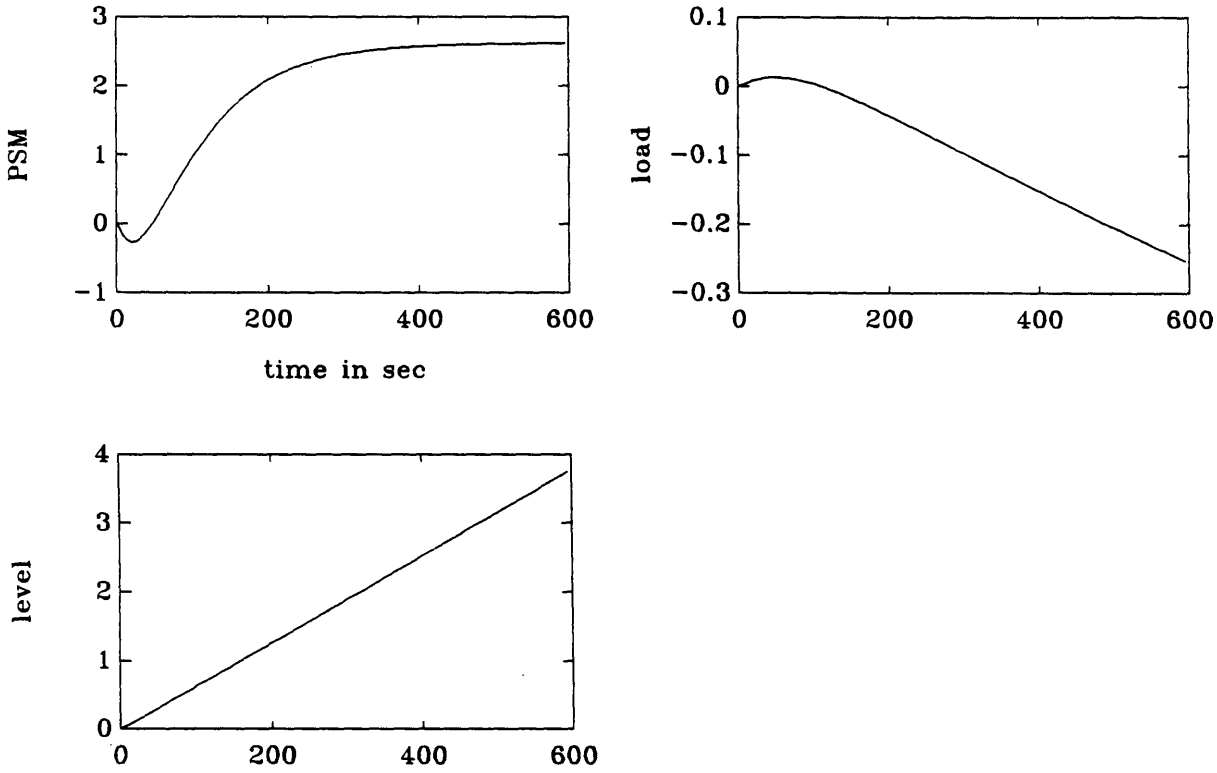

Figure C.5.1 :Response of full order model to a unit step in SFW

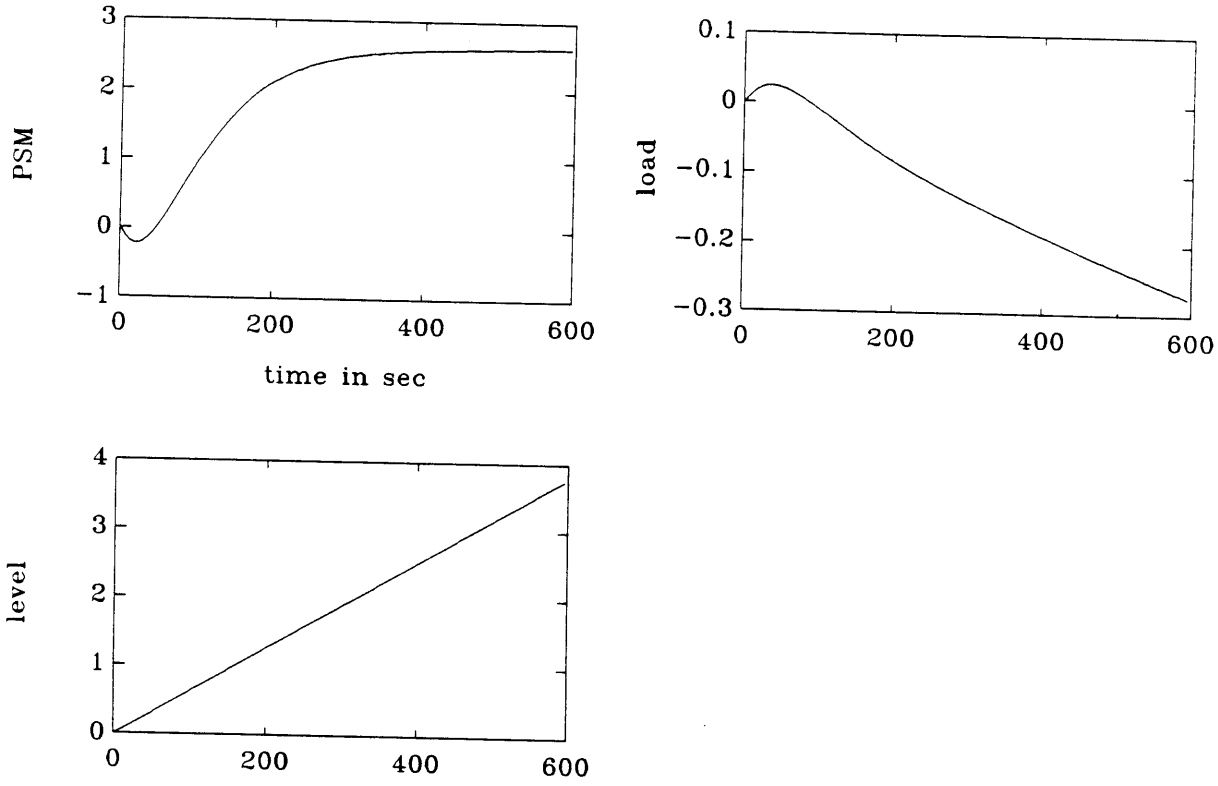

Figure C.5.2 :Response of reduced model to a unit step in SFW

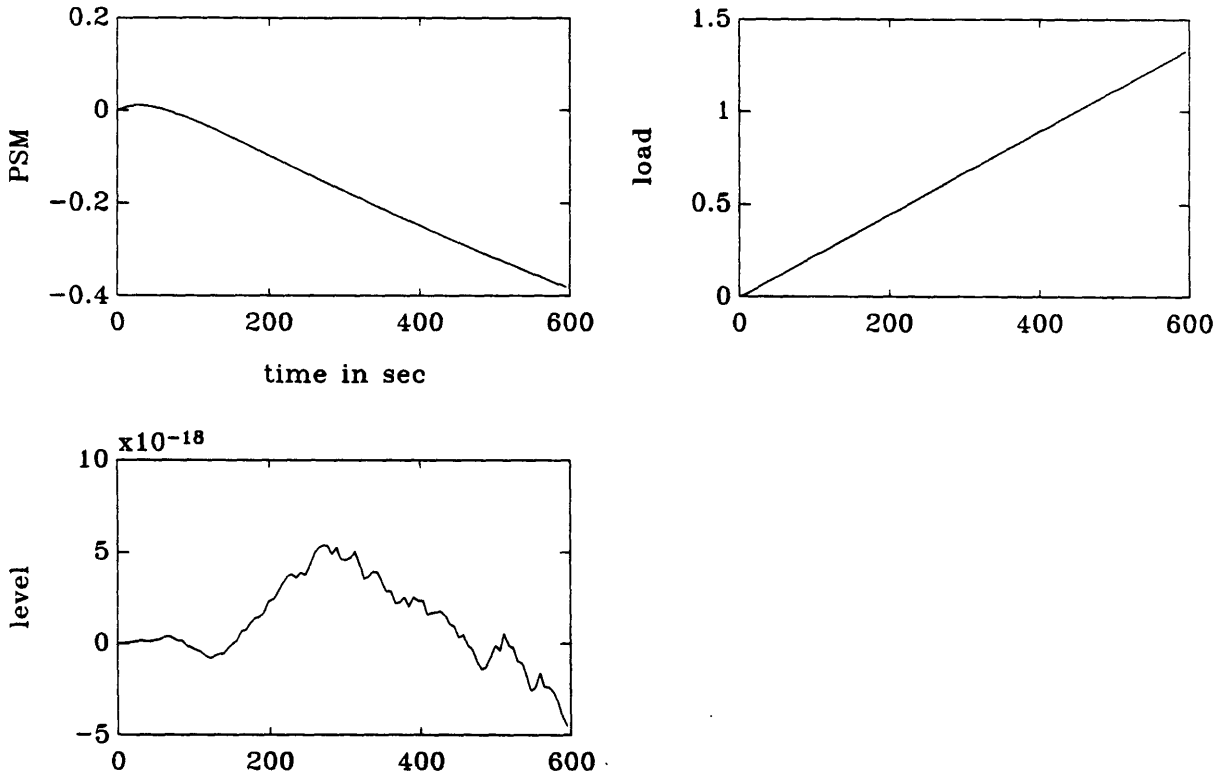

Figure C.5.3 :Response of full order model to a unit step in SLF

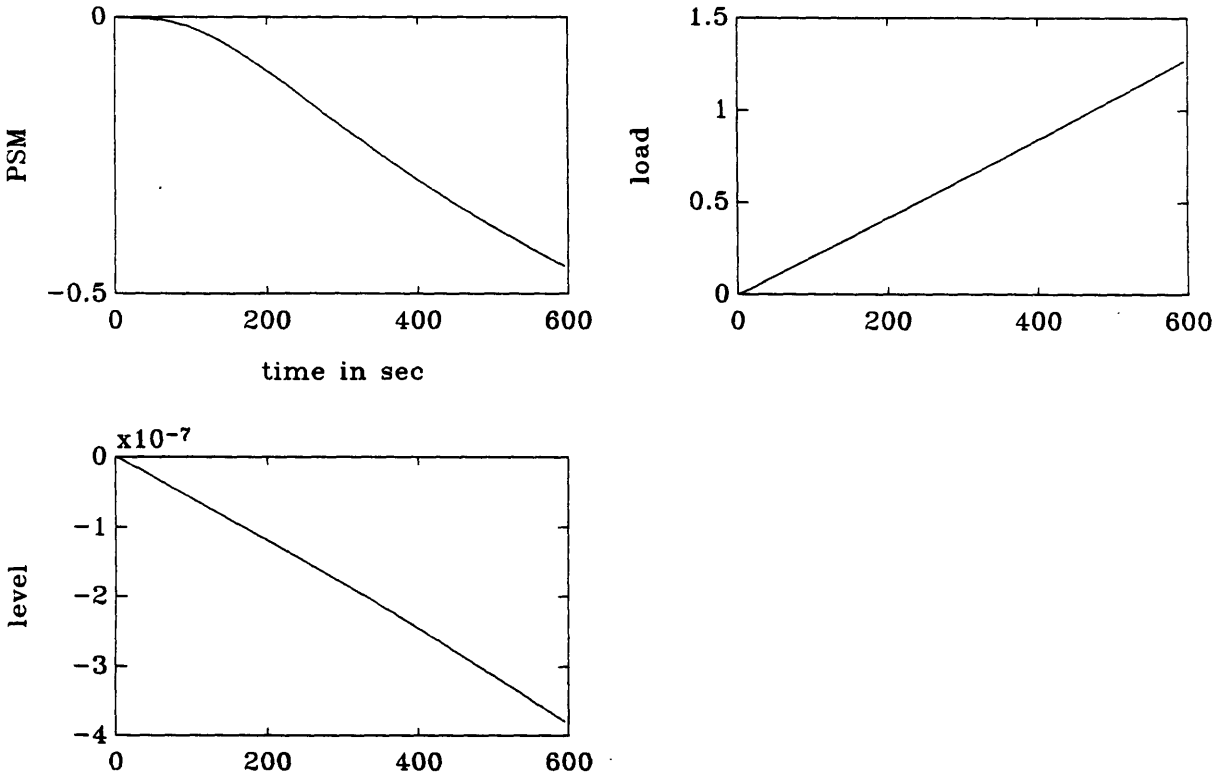

Figure C.5.4 :Response of reduced model to a unit step in SLF

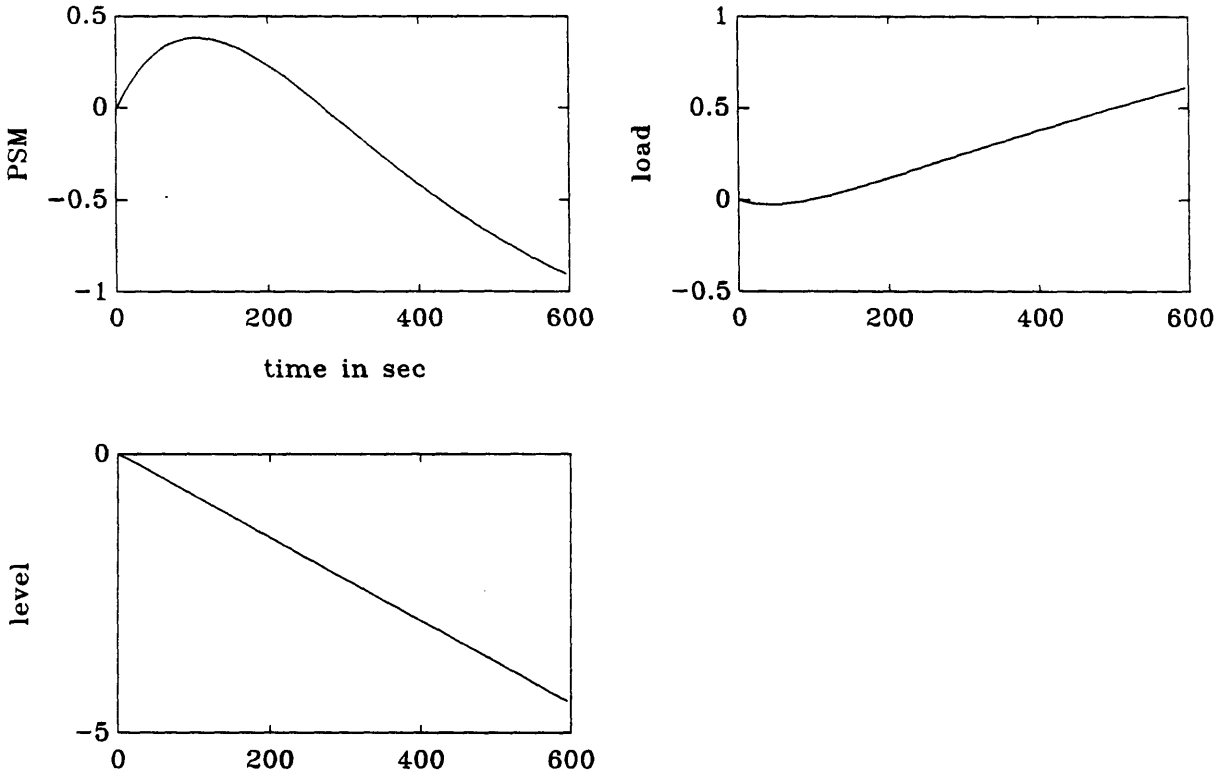

Figure C.5.5 :Response of full order model to a unit step in CFF

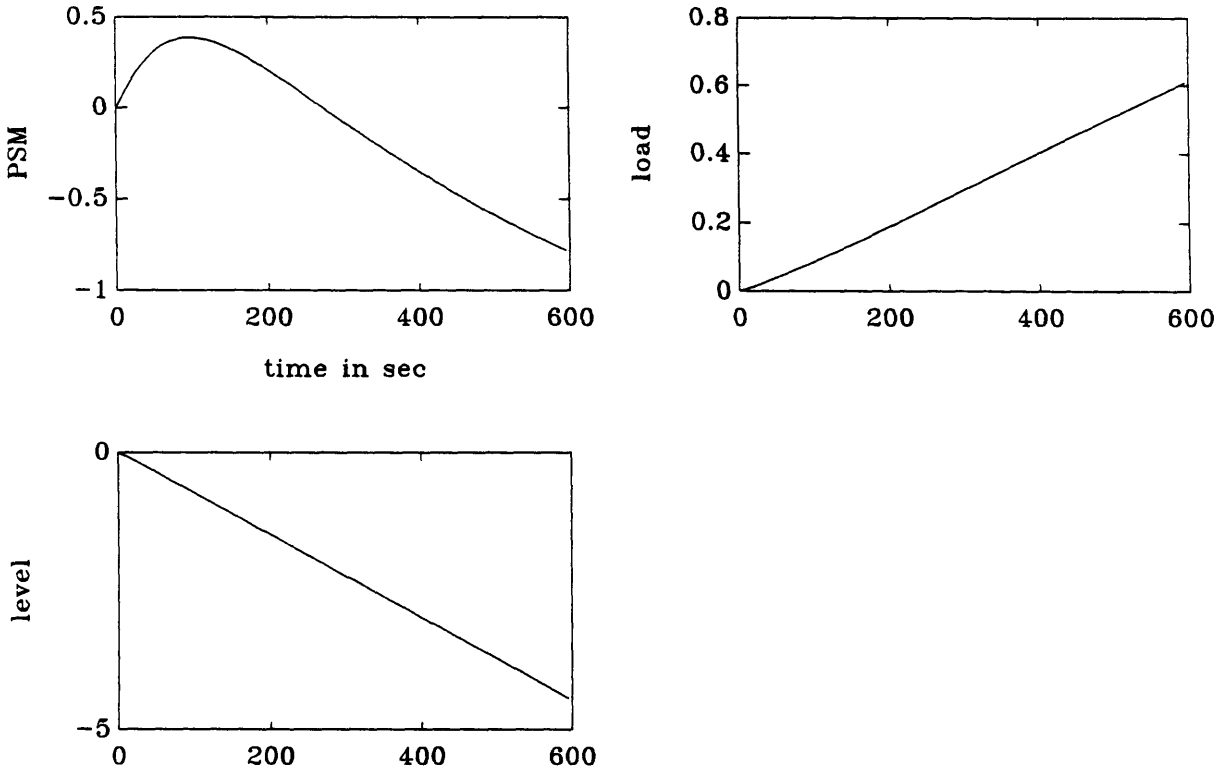

Figure C.5.6 :Response of reduced model to a unit step in CFF

Figure C.5.7 :Singular values of full order model G(s)

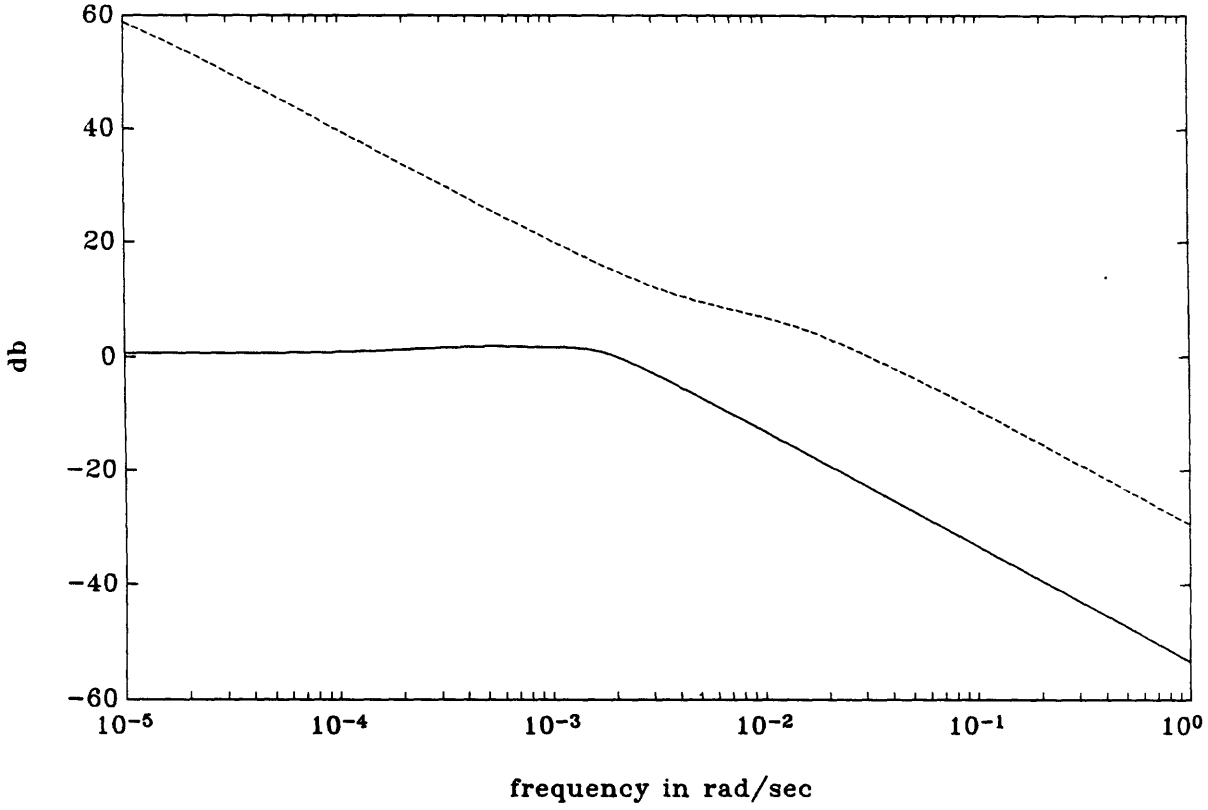

Figure C.5.8 :Singular values of reduced model Gm(s)

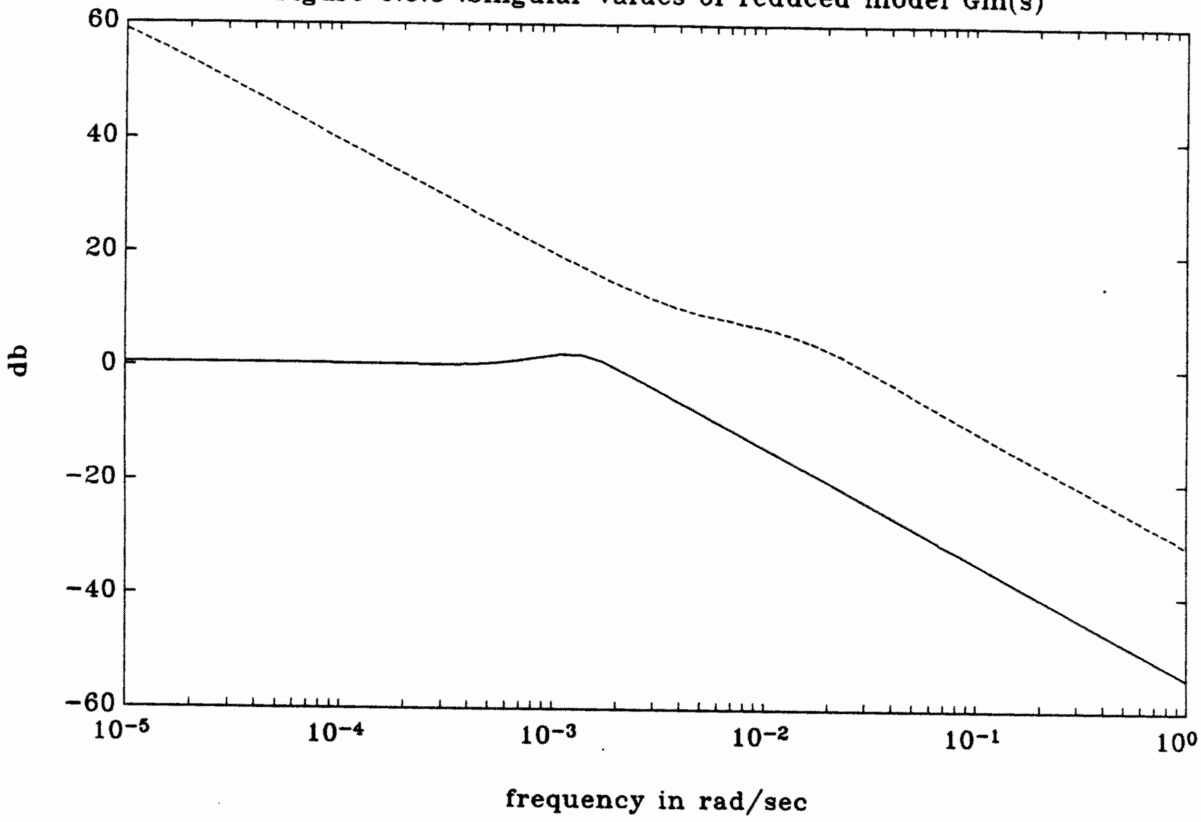

APPENDIX D

DERIVATION OF EQUATIONS USED IN SENSITIVITY STUDIES

D.1 Derivatives of Eigenvalues and Eigenvectors

In this section, an expression is derived for the derivative of an eigenvalue of a matrix. Second order terms are included in this expression which implies that the first order terms of the derivative of an eigenvector of a matrix, must also be found. Reference [27] provides a detailed description of material covered here, including alternate proofs for theorems given in this section.

Assumptions and Definitions: A is a square n x n matrix with distinct eigenvalues λ_i and corresponding right and left eigenvectors v_i and w_i respectively, such that,

1 $$Av_i = \lambda_i v_i \qquad ; i = 1,\ldots,n$$

2 $$w_i^T A = \lambda_i w_i^T$$

3 $$w_j^T v_i = 1 \qquad ; i = j$$
$$= 0 \qquad ; i \neq j$$

4 **Theorem** : The derivative of a right eigenvector v_i of the matrix A described by (1), including only first order terms, is given by:

5 $$dv_i = \sum_{\substack{k=1 \\ k \neq i}}^{n} \alpha_{ik} v_k \qquad ; \alpha_{ij} \in \mathbb{C}$$

Proof: Let p_i be a right eigenvector of the n x n matrix A + dA, with the corresponding distinct eigenvalue μ_i such that,

$$(A + dA)p_i = \mu_i p_i$$

p_i can be expressed as a linear combination of the right eigenvectors v_i (i = 1,...,n) which spans $\mathbb{C}^{nxn}$ i.e.,

$$p_i = \gamma_{i1} v_1 + \ldots + \gamma_{ii} v_i + \ldots + \gamma_{in} v_n \qquad ; \gamma_{ij} \in \mathbb{C}$$

or

6 $$\frac{p_i}{\gamma_{ii}} = v_i + \sum_{\substack{k=1 \\ k \neq i}}^{n} \alpha_{ik} v_k$$

with

$$\alpha_{ik} = \frac{\gamma_{ik}}{\gamma_{ii}}$$

Now let $v_i + dv_i = \frac{p_i}{\gamma_{ii}}$. (5) follows from substituting $v_i + dv_i$ in (6).

7 **Theorem :** α_{ij} used in (4) is given by the equation,

8 $$\alpha_{ij} = \frac{w_j^T \, dA \, v_i}{\lambda_i - \lambda_j} \qquad ; i \neq j$$

Proof: Let $\lambda_i + d\lambda_i$ be a distinct eigenvalue of the n x n matrix A + dA, with the associated right eigenvector $v_i + dv_i$. From (1) it follows that,

9 $$(A + dA)(v_i + dv_i) = (\lambda_i + d\lambda_i)(v_i + dv_i)$$

Neglecting second order terms and multiplying (9) from the left by w_j^T ($i \neq j$), results in,

10 $$w_j^T A dv_i + w_j^T dA v_i = \lambda_i w_j^T dv_i + d\lambda_i w_j^T v_i$$

Now using (2) and (3) in conjunction with (4), (10) results in (8) which concludes the proof.

11 **Theorem :** The derivative of an eigenvalue λ_i described by (1) and (2), which includes second order terms, is given by,

12 $$d\lambda_i = \gamma_{ii} + \sum_{\substack{k=1 \\ k \neq i}}^{n} \frac{\gamma_{ki}\gamma_{ik}}{\lambda_i - \lambda_k}$$

with $$\gamma_{ij} = w_i^T dA v_j$$

Proof : Let $v_i + dv_i$ be the right eigenvector of the n by n matrix A + dA, with the associated eigenvalue $\lambda_i + d\lambda_i$. From (1) it follows that,

13 $$(A + dA)(v_i + dv_i) = (\lambda_i + d\lambda_i)(v_i + dv_i)$$

Now multiplying (13) from the left by w_i^T and rearranging terms, results in,

14 $$d\lambda_i w_i^T v_i + d\lambda_i w_i^T dv_i = (w_i^T A - \lambda_i w_i^T)dv_i + w_i^T dA v_i + w_i^T dA dv_i$$

Letting (2), (3) and (5) act on (14), the following equation results,

15 $$d\lambda_i = w_i^T dA v_i + w_i^T dA \sum_{\substack{k=1 \\ k \neq i}}^{n} \alpha_{ik} v_k$$

Substituting (8) in (15) results in (12), which concludes the proof.

D.2 Derivatives of Singular Values and Singular Vectors

In this section the derivative of a singular value will be derived up to second order. This implies that the first order terms of the derivative of a singular vector of a matrix, must also be found. The results given here are for square matrices but can easily be generalized to the nonsquare case.

Assumptions and Definitions: G is a complex, square n x n matrix with a singular value decomposition given by,

16 $$G = U\Sigma V^H$$

with

17 $\Sigma = U^H G V$

18 Σ is a diagonal, n x n real matrix with singular values σ_i along the diagonal

19 U is a n x n unitary matrix ($U^H = U^{-1}$)

20 column vectors u_i of U (called left singular vectors of G), are orthonormal, i.e. $u_i^H u_j = \delta_{ij}$.

21 column vectors u_i of U are also the right eigenvectors of the Hermitian matrix GG^H. The eigenvalues λ_i of this matrix are the squares of the singular values of G, i.e. $\lambda_i = \sigma_i^2$

22 V is a n x n unitary matrix ($V^H = V^{-1}$)

23 column vectors v_i of V (called right singular vectors of G), are orthonormal, i.e. $v_i^H v_j = \delta_{ij}$

24 column vectors v_i of V are also the right eigenvectors of the Hermitian matrix $G^H G$. The eigenvalues λ_i of this matrix are the squares of the singular values of G, i.e. $\lambda_i = \sigma_i^2$

25 the left eigenvector w_i^T of an Hermitian matrix is equal to the hermitian of the corresponding right eigenvector, i.e. $w_i^T = u_i^H$ in the case of (21)

26 $$\delta_{ij} = 1 \quad ; i = j$$
$$= 0 \quad ; i \neq j$$

27 **Theorem :** The derivative of the left singular vector u_i of G, is given by,

28 $$du_i = \sum_{\substack{k=1 \\ k \neq i}}^{n} \alpha_{ik} u_k \quad ; \alpha_{ik} \in \mathbb{C}$$

Proof : Analogous with proof of (4), where the matrix $A = GG^H$ have right eigenvectors u_i.

30 **Theorem :** α_{ij} used in (28) is given by the equation,

31
$$\alpha_{ij} = \frac{u_j^H (dGG^H + GdG^H) u_i}{\sigma_i^2 - \sigma_j^2} \qquad ; i \neq j$$

Proof: Let $\lambda_i + d\lambda_i$ be a distinct eigenvalue of the n x n matrix A + dA, with the associated right eigenvector $u_i + du_i$. Let $A = GG^H$, then it follows from (21) that u_i is also a left singular vector of G. From (1) it follows that,

32
$$(A + dA)(u_i + du_i) = (\lambda_i + d\lambda_i)(u_i + du_i)$$

Neglecting second order terms and multiplying (32) from the left by a left eigenvector u_j^H ($i \neq j$) of A according to (25) results in:

33
$$u_j^H A du_i + u_j^H dA u_i = \lambda_i u_j^H du_i + d\lambda_i u_j^H u_i$$

Now using (2) and (20) in conjunction with (28), and noting that $\lambda_i = \sigma_i^2$ and that $dA = dGG^H + GdG^H$,(33) results in (31) which concludes the proof.

34 **Theorem :** The derivative of a singular value σ_i described by (16) and (18), which includes second order terms, is given by,

35 $$d\sigma_i = \frac{1}{2\sigma_i}(\gamma_{ii} + \sum_{\substack{k=1 \\ k\neq i}}^{n} \frac{\gamma_{ki}\gamma_{ik}}{\sigma_i^2 - \sigma_k^2})$$

with

$$\gamma_{ij} = u_i^H(dGG^H + GdG^H)u_j$$

Proof: Let $u_i + du_i$ be the right eigenvector of the n x n matrix A + dA, with the associated eigenvalue $\lambda_i + d\lambda_i$. Let $A = GG^H$, then it follows from (21) that u_i is also a left singular vector of G. From (1) it follows that,

36 $$(A + dA)(u_i + du_i) = (\lambda_i + d\lambda_i)(u_i + du_i)$$

Now multiplying (36) from the left by the left eigenvector u_i^H of A according to (25), and rearranging terms, results in,

37 $$d\lambda_i u_i^H u_i + d\lambda_i u_i^H du_i = (u_i^H A - \lambda_i u_i^H)du_i + u_i^H dAu_i + u_i^H dAdu_i$$

Letting (2), (20) and (28) act on (37), the following equation results,

38 $$d\lambda_i = u_i^H dAu_i + u_i^H dA \sum_{\substack{k=1 \\ k\neq i}}^{n} \alpha_{ik}u_k$$

(35) follows from substituting (31) into (38), and noting that $\lambda_i = \sigma_i^2$, $d\lambda_i = 2\sigma_i d\sigma_i$ and $dA = dGG^H + GdG^H$, which concludes the proof.

What is dG, where $G = C_p(sI_{nxn} - A_P)^{-1}B_p$, if A_P is perturbed? Differentiating G with respect to A_P, it follows that,

$$dG = C_p(sI_{nxn} - A_P)^{-1}\, dA_P\, (sI_{nxn} - A_P)^{-1}B_p$$

APPENDIX E

FICTITIOUS PLANTS

In this appendix, state space descriptions are given for the two fictitious plants described in section 4.3.3. Weighting functions used in the H_∞ design for these plants are given in section E.3.

E.1 Plant I

The state space description of plant I is given by,

$$G_1(s) = \left[\begin{array}{c|c} A_1 & B_1 \\ \hline C_1 & D_1 \end{array}\right]$$

with

$$A_1 = \begin{bmatrix} -2.0418e{+}00 & 9.6489e{-}02 & -4.5784e{-}02 \\ -4.1042e{-}01 & -1.8398e{+}00 & 1.3475e{+}00 \\ -1.7004e{+}00 & 2.4946e{-}01 & 8.8163e{-}01 \end{bmatrix}$$

$$B_1 = \begin{bmatrix} 9.1287e{-}01 & 0 \\ -1.7501e{-}01 & 9.0345e{-}01 \\ 3.6883e{-}01 & 4.2869e{-}01 \end{bmatrix}$$

$$C_1 = \begin{bmatrix} 0 & -1.4661e{-}01 & 2.6417e{+}00 \\ 0 & 9.0345e{-}01 & 4.2869e{-}01 \end{bmatrix}$$

$$D_1 = \begin{bmatrix} 0 & 0 \\ 0 & 0 \end{bmatrix}$$

E.2 Plant II

The state space description of plant II is given by,

$$G_2(s) = \left[\begin{array}{c|c} A_2 & B_1 \\ \hline C_1 & D_1 \end{array}\right]$$

with

$$A_2 = \begin{bmatrix} 1.0055e{+}00 & -2.7103e{-}01 & -5.4082e{+}00 \\ 7.4706e{-}04 & -1.8894e{+}00 & 6.2396e{-}01 \\ 3.0952e{-}03 & 4.4009e{-}02 & -2.1161e{+}00 \end{bmatrix}$$

with B_1, C_1 and D_1 as given in E.1.

E.3 Weighting Functions

The weighting functions used in the design of H_∞ compensators for plant I and II are given by,

$$W_1(s) = \frac{1}{s + .0001} I_{2x2}$$

$$W_2(s) = \epsilon\, I_{2x2}\,, \quad \epsilon = 0$$

$$W_3(s) = \frac{s}{1} I_{2x2}$$

REFERENCES

[1] B.A. Francis, *A Course in H_∞ Control Theory*, Lecture Notes in Control and Information Sciences, Springer–Verlag, Berlin, 1987.

[2] P. Dorato, *Robust Control*, IEEE Press, 1987.

[3] P. Voulgaris and L. Valavani, "High Performance Multivariable Control of the 'Supermaneuverable' F18/HARV Fighter Aircraft", accepted for publication in *AIAA Journal of Guidance, Control, and Dynamics*, 1989.

[4] G. Stein and M. Athans, "The LQG/LTR Procedure for Multivariable Feedback Control Design", *IEEE Trans. on Auto. Control*, Vol AC–32, No. 2, pp. 105–114, 1987.

[5] M. Athans, "Multivariable Control Systems 1 – Class notes", MIT, Cambridge, MA, Fall 1987.

[6] N.A. Lehtomaki, "Practical Robustness Measures in Multivariable Control System Analysis", Ph.D. Thesis, LIDS–TH–1093, MIT, Cambridge, MA, May 1981.

[7] M.G. Safonov and M. Athans, "Gain and Phase Margins for Multi–Loop LQG Regulators", *IEEE Trans. on Auto. Control*, Vol AC–22, No. 2, pp. 173–179, 1977.

[8] G. Stein, "Latest H_∞ Results", unpublished note, Oct. 1987.

[9] M.G. Safonov, "Simplifying the H_∞ Theory via Loop Shifting", *Proc. IEEE Conf. on Decision and Control*, Austin, TX, 1988, pp. 1399–1404

[10] G. Stein, "Formal Control System Synthesis with H_2/H_∞ Criteria", Lectures in Multivariable Control Systems 2, MIT, Cambridge, MA, Spring 1988.

[11] J.C. Doyle, K. Glover, P. Khargonekar and B. Francis, "State Space Solutions to Standard H_2 and H_∞ Control Problems", *Proc. American Control Conference*, Atlanta, GA, June 15–17, 1988. To appear in *IEEE Trans. on Auto. Control*, Aug. 1989.

[12] D.A. Millich, "A Methodology for the Synthesis of Robust Feedback Systems", Ph.D. Thesis, LIDS–TH–1748, MIT, Cambridge, MA, 1988.

[13] G. Strang, *Linear Algebra and its Applications*, Academic Press, New York, 1980.

[14] B. Ridgely, "H_∞ Optimization with an H_2 Superoptimization Criterion" ,Ph.D. Thesis, MIT, Cambridge, MA, 1989.

[15] H. Kwakernaak and R. Sivan, *Linear Optimal Control Systems*, Wiley–Interscience, New York, 1972.

[16] R.Y. Chaing and M.G. Safonov, "Robust–Control Toolbox: for use with MATLAB and the Control Systems Toolbox", User's Guide, The MathWorks, Jun. 1988.

[17] B. Bacon, NASA Langley, Private Communication, 1988.

[18] D.G. Hulbert, MINTEK, Private Communication, 1989.

[19] D. McRuer, I. Ashkenas and D. Graham, *Aircraft Dynamics and Automatic Control*, Princeton University Press, Princeton, NJ, 1973.

[20] J.S. Freudenberg and D.P. Looze, "Right Half Plane Poles and Zeros and Design Tradeoffs in Feedback Systems", *IEEE Trans. on Auto. Control*, Vol AC–30, No. 6, pp. 555–565, Jun. 1985.

[21] K.M. Sobel and E.Y. Shapiro, "A Design Methodology for Pitch Pointing Flight Control Systems", *AIAA Journal of Guidance, Control, and Dynamics*, Vol. 8, pp. 181–187, 1985.

[22] M. Athans, "Multivariable Control Systems 2 – Class notes", MIT, Cambridge, MA, Spring 1988.

[23] J.C. Doyle, "Analysis of Feedback Systems with Structured Uncertainties", *IEE Proceedings*, Vol. 129, Part D, No. 6, pp.242–250, Nov. 1982.

[24] J.S. Shamma, "Analysis and Design of Gain Scheduled Control Systems", Ph.D. Thesis, LIDS–TH–1770, MIT, Cambridge, MA, 1988.

[25] T. Kailath, *Linear Systems*, Prentice–Hall, Englewood Cliffs N.J., 1980.

[26] M.G. Safonov and R.Y. Chiang, "Schur Balanced Model Reduction", *Proc. American Control Conference*, Atlanta, GA, June 15–17, 1988.

[27] J. H. Wilkinson, *The Algebraic Eigenvalue Problem*, Clarendon Press, Oxford, 1965.